Warsaw University of Technology
Faculty of Power and Aeronautical Engineering

Thermodynamic optimization of downhole coaxial heat exchanger for geothermal applications

(Project)

Student: Marc Domínguez Masalias
Supervisor: Piotr Furmański

Warsaw, July 2011

Contents

Introduction

Currently fossil fuels - coal, oil and natural gas - provide about 85% of the world's total energy demand (including heating, transport, electricity generation and other uses). But, unfortunately, these types of energy resources have some negatives points.

Fossil fuels are non-renewable resources because they take millions of years to form, and reserves are being depleted much faster than new ones are being formed. Another negative aspect is that burning such fossil fuels results in major environmental deterioration. Trying to restrain this rapidly growing environmental pollution, authorities have more and more frequently turned towards alternative energy sources (renewable), among which geothermal energy plays a significant role in some countries.

Geothermal energy is the heat from the Earth. Resources of geothermal energy range from the shallow ground to hot water and hot rock found a few kilometres beneath the Earth's surface. The main inconvenience of this energy source is the hardly economical cost of drilling new wells. Therefore, attempts are being made to adapt existing boreholes, mostly drilled by the hydrocarbon industry, for geothermal utilization.

In this context, deep borehole heat exchangers are an environmentally advantageous way for geothermal energy production. In this project, a downhole coaxial heat exchanger (DCHE)/heat pump (HP) system is simulated for shallow geothermal resources exploitation. The downhole, coaxial heat exchanger is designed for two different scenarios according to the working medium; one using water as a working fluid and the other one using air. The hot water produced will be used for space heating and domestic hot water production for a Central European home offering an attractive way to supply local housing with heat for direct use.

All these systems need an electrical heat pump (HP) by which the low DCHE output temperature (rarely above 10 ºC) can be lifted to the required level (35-50 ºC). Heat extraction is established by closed-circuit fluid circulation.

In this project, a thermodynamic design for determining some optimal parameters of the heat exchanger is presented. In this study, optimum diameter and thermal resistance for the insulated inner pipe is determined by using the second law of thermodynamics. The purpose of a thermodynamic design is to achieve a working system. A goal of the design is high efficiency; minimization of entropy generated (exergy destruction) is a way to achieve this.

Chapter 1

Literature review

1.1 Review of downhole coaxial heat exchangers of Field type

Downhole coaxial heat exchanger (DCHE) of Field type is a kind of heat exchanger used for exploitation of geothermal resources such as Hot Wet Rock, Super Hot Rock adjacent to magma and magma. Depending on the geothermal resources features can differentiate between shallow geothermal resources (the heat content of rocks in the top few 100-200 meters of the earth's crust) and high temperature and deep potential geothermal resources with basin drilling depths of 2000-5000 meters.

The DCHE is applicable to various geological conditions and formation temperatures, and can be utilized not only for power generation, but also for space heating and cooling, indoor swimming pools and melting snow on roads.

The downhole, coaxial heat exchanger for geothermal applications consists of an outer steel pipe (casing) and a thin production pipe coaxial in the casing (fig. 1.1 and fig. 1.2). As is shown in fig. 1.1, cold fluid is pumped into the annulus of the geothermal well. On the way down to the bottom of the well it takes up heat from the surrounding rock. Once at the base of the heat exchanger the hot fluid flows back to the surface via the central production pipe. The heat exchanger has a closed fluid circulation and does not use hot fresh fluid in the subsurface. Back on the surface the hot water passes cascade like through radiators as well as ceiling-and floor-heating systems thus supplying heat to buildings, bathes and many more. In summer, the geothermal heat may serve as driving energy for an adsorption cooling machine. Once the previously hot water has cooled down it is conducted back into the geothermal heat exchanger and fluid circuit closes.

The major features of the DCH include the utilization of a highly insulated inner pipe, reverse circulation (i.e., cold water down the annulus and hot water up through the inner pipe) and a completely closed system (fig. 1.1).

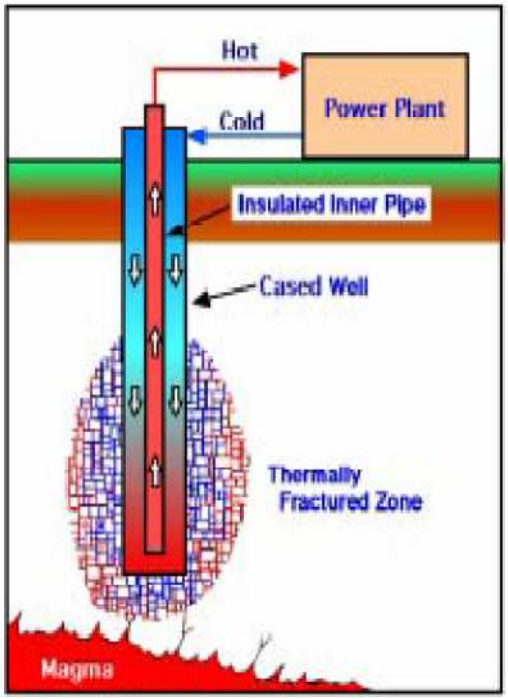

Fig. 1.1:Concept of the DCHE [10].

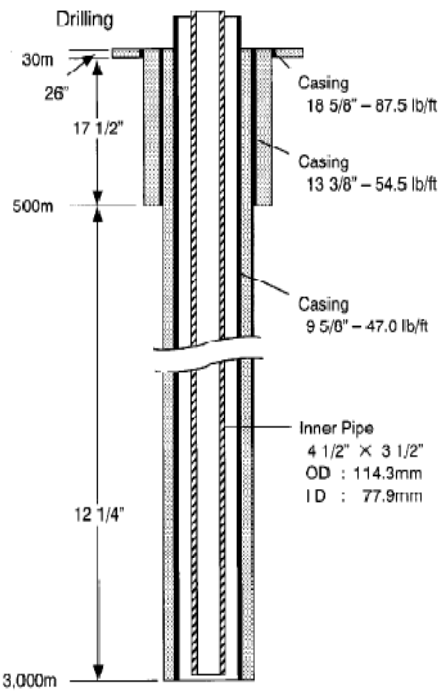

Fig. 1.2: Structure of the DCHE for high temperature and deep potential geothermal resource exploitation application [10].

The heat extraction is limited below the depth where the hot water temperature reaches the same temperature as the formation temperature. In another way, heat loss from hot water in the annulus to the surrounding formation should occur in the section where the hot water temperature is higher than the formation temperature.
In order to achieve efficient heat extraction from the formation, it is necessary to maximize the temperature difference between the heat extraction medium and the formation, and to minimize the heat loss. Reverse circulation minimizes the heat loss from the heat exchanger to the formation. Also, the insulated inner pipe makes possible a greater temperature difference between the working fluid and the surrounding formation, and prevents temperature drops in the inner pipe. These functions result in greater thermal output. Hence, the DCHE is thought to be the most efficient downhole heat exchanger.

Advantages of DCHE:

- Only one borehole.
- No risk to find an aquifer.
- Filled with clear water.
- Closed loop, therefore almost no maintenance, no abrasion, long living, reliable in operation.
- Environment friendly because there is no mass exchange.

1.2 Applications

These kinds of heat exchangers are used in many applications, being an excellent technology for the extraction of geothermal energy. The site of a project of this type at a given location depends on the geothermal resources and formation characteristics, at the same time, the application that you want to give that energy is an important feature.

It is clear that depending on the application desired the thermal requirements will be one or the other. Thus the required temperature output of the working fluid will not be the same for thermal generation for the production of electricity or other application like house space heating.

Below are a series of projects that use this type of heat exchangers for different areas. This will help us to get an idea of thermal requirements required for a specific type of application and what heat exchanger dimensions are most appropriate.

Transforming liquidated hydrocarbon wells to geothermal deep borehole heat exchanger for sports center heating [12]

In this project, a depleted hydrocarbon well has been redesigned to a deep borehole heat exchanger with two coaxial tubing, circulating a heat transport medium in the annulus without establishing a mass transport to the surrounding formation.
In populated regions, the redesign of depleted hydrocarbon wells to borehole heat exchanger is an attractive option to generate base-load heat.

Parameters:

- **Working fluid:** Air
- **Mass flow =** 2 kg/s
- **Injection temperature =** 303 K
- **Production temperature =** 316 K
- **Insulation type:** Nitrogen Gas
- **Insulation =** 0.17 W/m·K
- **C_p cement ≈** 2 kJ/kg·K
- **C_p rocks ≈** 2 kJ/kg·K
- **C_p heating medium =** 3.93 kJ/kg·K
- **Casing =** 7” = 17.78 cm
- **Outer pipe =** 4 ½” = 11.43 cm
- **Inner tubing =** 2 3/8” = 6.03 cm
- **DCHE length ≈** 2100 m
- **Thermal power =** 50 kW

- **Downhole temperature** = 333 K

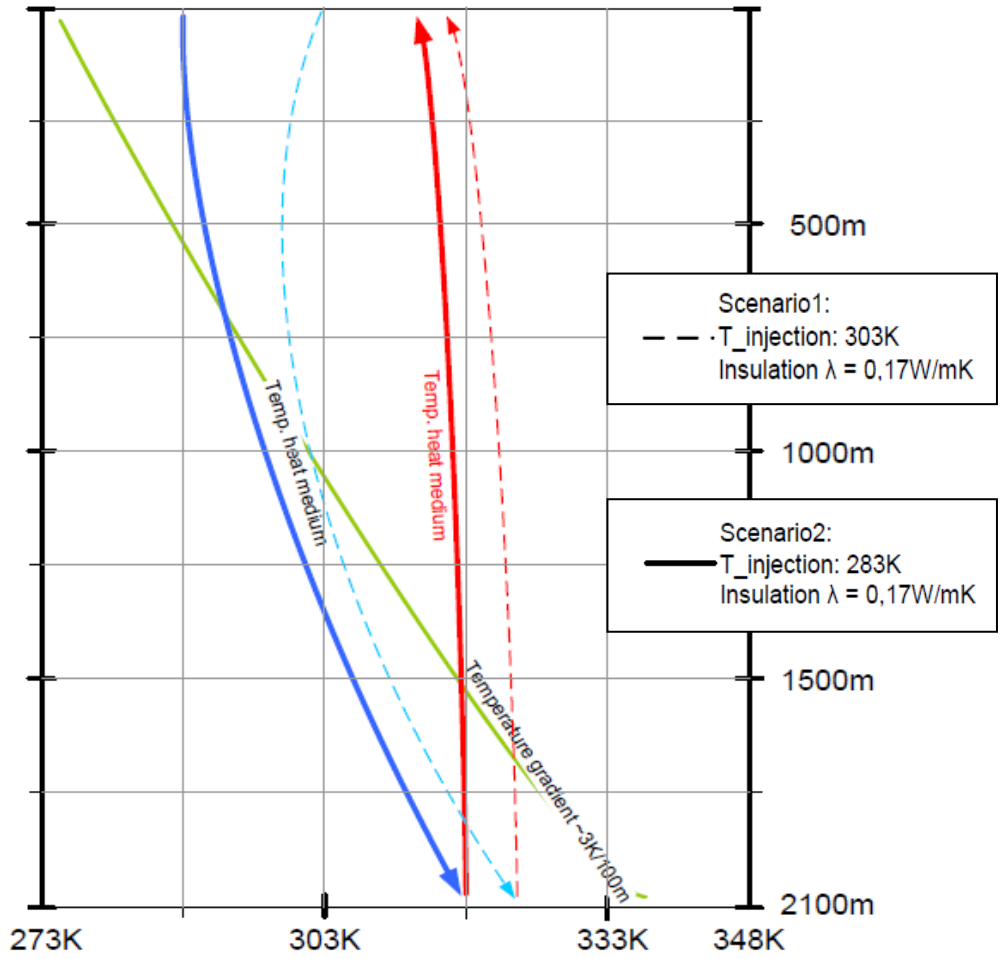

Fig. 1.3: Temperature profile of the working fluid for two different "scenarios" (Application: Transforming liquidated hydrocarbon wells to geothermal deep borehole heat exchanger for sports center heating) [12].

Fig. 1.3 shows the temperature profile along the borehole heat exchanger for two different scenarios according with the injection temperature. Conventional heating systems do not operate at these temperature levels. For this reason, a heat-pump energy cascade will be used to increase the overall power output.

The Gaia Snow-Melting System

The Gaia Snow-Melting system which utilizes the ground as a heat source and a heat storage body (Morita, 1997; Morita and Tago, 2000) consists of DCHEs, a heat pump and heating pipes embedded in the pavement (fig. 1.4).

The first Gaia system was installed in December 1995 by the government of Ninohe City (Japan) at the downhill section of a curved road with a 9 % gradient in order to

prevent accidents caused by skidding and sliding vehicles in winter. The area covered by the snow-melting system is 4 m wide and 65 m long, covering a total area of 266 m^2.

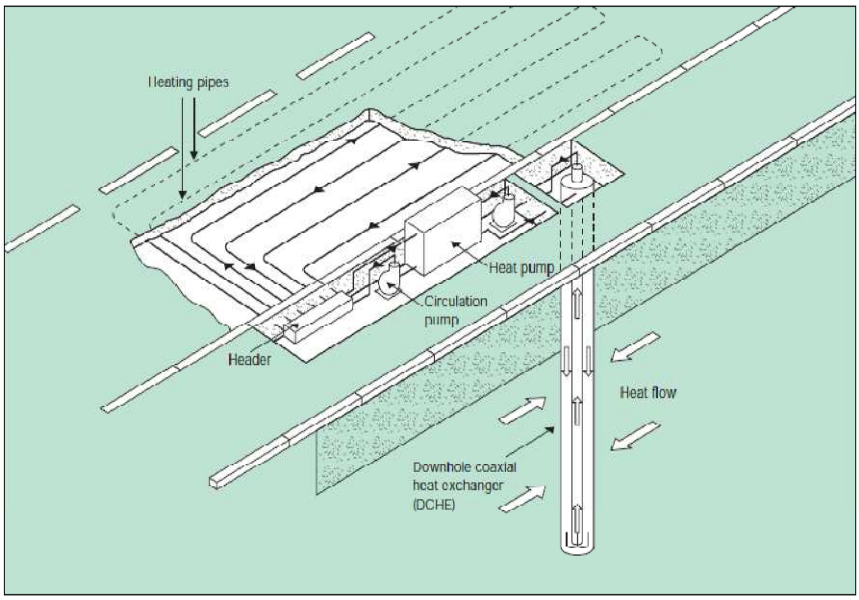

Fig. 1.4: Conceptual drawing of the Gaia Snow-Melting System [6].

In this system, solar heat absorbed in a pavement is recovered and stored in the ground over summertime. Hence, both geothermal heat and solar heat are used for melting snow in winter.

In winter, heat extracted from the ground with the DCHEs is transferred to the heat pump. After the heat pump increases the temperature, the thermal energy is transmitted to a heating medium circulating through a network of heating pipes for melting snow. Antifreeze is used as both a heat extraction medium and a heating medium.

In summer, solar heat raises the temperature of the pavement, in which the heating pipes are embedded, up to between 30 to 50 ºC. The solar heat is recovered from the pavement and charged into the ground by directly connecting the DCHEs and heating pipes, and by circulating antifreeze in this loop. Forward circulation is employed for efficient heat charging. Thus, geothermal heat and summertime solar heat are used for melting snow in winter. A newly developed control system operates the Gaia system automatically when road conditions meet specified criteria for melting snow or charging heat.

Fig. 1.5 shows the changes in the delivery temperatures of the heating medium from the heat pump to the heating pipes. Except in the case of short daily operation times, daily high temperatures of delivery temperatures roughly ranged from 28 to 36 ºC and daily average temperatures 25 to 30 ºC.

Fig. 1.6 shows the changes in the antifreeze temperature at the outlet of the observation DCHE and in the ambient temperature at the weather station. The Gaia snow-melting system normally works in an ambient temperature range between the average and the low temperatures. Hence, the ambient temperature ranges shown in fig. 1.6 are ranges between the average and low temperatures. It can be seen that the outlet temperatures of the DCHE are higher than the ambient temperatures by 1.4 to 20.4 ºC.

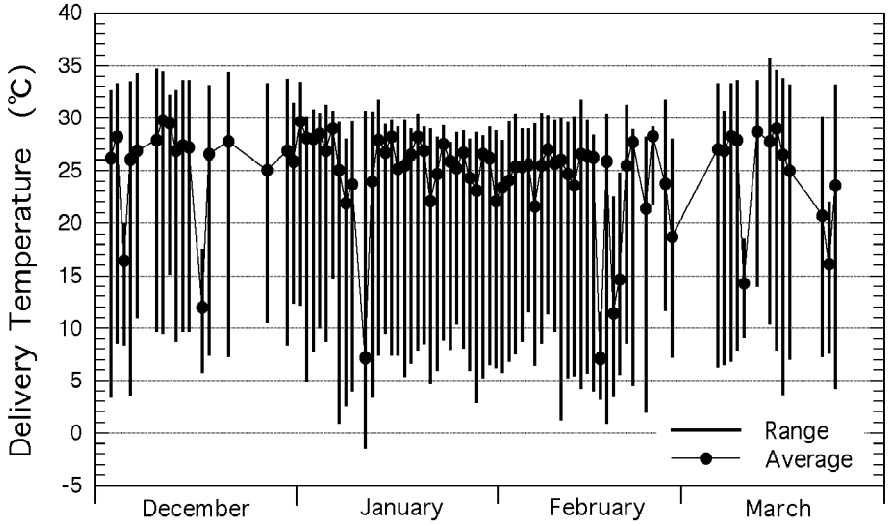

Fig. 1.5: Change in delivery temperature in the 1997 snow-melting season [11].

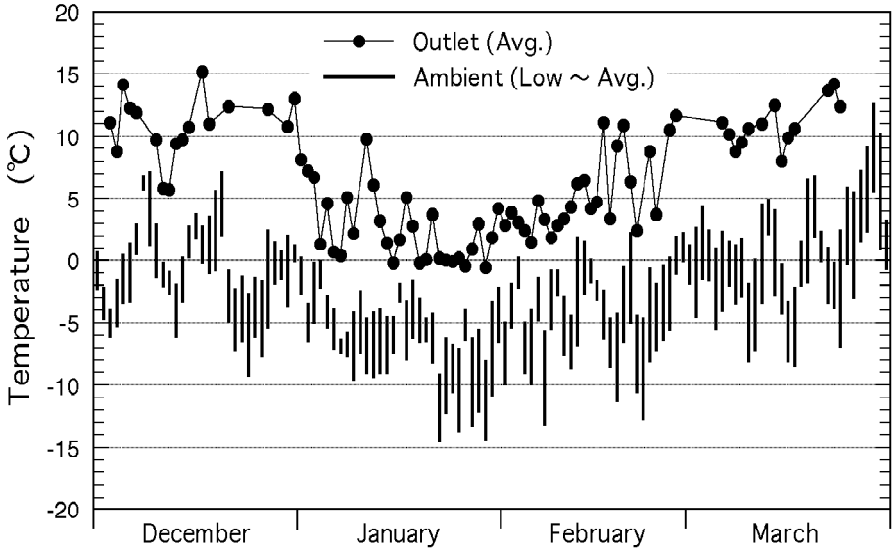

Fig. 1.6: Daily average outlet temperatures of DCHE and ambient temperatures in the 1997 snow-melting season [11].

The next table summarizes the major characteristic values of the system in snow-melting operations for four winters.

Snow Melting Season	1995	1996	1997	1998
Total Snowdepth Difference (cm)	234	149	223	323
Avg. Low Temp. for January (°C)	-7.1	-4.6	-8.3	-6.2
Operation Time of System (h)	460.0	417.7	491.9	597.2
Operation time of HP (h)	381.5	393.4	460.7	507.3
Avg. Inlet Temp. of DCHE (°C)	1.7	2.1	0.2	1.1
Avg. Outlet Temp. of DCHE (°C)	4.8	5.3	3.4	4.3
Avg. Delivery Temp. of HP (°C)	26.2	26.6	26.2	25.4
Avg. Return Temp. to HP (°C)	19.3	19.4	19.2	18.5
Extracted Heat ($kW_t h$)	12,330	14,740	16,600	18,870
Supplied Heat ($kW_t h$)	16,230	19,360	21,810	24,650
Avg. Outlet of HP (kW_t)	42.5	49.2	47.3	48.6
Heat Supply Rate per Unit Area (W_t/m^2)	160	185	178	183
Specific Heat Extraction Rate (W_t/m^m)	71.8	83.2	80.0	82.5
Electric Power Consumption ($kW_e h$)	5,164	5,939	6,641	7,363
Power Consumption of HP ($kW_e h$)	3,899	4,617	5,211	5,779
Avg. COP of HP (-)	4.16	4.19	4.19	4.27
Avg. COP of Total System (-)	3.42	3.59	3.57	3.60
Seasonal Performance Factor (-)	3.14	3.26	3.28	3.33

Note: Data for each winter are for a period from the first of December to the end of March except for the 1995 snow-melting season. Data for 1995 are for a period from December 27, 1995 to March 31, 1996.

Table 1.1: Characteristic values for snow-melting seasons [11].

Fig. 1.7 shows measured temperature profiles in the observation DCHE at the beginning of the snow-melting season. As can be seen in this figure, temperature profiles have changed year by year. However, average temperatures in the DCHE over a section from 10 m in depth to the bottomhole have remained almost the same. The average temperatures for 1995, 1996, 1997 and 1998 were 17.04, 16.95, 16.88 and 17.07 ºC, respectively. It is clear that the heat charging operation has been effective in preventing deterioration of the ground's function as a heat source.

The temperature profiles are becoming more vertical year by year. This is mainly due to self-circulation in the DCHE and vertical redistribution of heat in it and in the surrounding formation. Collected data from a flow meter in the snow melting seasons indicate that self-circulation occurs after the end of each operation of the system.

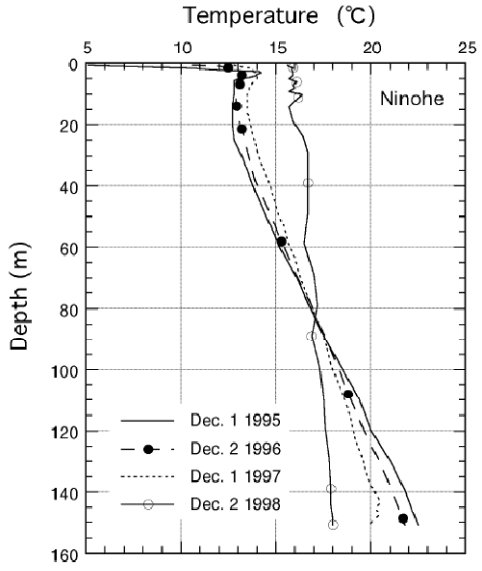

Fig. 1.7: Change in temperature profiles in the observation DCHE [11].

Parameters:

- **Formation type:** Tertiary sandy tuff.
- **Formation thermal conductivity =** 1.3 W/m·K
- **Number DCHE =** 3
- **Length DCHE =** 150.2 m
- **Outer diameter =** 8.9 cm
- **Power electric motor (Heat pump) =** 15 kW
- **Number of circulation pumps =** 2
- **Power circulation pump =** 0.75 kW
- **Heating pipes type (pavement):** Polybutene
- **Inner diameter heating pipes =** 16 mm
- **Depth top of the heating pipes =** 10 cm
- **Thermal capacity of the Gaia System =** 50 kW_t

Downhole, coaxial heat exchanger for electrical power generation[20]

The system sketch used for electrical power generation is shown in fig. 1.8. Hot water production is delivered to a turbine-generator system where electrical generation power takes place.

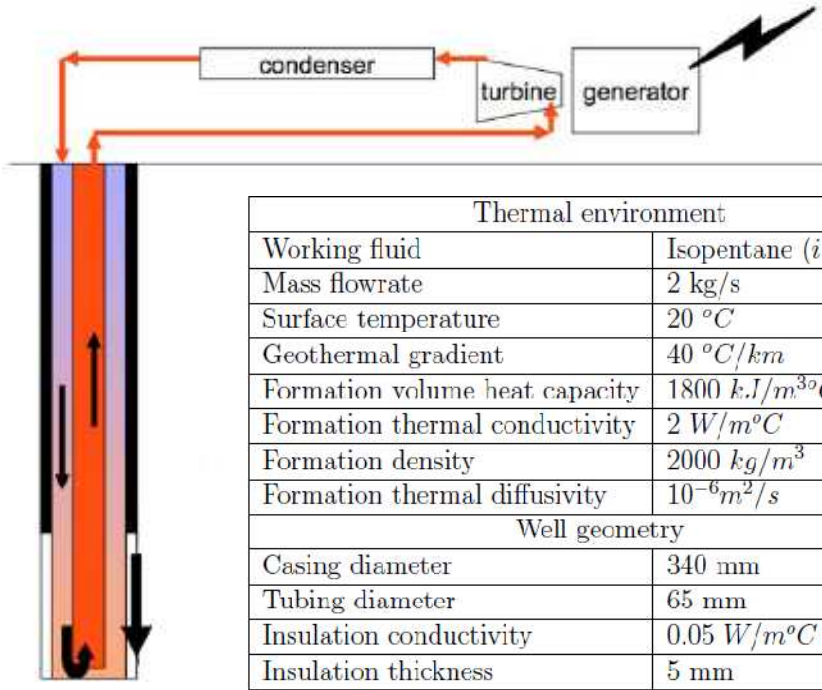

Fig. 1.8: Sketch of single-well, coaxial downhole heat Exchanger [20].

Thermal environment	
Working fluid	Isopentane $(i - C_5H_{12})$
Mass flowrate	2 kg/s
Surface temperature	20 ^oC
Geothermal gradient	40 $^oC/km$
Formation volume heat capacity	1800 $kJ/m^{3o}C$
Formation thermal conductivity	2 W/m^oC
Formation density	2000 kg/m^3
Formation thermal diffusivity	$10^{-6}m^2/s$
Well geometry	
Casing diameter	340 mm
Tubing diameter	65 mm
Insulation conductivity	0.05 W/m^oC
Insulation thickness	5 mm
Binary cycle specification	
Condenser temperature	320 K
Turbine isentropic efficiency	85% mm

Table 1.2: Common parameters [20].

In the above table is summarized the basic configuration. For electrical power generation, is assumed a constant condenser condition at 320 K, which corresponds to a saturated pressure of 1.866 bars, which is also the condition for the working fluid injected back into the wellbore. Another assumption for the turbine process is an isentropic turbine efficiency of 85%. Paying attention for the temperature profile (fig. 1.9), you can appreciate the difference between the cases with insulated inner pipe and without insulation. In fig. 1.10 can be determined the optimal insulation length from the point of view of the thermal production energy.

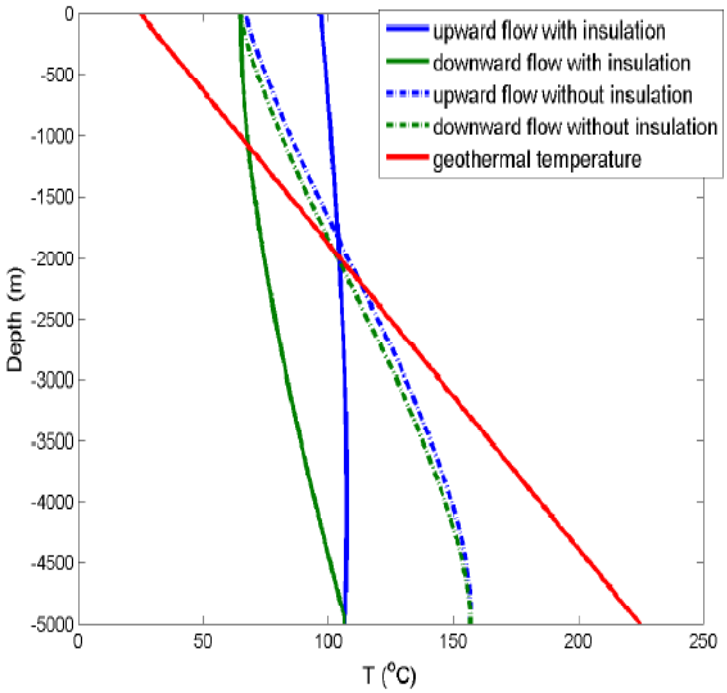

Fig. 1.9: Wellbore temperature profiles (Application: Electrical power generation) [20].

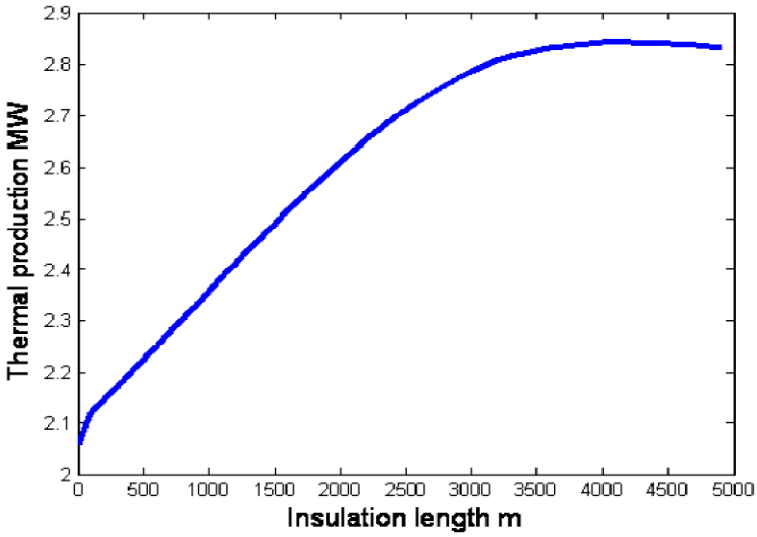

Fig. 1.10: Heat production for different insulation length (Application: Electrical power generation) [20].

Chapter 2

Description of heat transfer in DCHE

2.1 Mean temperature profile of the working fluid along the heat exchanger

Coaxial heat exchangers of Field type can present different heat transfer configurations depending of the working fluid circulation inside the heat exchanger and the external fluid circulation (fig. 2.1).
We can divide the working fluid circulation between reverse circulation (cold fluid is pumped into the annulus of the geothermal well) and forward circulation (cold fluid is pumped into the tubing of the geothermal well).
External flow is divided between parallel flow, counter flow or cross flow.

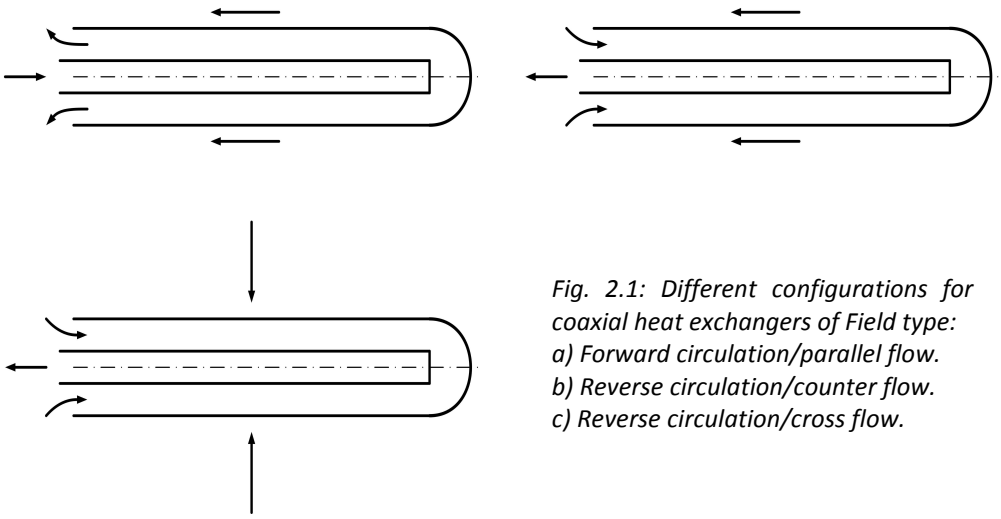

Fig. 2.1: Different configurations for coaxial heat exchangers of Field type:
a) Forward circulation/parallel flow.
b) Reverse circulation/counter flow.
c) Reverse circulation/cross flow.

Temperature profile of the working fluid along the heat exchanger and external fluid temperature profile for a particular heat exchanger Field configuration (forward circulation/parallel flow) are shown in fig. 2.2. Part of the heat flux transferred to the heat exchanger by the external fluid is transferred to the annular flow and the other part is transferred to the inner tubing flow.

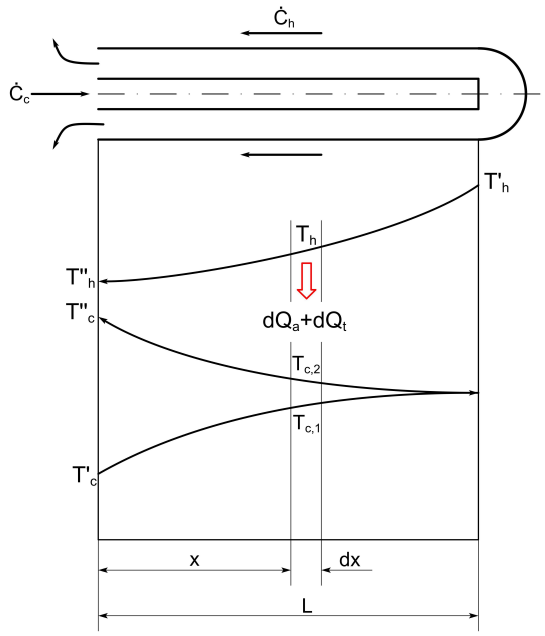

Fig. 2.2: Temperature profile of the fluids in the heat exchanger of Field type (Forward circulation/parallel flow).

The temperature of the working medium inside the inner tube is expressed by $T_{c,1}$ and inside the annulus is characterized by $T_{c,2}$. Both are part of the cold stream. In the other hand, hot stream is expressed by T_h which consists in the external fluid.
Fluid inlet temperature is characterized by T' while fluid outlet temperature is characterized by T''.

As is shown in fig. 2.2, heat flow transferred from the external fluid to the annulus flow is expressed by dQ_a while the heat flow transferred from the external fluid to the tubing flow is expressed by dQ_t.

In operation of the heat exchanger of Field type studied in this thesis there is two heat flows. The first heat flow takes place from the formation to the annular flow (dQ_1) and the second one from the inner pipe flow to the annular flow (dQ_2) (fig. 2.3).

As is mentioned above, in this kind of heat exchangers of Field type cold fluid is pumped into the annulus of the geothermal well (reverse circulation). On the way down to the bottom of the well it takes up heat from the ground.
Is assumed that the heat exchanger operate by conduction; there is no groundwater flow in the formation. In the other hand, hot production flow is obtained through the inner pipe. On the way to the surface of the well the hot flow loses heat to the annular flow. For this reason it is necessary insulate the inner pipe. The geometric model of the borehole heat exchanger studied in this project (see section 6.1) has two outer layers in contact with the formation; the outer pipe and the casing which is in contact with the soil. This can be observed in fig. 2.3 where the heat flow diagram inside the downhole coaxial heat exchanger of Field type is described.

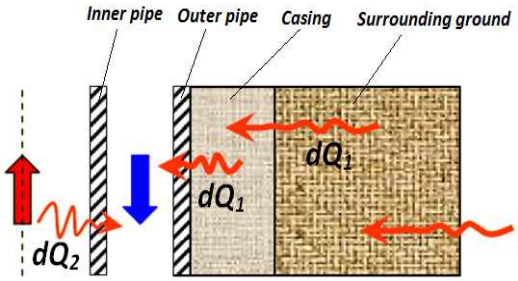

Fig. 2.3: Heat flow diagram for the DCHE of field type [19].

In this situation there is no external flow (hot stream) which transfers heat flow into the heat exchanger; now heat flow is provided by the surrounding rocks (without groundwater movement), assuming it as a heat source.

At a considerable distance from the heat exchanger can be assumed constant temperature profile of the ground, approaching it by a linear temperature profile. So, ground acts as a heat source of variable temperature.

The temperature profile description of the working fluid along the heat exchanger depends of the relation between ground surface temperature and the temperature of the working fluid in the heat exchanger inlet (fig. 2.4 and fig. 2.5). The heat exchanger loses heat from the annulus to the formation if the annular flow temperature is higher than the formation temperature. Otherwise the heat exchanger is taking heat from the formation.

Temperature profile along the heat exchanger for these two different configurations is shown in fig. 2.4 and fig. 2.5.

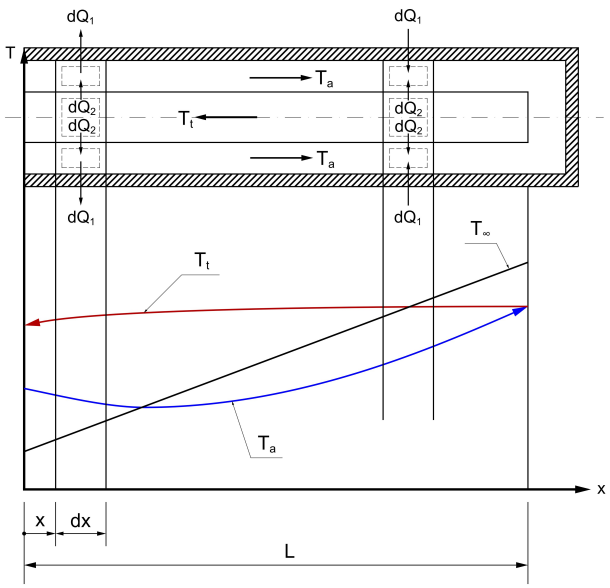

Fig. 2.4: Temperature profile of the working fluid along the heat exchanger (ground surface temperature lower than working fluid inlet temperature).

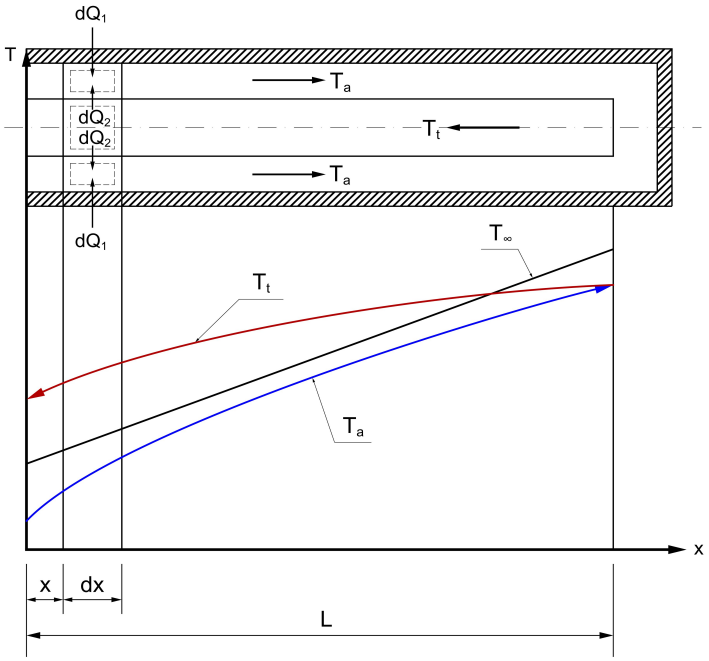

Fig. 2.5: Temperature profile of the working fluid along the heat exchanger (ground surface temperature higher than working fluid inlet temperature).

In above figures, the temperature of the working medium inside the annulus and tubing are denoted respectively by; T_a and T_t. Ground temperature is expressed by T_∞.

2.2 Effectiveness of the heat exchanger

The heat exchanger *effectiveness* (ε) is the ratio between the actual heat transfer rate between the two streams, $\dot{Q}$, and the thermodynamic maximum value of that heat transfer rate:

$$\varepsilon = \frac{actual\ heat\ transfer\ rate}{maximum\ heat\ transfer\ rate} = \frac{\dot{Q}}{\dot{Q}_{max}} \tag{2.1}$$

In a *counterflow* heat exchanger the effectiveness definition of above equation reduces to:

$$\varepsilon = \frac{\dot{C}_h(T_{h,in} - T_{h,out})}{\dot{C}_{min}(T_{h,in} - T_{c,in})} = \frac{\dot{C}_c(T_{c,out} - T_{c,in})}{\dot{C}_{min}(T_{h,in} - T_{c,in})} \tag{2.2}$$

Where the subscripts *in* and *out* indicate the inlet and outlet temperatures of the hot (*h*) and cold (*c*) streams respectively. C_h and C_c represent the capacity flow rates of the

two streams flowing along the sides of the heat exchanger surface, where C denotes $\dot{m}c_p$. C_{min} is the smaller of the two capacity rates.

Fig. 2.6 shows a hot-fluid stream being cooled by a cold-fluid stream in a counterflow heat exchanger. When the hot stream exits the exchanger, it must be warmer than the inlet temperature of the cold stream. In an ideal heat exchanger, with $\varepsilon = 1$, the outgoing hot stream's temperature equals the incoming cold stream's temperature. In addition, this heat exchanger's cold stream exits at a temperature lower than the inlet temperature of the hot stream.

In a *counterflow* heat exchanger the effectiveness can be also expressed as:

$$\varepsilon = \frac{1 - exp[-NTU(1 - \dot{C}_{min}/\dot{C}_{max})]}{1 - (\dot{C}_{min}/\dot{C}_{max})exp[-NTU(1 - \dot{C}_{min}/\dot{C}_{max})]} \tag{2.3}$$

And in a concurrent flow (parallel flow) configuration, effectiveness is expressed as:

$$\varepsilon = \frac{1 - exp\left[-NTU\left(1 + \frac{\dot{C}_{min}}{\dot{C}_{max}}\right)\right]}{1 + \frac{\dot{C}_{min}}{\dot{C}_{max}}} \tag{2.4}$$

Where:

$$NTU = ["The\ number\ of\ heat\ exchanger\ (or\ heat\ transfer)\ units"] = \\ = \frac{UA}{\dot{C}_{min}}$$

$$U = "Overall\ heat\ transfer\ coefficient"$$

$$A = "Heat\ transfer\ area"$$

$$\dot{C}_{min} = "Lower\ of\ the\ two\ fluids\ heat\ capacities"$$

$$\dot{C}_{max} = "Higher\ of\ the\ two\ fluids\ heat\ capacities"$$

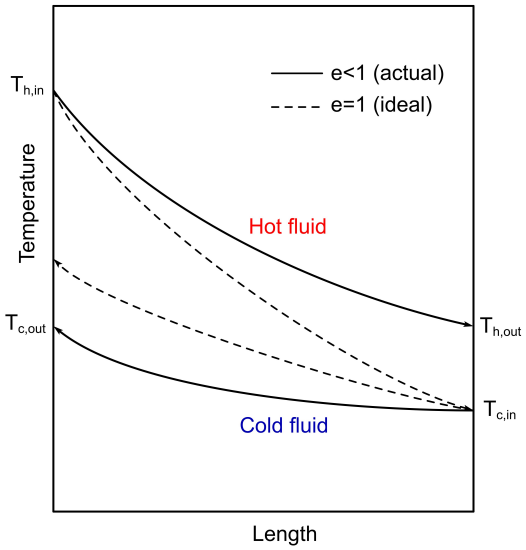

Fig. 2.6: Stream temperatures through a heat exchanger in counter-current flow.

Hence, the heat exchanger's outlet temperature can be calculated in a simplified way by calculating the effectiveness of the heat exchanger. For the Field type heat exchanger the outlet temperature can be obtained by the following expressions:

$$\dot{Q} = A_e k_e \Delta\overline{T} \tag{2.5}$$

where:

$\dot{Q}$=Heat rate transferred from the formation to the heat exchanger.
A_e=External surface area of the heat exchanger.
k_e=Heat transfer coefficient referred to the heat exchanger's external surface.
$\Delta\overline{T}$=Logarithmic mean temperature difference.

The logarithmic mean temperature difference takes the following form in this kind of heat exchangers (see fig. 2.2):

$$\Delta\overline{T} = \frac{2E(T_c'' - T_c')}{ln\left(\frac{D+E}{D-E}\right)} \tag{2.6}$$

Where:

$$D = \frac{1}{2}(1+R) + R\frac{T_h'' - T_c''}{T_h' - T_h''} \tag{2.7}$$

$$R = \frac{\dot{C}_c}{\dot{C}_h} \tag{2.8}$$

For parallel flow:

$$E = \frac{1}{2}\sqrt{(1+R)^2 + \frac{4k_i A_i}{k_e A_e}} \tag{2.9}$$

For the countercurrent flow:

$$E = \frac{1}{2}\sqrt{(R-1)^2 + \frac{4k_i A_i}{k_e A_e}} \tag{2.10}$$

where, A_i and k_i are the area and heat transfer coefficient referred to the internal surface of the heat exchanger.

In the heat exchanger of Field type:

$$\dot{C}_h \gg \dot{C}_c \Longrightarrow \boxed{R = 0}$$

Hence,

$$E = \frac{1}{2}\sqrt{1 + \frac{4k_i A_i}{k_e A_e}}$$

$$D = \frac{1}{2}$$

Chapter 3

Correlations for the convective heat transfer and friction coefficients

The convective heat transfer coefficient is determined by previously calculation of the *Nusselt number*. In heat transfer at a boundary (surface) within a fluid, the *Nusselt number* is the ratio of convective to conductive heat transfer across the boundary, it is a dimensionless number. The conductive component is measured under the same conditions as the heat convection but with a stagnant fluid.

$$Nu_L = \frac{hL}{\lambda_f} = \frac{Convective\ heat\ transfer\ coefficient}{Conductive\ heat\ transfer\ coefficient} \tag{3.1}$$

Where,

$L = characteristic\ length.$
$\lambda_f = thermal\ conductivity\ of\ the\ fluid.$
$h = convective\ heat\ transfer\ coefficient.$

In coaxial heat exchanger of Field type are two different regions to be considered; annulus and tubing.
The characteristic length for the tube flow is the inner pipe diameter (D_i) while for the annular flow is the *hydraulic diameter* (a measure of the duct cross section) defined as:

$$D_h = \frac{4A}{p} \tag{3.2}$$

Where,

$A = cross\ section\ area.$
$p = internal\ wetted\ perimeter.$

For an annular geometry the *hydraulic diameter* is expressed as:

$$D_h = \frac{4(\pi/4)\left(D_o^2 - D_i^2\right)}{\pi(D_o + D_i)} = \frac{D_o^2 - D_i^2}{D_o + D_i} = \frac{(D_o - D_i)(D_o + D_i)}{(D_o + D_i)} = (D_o - D_i) \tag{3.3}$$

Heat transfer in these heat exchangers is governed by forced convection mechanisms. For forced convection, the *Nusselt number* is generally a function of the *dimensionless Reynolds number (Re)* and the *dimensionless Prandtl (Pr) number*, or $Nu = f(Re, Pr)$. Empirical correlations for a wide variety of geometries are available that express the *Nusselt number* in the aforementioned forms. Depending on laminar or turbulent flow regimes different formulations of the *Nusselt number* are applicable. For forced convection in fully developed turbulent pipe flow, the *Nusselt number* can be calculated from the *Gnielinski* correlation, taking as the characteristic length the hydraulic diameter [7]:

$$Nu_{D_h} = \frac{(f/2)\left(Re_{D_h} - 1000\right)Pr}{1 + 12{,}7(f/2)^{1/2}(Pr^{2/3} - 1)} \tag{3.4}$$

Where, f is the friction coefficient that can be obtained from the Moody chart or for smooth tubes from correlation developed by *Filonenko*:

$$f(filonenko) = \frac{1}{\left(1{,}58 ln Re_{D_h} - 3{,}28\right)^2} \tag{3.5}$$

The *Gnielinski* correlation is valid for:

$$\begin{cases} 0{,}5 < Pr < 2000 \\ 3000 < Re_{D_h} < 5 \times 10^6 \end{cases}$$

Thermal properties of the fluid are evaluated at the average of the bulk fluid temperature. With this correlation is obtained the average *Nusselt number*. In order to account for the inlet flow effect, equation (3.4) is changed by *Hausen correction*:

$$Nu_{D_h} = \frac{(f/2)\left(Re_{D_h} - 1000\right)Pr\left[1 + \left(\frac{D_h}{L}\right)^{2/3}\right]}{1 + 12{,}7(f/2)^{1/2}(Pr^{2/3} - 1)} \tag{3.6}$$

Gnielinski correlation is also changed for the variation of fluid properties with the temperature (table. 3.1).

$$Nu_{D_h} = \frac{(f/2)\left(Re_{D_h} - 1000\right)Pr\left[1 + \left(\frac{D_h}{L}\right)^{2/3}\right]\phi^n}{1 + 12{,}7(f/2)^{1/2}(Pr^{2/3} - 1)} \tag{3.7}$$

Fluid	$\boldsymbol{\phi}$	**Process**	**p**	**n**
Gas	(T_m/T_0)	heating	0,52	0,47
		cooling	0,38	0,36
Liquid	(μ_m/μ_0)	heating	-0,33	0,11
		cooling	-0,24	0,25

Table 3.1: Correction factor for variation of fluid properties with temperature.

Where T_m and μ_m are the temperature and viscosity at the average of the bulk fluid temperature, respectively. T_0 and μ_0 are the temperature and viscosity at the wall surface temperature, respectively.

Another correlation used in these kinds of heat exchangers is the *Dittus-Boelter* equation (see equation (3.8)). The *Dittus-Boelter* equation (for turbulent flow) is an explicit function for calculating the *Nusselt number*. It is easy to solve but is less accurate when there is a large temperature difference across the fluid. It is tailored to smooth tubes, so use for rough tubes (most commercial applications) is cautioned.

$$Nu_{D_h} = 0{,}023 Re_{D_h}^{4/5} Pr^n \tag{3.8}$$

Where:

$D_h = Hydraulic\ diameter.$
$Re = Reynold\ number.$
$Pr = Prandtl\ number.$
$n = \begin{cases} 0.4\ (for\ heating\ of\ the\ fluid) \\ 0.3\ (for\ cooling\ of\ the\ fluid) \end{cases}$

The *Dittus-Boelter* equation is valid for:

$$\begin{cases} 0{,}7 < Pr < 160 \\ Re_{D_h} \gtrsim 10000 \\ \dfrac{L}{D_h} \gtrsim 10 \end{cases}$$

Similarly friction coefficient is given by the next correlation:

$$f = 0{,}046 Re_{D_h}^{-0{,}2} \qquad \left(2 \times 10^4 < Re_{D_h} < 10^6\right) \tag{3.9}$$

For the laminar flow ($Re \leq 2300$), the *Nusselt number* can be calculated from the *Prandtl number* (Pr), the *Reynolds number* (Re), the dynamic viscosity of the fluid (μ) and the dynamic viscosity at the wall temperature (μ_0), formulated as the Sieder-Tate equation:

$$Nu_{D_h} = 1.86 \left(\frac{Re_{D_h} Pr}{(L/D_h)}\right)^{1/3} \left(\frac{\mu}{\mu_0}\right)^{0.14} \tag{3.10}$$

The friction factor for laminar flow is expressed as:

$$f = \frac{64}{Re_{D_h}} \tag{3.11}$$

Chapter 4

Fundamentals of thermodynamic analysis of heat exchangers based on the 2nd Law of Thermodynamics

The purpose of a thermodynamic design is to achieve a working system. A goal of the design is high efficiency; minimization of entropy production is a way to achieve this. For the determination of the downhole coaxial heat exchanger optimum sizes, the total generated entropy should be minimized in the heat exchanger because, for a given heating load, there is a direct relationship between entropy generated and the required power input.

The use of the Second Law of Thermodynamics offers a more appropriate approach carrying out the thermodynamic analysis with the minimization of the irreversibility. The entropy generation minimization was first applied in heat exchangers by Bejan (1977), Ciampi and Tuoni (1979) and also by El Sayed (1996).

For the opened system the differential balance of entropy results like:

$$dS = \delta S_{gen} + \left(\frac{\delta Q}{T}\right)_b + dm_1 s_1 - dm_2 s_2 \tag{4.1}$$

and after integration between two states:

$$S_2 - S_1 = S_{gen\,1,2} + \int_1^2 \left(\frac{\delta Q}{T}\right)_b + \int_1^2 dm_1 s_1 - \int_1^2 dm_2 s_2 \tag{4.2}$$

Where dm_1, dm_2 are the elementary masses flowing *in* and *out*; and s_1, s_2 are the specific entropies of their masses.

The left side of equation (4.2) represent the total entropy change between the two states. The first term on the right side represent the entropy generated, this term is positive when internal irreversibilities are present during the process and vanishes when internal irreversibilities are absent. This can be described by saying that entropy

is generated (or produced) within the system by action of irreversibilities. The second term on the right side is associated with heat transfer to or from the system during the process. This term can be interpreted as the entropy transfer associated with (or accompanying) heat transfer. And the others terms on the right side corresponds to the entropy associated to the inlet and outlet mass flows.

In heat exchangers the destruction of exergy, or equivalently entropy generation, is due to two mechanisms: the heat transfer across a finite temperature difference and the flow with friction through ducts. We shall refer to these mechanisms as the heat transfer irreversibility and the fluid flow irreversibility, respectively. We have to considerer their simultaneous effect on entropy generation. Heat transfer and fluid friction irreversibilities tend *to compete* with one another, and that the total rate of entropy generation can be minimized by adjusting the size of one irreversibility against the other. These adjustments can be made by properly selecting the physical dimensions of the solid parts.

In this project, the temperature and pressure distribution along the heat exchanger is analytically determined, and then with regard to the Second Law of Thermodynamics, an equation is presented for the calculation of the generated entropy in the heat exchanger. By using this equation, the optimum Reynolds number and therefore the optimum inner's pipe diameter of the heat exchanger is determined.

In the steady state and conservation of the mass case, equation (4.1) becomes:

$$\delta S_{gen} = dm(s_2 - s_1) - \left(\frac{\delta Q}{T}\right)_b \tag{4.3}$$

Focusing on a slice of thickness dx as a system (fig. 4.1) and if the exit from the system is close to the inlet the specific entropies s_2 and s_1 have the following form:

$$\begin{cases} s_1 = s(x) \\ s_2 = s(x + dx) \cong s(x) + \dfrac{ds}{dx}dx + \cdots \end{cases}$$

Hence if:

$$\delta S_{gen} = \delta S'_{gen} dx \quad and \quad \delta Q = qpdxdt = q'dxdt$$

Where,

- S'_{gen}, is the entropy generation per unit length.
- q, is the heat flux rate transferred to the stream through the surface of the channel $[W/m^2]$.
- p, is the channel perimeter.
- q', is the heat rate flowing per unit length $[W/m]$.

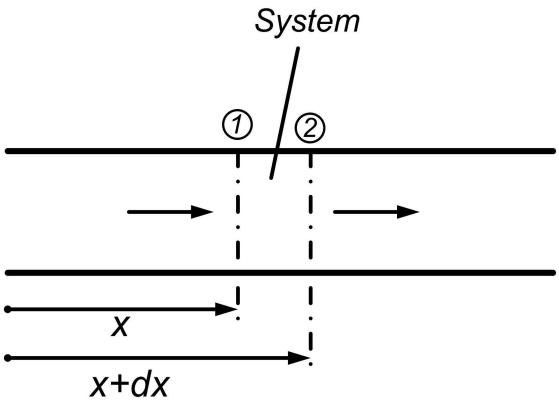

Fig. 4.1: Schematic of the entropy balance system.

The temperature in the border or in the surface of the channel (T_b) is expressed as a sum between the bulk temperature of the stream (T) and a finite temperature difference (ΔT).

$$T_b = T + \Delta T$$

After substitution into equation (4.3) and dividing by elementary time dt:

$$\dot{S}'_{gen} = \dot{m}\frac{ds}{dx} - \frac{q'}{T + \Delta T} \tag{4.4}$$

Where,

- $\dot{S}'_{gen}$, is the rate of entropy generation per unit duct length.
- $\dot{m}$, is the mass flow rate.

In order to illustrate the dependence of $\dot{S}'_{gen}$ on the Stanton number and friction factor information, consider the case where the heat transfer rate per unit length q' and the mass flow rate $\dot{m}$ are specified; combining definition with formula yields and rewriting above equation using the friction factor f, Stanton number $\left(St = \bar{h}/\rho c_p\, U\right)$, mass velocity $(G = \dot{m}/A)$, Reynolds number $(Re = GD_h/\mu)$, and hydraulic diameter $(D_h = 4A/p_w)$:

$$\dot{S}'_{gen} = \underbrace{\frac{(q')^2 D_h}{4T^2 \dot{m} c_p S_t}}_{\dot{S}'_{gen,\Delta T}} + \underbrace{\frac{2\dot{m}^3 f}{\rho^2 T D_h A^2}}_{\dot{S}'_{gen,\Delta p}} \tag{4.5}$$

Under the present assumptions, above equation has two degrees of freedom, the wetted perimeter p_w and the cross-sectional area A or any other couple of independent parameters such as (Re, D_h) or (G, D_h).

Chapter 5

Objective of the thesis

- Optimization of the diameter of the inner pipe
- Optimization of the thermal resistance of the inner pipe

The objective of the thesis is the thermodynamic optimization of a downhole coaxial heat exchanger, minimization of entropy production is a way to achieve this.

First of all selection of a particular downhole, coaxial heat exchanger for our field of application is performed and setting some geometrical parameters we determine the dimensions of this.
These geometrical parameters are dimension of the external pipe and heat exchanger length.

Minimizing entropy production across the heat exchanger will find the optimum inner pipe diameter and the optimum annular hydraulic diameter. In this configuration, heat exchanger irreversibilities are minimized and heat transfer occurs optimally.

On the other hand, as we known, the inner pipe should be insulated for minimize heat loss from inner pipe to the annulus. Thermal resistance of the inner pipe is the other variable that defines the heat exchanger features; in this case, this variable is not related in geometrical characteristics if not in heat transfer aspects. Just as inner pipe dimension, thermal resistance of the inner pipe should be optimized to minimize entropy generation.

Chapter 6

Selection of the particular downhole coaxial heat exchanger

6.1 Description of the DCHE geometric and property parameters

The ground temperature changes at the zones around the heat exchanger. The ground temperature changes decrease, as the distance from the heat exchanger increases. To determine the heat flux due to heat transfer from the ground, we can assume the heat flux is absorbed by the heat exchanger radially at steady state heat conduction.

We can divide the area around the heat exchanger into six coaxial cylinders whose radiuses definitions are (fig. 6.1, fig. 6.2 and fig. 6.3):

r_1: $inner\ radius\ of\ the\ insulated\ inner\ pipe.$
r_2: $outer\ radius\ of\ the\ insulated\ inner\ pipe.$
r_3: $inner\ radius\ of\ the\ outer\ pipe.$
r_4: $outer\ radius\ of\ the\ outer\ pipe.$
r_5: $casing\ radius.$
r_6: $position\ where\ the\ ground\ is\ not\ affected\ by\ the\ heat\ exchanger.$

Hence for the study of the downhole, coaxial heat exchanger six distinct parts where different heat transfer mechanisms take part, be considered:

- *Inner tubing flow.*
- *Inner insulated pipe.*
- *Annular flow.*
- *Outer pipe.*
- *Casing.*
- *Surrounding ground.*

At the same time DCHE property parameters are defined below:

R_{ip}: $insulated\ inner\ pipe\ thermal\ resistance.$
λ_{op}: $outer\ pipe\ thermal\ conductivity.$
λ_c: $casing\ thermal\ conductivity.$
λ_{rock}: $rocks\ thermal\ conductivity.$

Where, r_1 (inner radius of the inner pipe) and R_{ip} (insulated inner pipe thermal resistance) are the system variables that should be optimized.

In fig. 6.1 are described the DCHE geometric parameters.

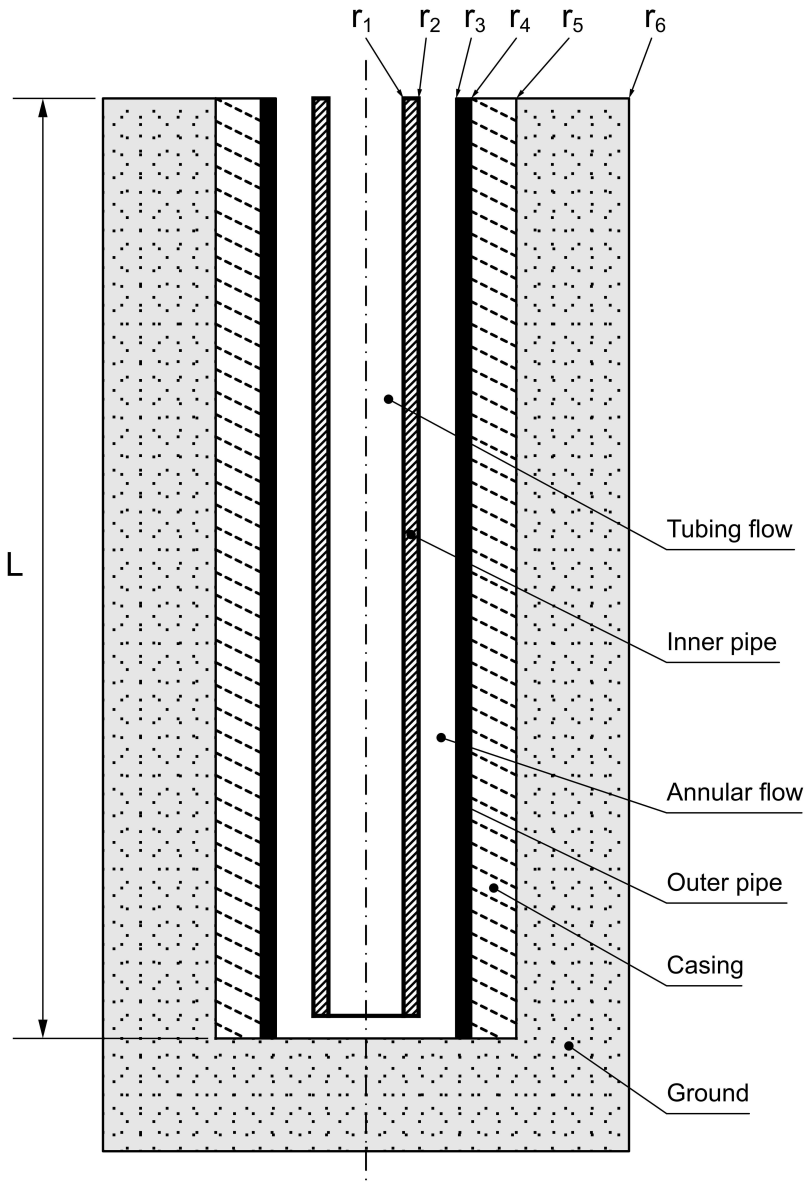

Fig. 6.1: DCHE geometric parameters description.

The downhole, coaxial heat exchanger geometric features are shown below.

Fig. 6.2: DCHE 3D view.

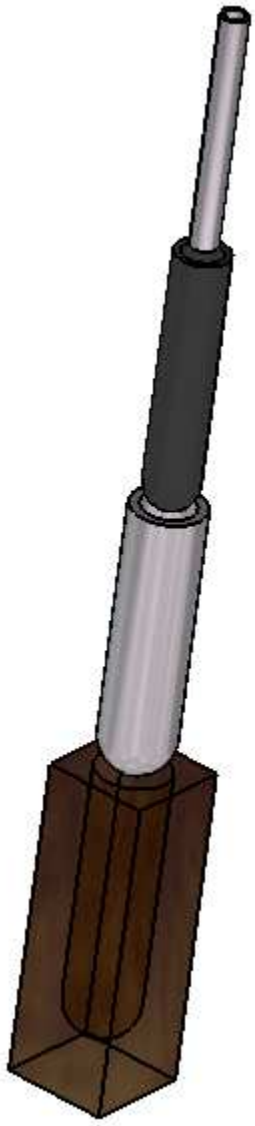

Fig. 6.3: Assembly of the DCHE.

6.2 Shallow geothermal energy

One of the most typical applications of a borehole heat exchanger is for shallow geothermal energy exploitation, for example, space heating/cooling in a Central European home (fig. 6.4).

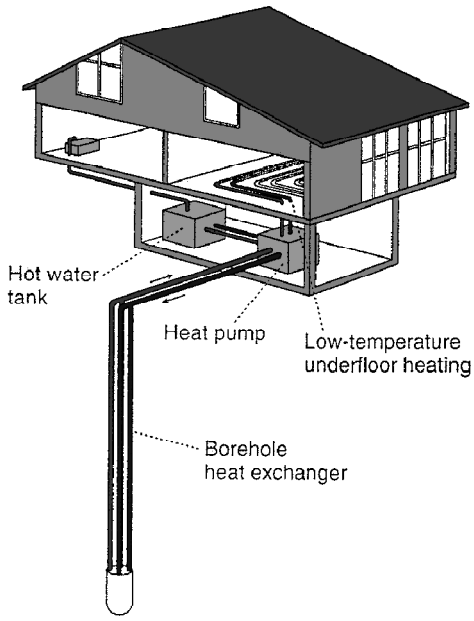

Fig. 6.4: Typical application of the Borehole Heat Exchanger (BHE) / heat pump (HP) system in a Central European home. Average BHE length: 100 m [18].

Shallow geothermal resources (The heat content of rocks in the top few 100-200 meters of the earth's crust) represent a major and ubiquitous energy source. There are several technical means to tap this vast resource by extracting heat from the ground, the most widespread technology of shallow heat extraction is by BHEs.

All systems need an electrical heat pump (HP) by which the low BHE output temperature (rarely above 10°C) can be lifted to the required level (35 – 50°C) and used in a heating system (fig. 6.5). For cooling in summertime, the system can be reversed, and heat from building cooling can be injected into the ground for a highly effective space cooling.

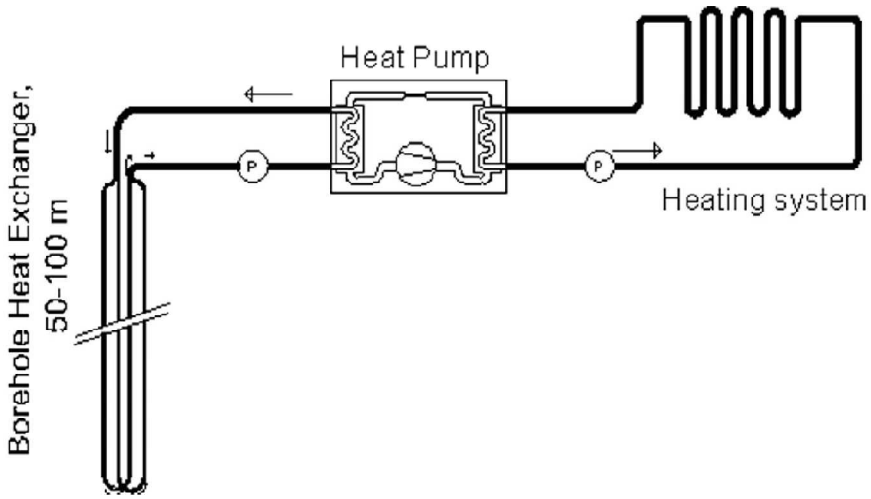

Fig. 6.5: Schematic of a ground-source heat pump [15].

BHEs can be installed in nearly all kinds of geologic media (except in material with low thermal conductivity like dry gravel). These systems operate by conduction, i.e. there are no formation fluids produced.

Downhole, coaxial heat exchanger design for this project will be applied for space heating/cooling and domestic hot water production in Central European home.

Diagram of the borehole heat exchanger (BHE)/heat pump (HP) system is shown in fig. 6.6.

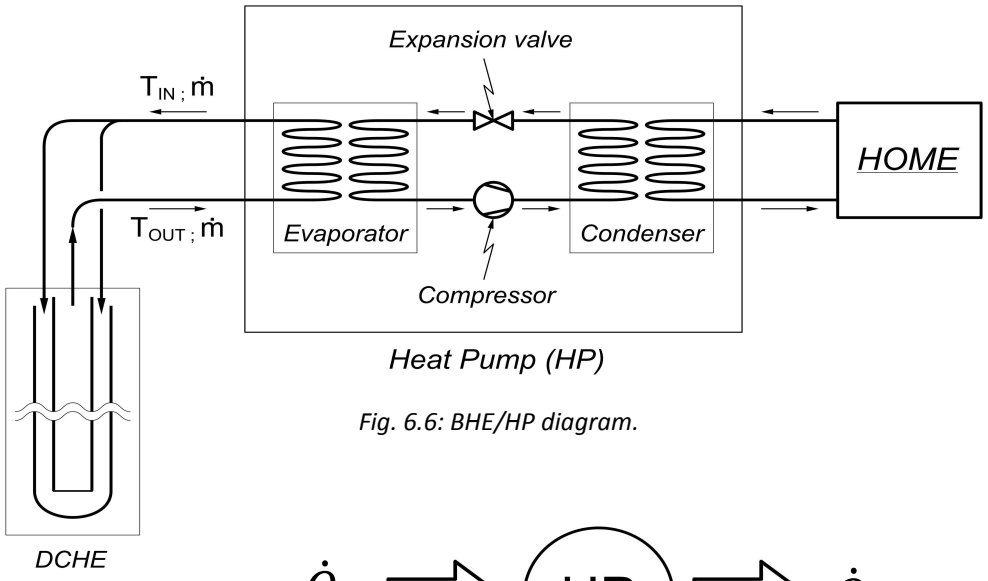

Fig. 6.6: BHE/HP diagram.

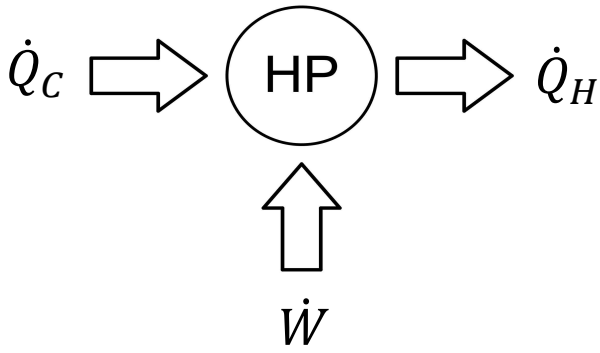

Fig. 6.7: BHE/HP energetic diagram.

One of the most heat pump features is the *coefficient of performance* or *COP*. The *coefficient of performance* of a heat pump is the ratio of the change in heat at the "output" (the heat reservoir of interest) to the supplied work. For heating the *coefficient of performance* is expressed as:

$$COP_{heating} = \frac{\dot{Q}_H}{\dot{W}} \tag{6.1}$$

Energy balance in the heat pump is written as following (fig. 6.7):

$$\dot{Q}_C + \dot{W} = \dot{Q}_H \tag{6.2}$$

Where,

- $\dot{Q}_H$, is the heat rate supplied to the hot reservoir.
- $\dot{W}$, is the work rate time consumed by the heat pump.
- $\dot{Q}_C$, is the heat rate supplied to the cold reservoir.

Hence, the *coefficient of performance* can be expressed as:

$$COP_{heating} = \frac{\dot{Q}_H}{\dot{Q}_H - \dot{Q}_C} \tag{6.3}$$

In the next table is summarized the energetic features of the borehole heat exchanger (BHE)/heat pump (HP) system.

BHE/HP system application	Heating + domestic hot water
Thermal power demand = $\dot{Q}_H$	20 kW_t
Heat pump *COP*	4
DCHE outlet temperature = T_{OUT}	*"calculated"*
DCHE inlet temperature = T_{IN}	*"calculated"*

Table 6.1: BHE/HP energetic features.

Below is described the method to calculate the downhole, coaxial heat exchanger inlet temperature (T_{IN}). This is an iterative process (see fig. 6.8):

1) Estimation of the DCHE inlet temperature (T_{IN})

   We have to take a DCHE inlet temperature initial value to start the iterative process.

2) Calculation of the DCHE outlet temperature (T_{OUT})

   DCHE outlet temperature is calculated for a given T_{IN} value using the heat transfer equations. This process will be described later (see section 9.1).

3) Calculation of the new DCHE inlet temperature ($T_{IN_{new}}$)

   The energy balance in the heat pump evaporator is written as:

$$\dot{Q}_C = \dot{m} \cdot c_p \cdot \Delta T_{BHE} = \dot{m} \cdot c_p \cdot (T_{OUT} - T_{IN}) \tag{6.4}$$

   Where,

   - $\dot{m}$, is the working medium mass flow rate.
   - c_p, is the working medium specific heat capacity.
   - ΔT_{BHE}, is the temperature variation along the heat exchanger.

   Hence, equation (6.3) is rewritten as:

$$\dot{Q}_C = \dot{Q}_H - \frac{\dot{Q}_H}{COP} \tag{6.5}$$

Combining equation (6.4) and equation (6.5) yields:

$$\dot{m} \cdot c_p \cdot (T_{OUT} - T_{IN}) = \dot{Q}_H - \frac{\dot{Q}_H}{COP} \Rightarrow T_{IN_{new}} = T_{OUT} - \left(\frac{\dot{Q}_H - \frac{\dot{Q}_H}{COP}}{\dot{m} \cdot c_p} \right) \tag{6.6}$$

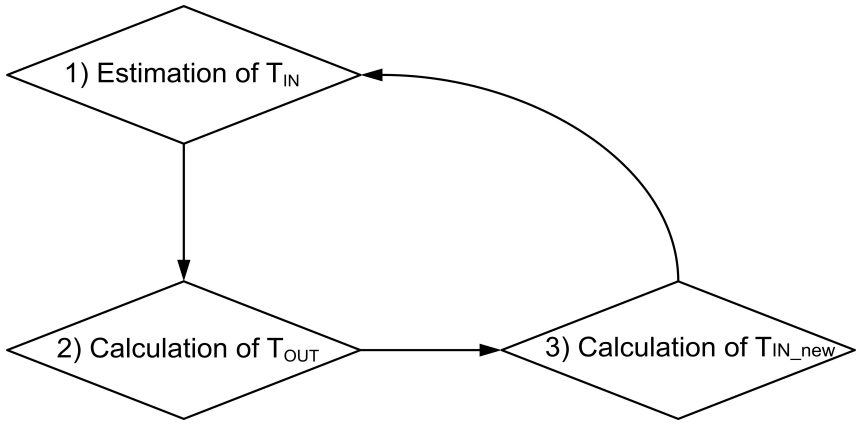

Fig. 6.8: Iterative process diagram to calculate the DCHE inlet temperature (T_{IN}).

6.3 DCHE dimensions and properties

In the next table is summarized the geometric and properties parameters of the DCHE. All the values are chosen to make the model realistic.

Parameter	Definition	Expression	Value (variable/fixed)
Geometric parameters			
r_1	Inner radius of the insulated inner pipe.	r_1	25 mm (variable)
e_{ip}	Insulated inner pipe thickness.	e_{ip}	5 mm (fixed)
r_2	Outer radius of the insulated inner pipe.	$r_1 + e_{ip}$	30 mm (variable)
r_3	Inner radius of the outer pipe.	r_3	50 mm (fixed)
e_{op}	Outer pipe thickness.	e_{op}	5 mm (fixed)
r_4	Outer radius of the outer pipe.	$r_3 + e_{op}$	55 mm (fixed)
e_c	Casing thickness.	e_c	10 mm (fixed)
r_5	Casing radius.	$r_4 + e_c$	65 mm (fixed)
e_{rock}	Distance from the BHE to the undisturbed ground temperature profile considered.	e_{rock}	100 mm (fixed)

r_6	Distance from the DCHE axis to the undisturbed ground temperature profile considered.	r_6	165 mm (fixed)
L	Heat exchanger length.	L	200 m (fixed)
Property parameters			
R_{ip}	Insulated inner pipe thermal resistance.	R_{ip}	0.008 m^2·K/W (Variable)
λ_{op}	Outer pipe thermal conductivity.	λ_{op}	15 W/m·K (fixed)
λ_c	Casing thermal conductivity.	λ_c	15 W/m·K (fixed)

Table 6.2: DCHE parameters.

As mentioned above, DCHE used for shallow geothermal energy exploitation have a length between 100-200 m [15]. In this project a DCHE length of 200 m is selected. The dimension of the outer pipe inner diameter is about 40-60 mm when the length of the heat exchanger is 100 m. In this case the heat exchanger length is doubled, for this reason the selected dimension of the outer pipe inner diameter of the model is 100 mm.

The temperature profile in the ground depends on the distance from the Borehole Heat exchanger to the point in the ground where is assumed that temperature profile (e_{rock}). This parameter is difficult to predict, for this reason is obtained through some ground tests. In this project is assumed that the temperature profile in the ground is given in 10 cm distance from the BHE. This value is a consequence of the review of some similar projects [16]. Then, is obvious, that must be considered a thermal conductivity resistance for the surrounding ground.

The other geometric parameters are selected according to the DCHE length and the inner diameter of the outer pipe.

As regards to the thermal conductivity of the outer pipe and casing, are chosen a typical values for pipes used in heat exchangers.

6.4 Working medium description

Downhole, coaxial heat exchanger will be designed for two different cases according with the working medium, in the first case using *water* as a working medium and in the second case using *air*.

Below are written the properties of the working medium fluids depending on the temperature.

Liquid water [5]:

$$\rho(density) = 741.966 + 1.9613 \cdot T - 0.00371211 \cdot T^2$$
$$c_p(specific\ heat\ capacity) = 2820 + 11.82 \cdot T - 0.03502 \cdot T^2 + \\ +3.599 \cdot 10^{-5} \cdot T^3$$
$$\lambda(thermal\ conductivity) = -0.3835 + 0.00525 \cdot T - 6.265 \cdot 10^{-6} \cdot T^2$$
$$\mu(dynamic\ viscosity) = 10^{\left(-13.73+\frac{1830}{T}+0.0197 \cdot T - 1.47 \cdot 10^{-5} \cdot T^2\right)}$$

Air [5]:

$$\rho(density) = 3.484 \cdot P/T$$
$$c_p(specific\ heat\ capacity) = 1004$$
$$\lambda(thermal\ conductivity) = (3.807 + 0.074 \cdot T) \cdot 10^{-3}$$
$$\mu(dynamic\ viscosity) = (2.469 + 0.0536 \cdot T + P/8280) \cdot 10^{-6}$$

(*International system of units:* $c_p\ [J/kg \cdot K]$, $P\ [kPa]$, $T\ [K]$)

The rest of the working medium parameters are described in the next table.

Parameter	Definition	Value
Liquid water		
$\dot{m}$	Mass flow rate.	0.8 kg/s
P_{IN}	DCHE's inlet pressure.	*"calculated"*
P_{OUT}	DCHE's outlet pressure.	1 atm=1.01325·10^5 Pa
Air		
$\dot{m}$	Mass flow rate.	2 kg/s
P_{IN}	DCHE' inlet pressure.	*"calculated"*
P_{OUT}	DCHE's outlet pressure.	1.5 atm=1.52·10^5 Pa

Table 6.3: Working medium parameters.

The DCHE's inlet pressure depends of the heat exchanger configuration according with the value of the inner radius of the inner pipe (r_1). The pressure drop along the heat exchanger varies extremely according with this variable. In section 9.2 is discussed this item in detail. Below is described the method to get the DCHE's inlet pressure (P_{IN}), an iterative process is again used (fig. 6.9).

1) Estimation of the DCHE's inlet pressure (P_{IN})

   We have to take a DCHE's inlet pressure initial value to start the iterative process.

2) Calculation of the pressure drop along the heat exchanger (ΔP)

   DCHE's pressure drop is calculated for a given P_{IN} value. This process will be described later (see section 9.2).

3) Calculation of the new DCHE's inlet pressure ($P_{IN_{new}}$)

$$P_{IN_{new}} = P_{OUT} + \Delta P$$

Where, P_{OUT} is a fixed value.

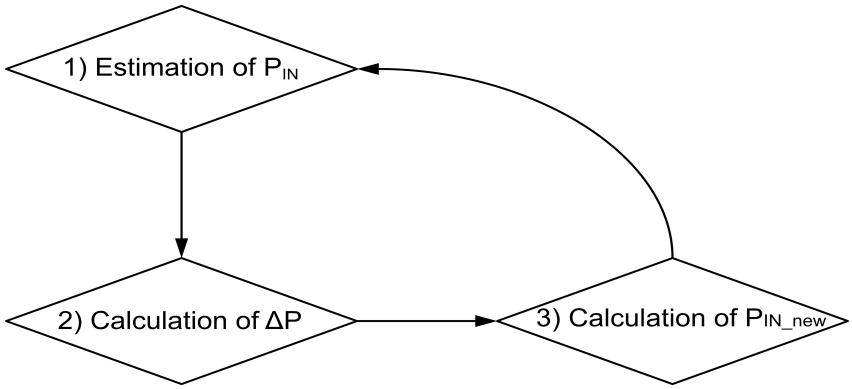

Fig. 6.9: Iterative process diagram for calculate the DCHE's inlet pressure (P_{IN}).

6.5 Surrounding ground properties and temperature

For the soil (formation) it's assumed that no underground water is present and the heat transfer mechanism is limited to heat conduction. Is assumed that the undisturbed natural rock temperature (T_∞), its distribution linear with depth (z):

$$T_\infty(z) = T_s + \gamma \cdot z \; [K] \tag{6.7}$$

Where, T_s is the annual mean temperature at the surface and γ is the geothermal gradient. Below are summarized the ground (formation) features [4].

Parameter	Definition	Type/Value
Formation type	Formation type	Unconsolidated rock, dry.
λ_{rock}	Formation thermal conductivity	3 W/m·K (fixed)
T_s	Annual mean surface temperature	6 ºC = 279.15 K (fixed)
γ	Geothermal gradient	4.5 ºC/100 m (fixed)

Table 6.4: Ground properties.

Chapter 7

Governing equations

The governing equations that describe the motion of fluid substances are the conservation equations for mass and momentum. For flows involving heat transfer, an additional equation for energy conservation is solved. Below, the conservation equations for a Newtonian fluid and laminar flow in an inertial (non-accelerating) reference frame are presented.

Mass Conservation-Continuity Equation [8]:

$$\frac{\partial \rho}{\partial t} + \nabla \cdot \left(\rho \vec{V}\right) = 0 \tag{7.1}$$

where,

- ρ is the fluid density.
- $\vec{V}$ is the velocity vector.

For 2D axisymmetric geometries, the continuity equation is given by,

$$\frac{\partial \rho}{\partial t} + \frac{\partial}{\partial z}(\rho V_z) + \frac{\partial}{\partial r}(\rho V_r) + \frac{\rho V_r}{r} = 0 \tag{7.2}$$

where, z is the axial coordinate, r is the radial coordinate, V_z is the axial velocity, and V_r is the radial velocity.

For steady state $\left(\frac{\partial}{\partial t}() \equiv 0\right)$ and assuming incompressible flow ($\rho = cte$) the continuity equation takes the next form:

$$\boxed{\nabla \cdot \vec{V} = 0 \Rightarrow \frac{\partial}{\partial z}(V_z) + \frac{\partial}{\partial r}(V_r) + \frac{V_r}{r} = 0} \tag{7.3}$$

Momentum Conservation (The Navier-Stokes equations) [8]:

$$\frac{\partial}{\partial t}\left(\rho \vec{V}\right) + \nabla \cdot \left(\rho \vec{V}\vec{V}\right) = -\nabla P + \nabla \cdot (\bar{\bar{\tau}}) + \rho \vec{g} + \vec{F} \tag{7.4}$$

where, p is the static pressure, $\bar{\bar{\tau}}$ is the stress tensor that represents the tangential surface forces (shear stresses) applied on a fluid particle and $\rho\vec{g}$ and $\vec{F}$ are the gravitational body force and external body forces, respectively. The stress tensor $\bar{\bar{\tau}}$ is given by:

$$\bar{\bar{\tau}} = \mu\left[\left(\nabla\vec{V} + \nabla\vec{V}^T\right) - \frac{2}{3}\nabla\cdot\vec{V}\bar{\bar{I}}\right] \tag{7.5}$$

where, μ is the molecular viscosity, $\bar{\bar{I}}$ is the unit tensor, and the second term on the right hand side is the effect of volume dilation.

For steady state and incompressible flow the *continuity equation* can be written as:

$$\nabla\cdot\vec{V} = 0 \Rightarrow \nabla\cdot\left(\rho\vec{V}\vec{V}\right) = -\nabla P + \rho\vec{g} + \mu\nabla^2\vec{V} \tag{7.6}$$

where, ∇^2 is the Laplacian operator.

For 2D axisymmetric geometries, the axial and radial momentum conservation equations are given by,

$$\rho\left[\frac{1}{r}\frac{\partial}{\partial z}(rV_zV_z) + \frac{1}{r}\frac{\partial}{\partial r}(rV_rV_z)\right] = \\ = -\frac{\partial P}{\partial z} + \frac{1}{r}\frac{\partial}{\partial z}\left[r\mu\left(2\frac{\partial V_z}{\partial z}\right)\right] + \frac{1}{r}\frac{\partial}{\partial r}\left[r\mu\left(\frac{\partial V_z}{\partial r} + \frac{\partial V_r}{\partial z}\right)\right] + F_z \tag{7.7}$$

and,

$$\rho\left[\frac{1}{r}\frac{\partial}{\partial z}(rV_zV_r) + \frac{1}{r}\frac{\partial}{\partial r}(rV_rV_r)\right] = \\ = -\frac{\partial P}{\partial r} + \frac{1}{r}\frac{\partial}{\partial z}\left[r\mu\left(\frac{\partial V_r}{\partial z} + \frac{\partial V_z}{\partial r}\right)\right] + \frac{1}{r}\frac{\partial}{\partial r}\left[r\mu\left(2\frac{\partial V_r}{\partial r}\right)\right] - 2\mu\frac{V_r}{r^2} \\ + F_r \tag{7.8}$$

<u>Energy conservation</u> [8]:

$$\rho\frac{D}{Dt}\left(u + \frac{1}{2}V^2\right) = -\nabla\cdot\vec{q} + \rho\vec{f}\cdot\vec{V} + \nabla\cdot\left(\vec{V}\bar{\bar{\sigma}}\right) \tag{7.9}$$

$$\frac{\partial}{\partial t}\left[\rho\left(u + \frac{1}{2}V^2\right)\right] + \nabla\cdot\left[\vec{V}\rho\left(u + \frac{1}{2}V^2\right)\right] = \\ = -\nabla\cdot\vec{q} + \rho\vec{f}\cdot\vec{V} - \nabla\cdot\left(P\vec{V}\right) + \nabla\cdot\left(\bar{\bar{\tau}}\cdot\vec{V}\right) \tag{7.10}$$

Internal flow energy is represented by u. The first term in the right-hand represent energy transfer due to conduction, this heat transfer mechanism is governed by Fourier's law:

$$\vec{q} = -k\nabla T \tag{7.11}$$

The next terms in the right-hand of the above equation represent energy transfer due to body forces, static pressure and viscous dissipation.

The unknown quantities of these equations are the velocity field $\vec{V}(\vec{x},t)$, pressure field $P(\vec{x},t)$ and the temperature field $T(\vec{x},t)$.

As mentioned above, these equations govern the motion of fluid for a laminar flow. In this thesis is considered turbulent flow of the working fluid, so mass, momentum and energy conservation equation must be changed for describe the turbulent regime.
The laminar regime is characterized by the orderly flow of fluid particles, existing streamlines and well defined pathlines. In the turbulent regime the particles have a chaotic movement without existing streamlines or pathlines defined.
Turbulent flows are characterized by fluctuating velocity fields (fig. 7.1). These fluctuations mix transported quantities such as momentum, energy, and cause the transported quantities to fluctuate as well. Since these fluctuations can be of small scale and high frequency, they are too computationally expensive to simulate directly in practical engineering calculations. Instead, the instantaneous (exact) governing equations can be time-averaged, ensemble-averaged, or otherwise manipulated to remove the small scales, resulting in a modified set of equations that are computationally less expensive to solve. However, the modified equations contain additional unknown variables, and turbulence models are needed to determine these variables in terms of known quantities. The analysis of turbulent duct flow and heat transfer is traditionally presented in terms of time-averaged quantities, which are denoted by a bar superscript. For example, the longitudinal velocity is decomposed as $u(\vec{x},t) = \bar{u}(\vec{x}) + u'(\vec{x},t)$, where $\bar{u}$ is the time-averaged velocity and u' is the fluctuation, or the time-dependent difference between u and $\bar{u}$.

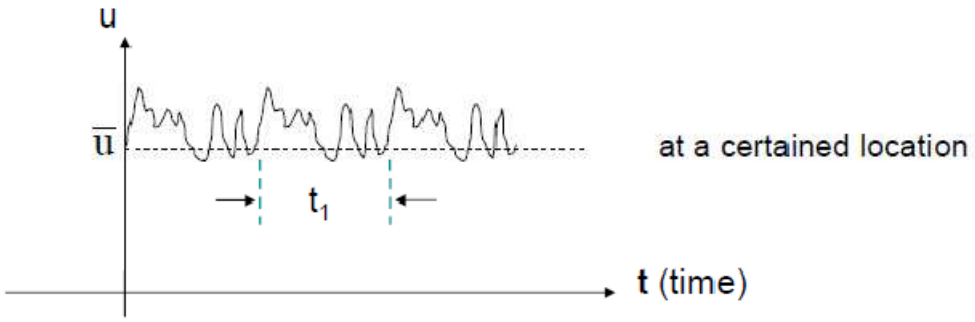

Fig. 7.1: Fluctuation of longitudinal velocity in turbulent flow region [13].

In general,

$$u_i = \bar{u}_i + u'_i \tag{7.12}$$

where, $\bar{u}_i$ and u'_i are the mean and fluctuating velocity components($i = 1,2,3$).

Likewise, for pressure and other scalar quantities:

$$\phi = \bar{\phi} + \phi' \tag{7.13}$$

where, ϕ denotes a scalar such as pressure, energy, or temperature.

$$P(\vec{x}, t) = \bar{P}(\vec{x}, t) + P'(\vec{x}, t) \tag{7.14}$$
$$T(\vec{x}, t) = \bar{T}(\vec{x}, t) + T'(\vec{x}, t) \tag{7.15}$$

Substituting expressions of this form for the flow variables into the instantaneous continuity and momentum equations and taking a time (or ensemble) average (and dropping the overbar on the mean velocity, $\bar{u}$) yields the ensemble-averaged momentum equations. They can be written in Cartesian tensor form as:

$$\frac{\partial \rho}{\partial t} + \frac{\partial}{\partial x_i}(\rho u_i) = 0 \tag{7.16}$$

$$\frac{\partial}{\partial t}(\rho u_i) + \frac{\partial}{\partial x_j}\left(\rho u_i u_j\right) = \\ = -\frac{\partial P}{\partial x_i} + \frac{\partial}{\partial x_j}\left[\mu\left(\frac{\partial u_i}{\partial x_j} + \frac{\partial u_j}{\partial x_i} - \frac{2}{3}\delta_{ij}\frac{\partial u_i}{\partial x_i}\right)\right] + \frac{\partial}{\partial x_j}\left(-\rho\overline{u'_\iota u'_j}\right) \tag{7.17}$$

Equations (7.16) and (7.17) are called Reynolds-averaged Navier-Stokes (RANS) equations. They have the same general form as the instantaneous Navier-Stokes equations, with the velocities and other solution variables now representing ensemble-averaged (or time-averaged) values.

Additional terms now appear that represent the effects of turbulence. These Reynolds stresses, $-\rho\overline{u'_\iota u'_j}$, must be modeled in order to close equation (7.17).

Assuming steady-state and incompressible flow:

$$\nabla \cdot \vec{V} = 0 \Rightarrow -\frac{2}{3}\delta_{ij}\frac{\partial u_i}{\partial x_i} = 0 \tag{7.18}$$

<u>$x - direction\ momentum\ equation\ (steady\ state\ and\ incompressible\ flow)$:</u>

$$\boxed{\vec{u}(\vec{x}, t) = u\vec{\imath} + v\vec{\jmath} + w\vec{k}} \tag{7.19}$$

$$\frac{\partial}{\partial x}(uu) + \frac{\partial}{\partial y}(uv) + \frac{\partial}{\partial z}(uw) = \\ = -\frac{1}{\rho}\frac{\partial P}{\partial x} + \nu\left(\frac{\partial^2 u}{\partial x^2} + \frac{\partial^2 u}{\partial y^2} + \frac{\partial^2 u}{\partial z^2}\right) - \frac{\partial}{\partial x}\overline{(u')^2} - \frac{\partial}{\partial y}\left(\overline{u'v'}\right) \\ - \frac{\partial}{\partial z}\left(\overline{u'w'}\right) \tag{7.20}$$

where, $\nu = \frac{\mu}{\rho}$ $(\nu = kinematic\ viscosity)$.

$$\frac{\partial}{\partial x}(uu)+\frac{\partial}{\partial y}(uv)+\frac{\partial}{\partial z}(uw)=$$
$$=-\frac{1}{\rho}\frac{\partial P}{\partial x}+\nu(\nabla^2 u)-\frac{\partial}{\partial x}\overline{(u')^2}-\frac{\partial}{\partial y}\left(\overline{u'v'}\right)-\frac{\partial}{\partial z}\left(\overline{u'w'}\right) \quad (7.21)$$

In tensor notation, i-direction time-averaged momentum equation is:

$$\frac{\partial}{\partial x_j}\left(u_i u_j\right)=-\frac{1}{\rho}\frac{\partial P}{\partial x_i}+\nu\left(\frac{\partial^2 u_i}{\partial x_j x_j}\right)+\frac{\partial}{\partial x_j}\left(-\overline{u'_i u'_j}\right) \quad (7.22)$$

The Reynolds-averaged approach to turbulence modeling requires that the Reynolds stresses in above equation be appropriately modeled. A common method employs the Boussinesq hypothesis to relate the Reynolds stresses to the mean velocity gradients:

$$-\overline{u'_i u'_j}=\frac{\mu_t}{\rho}\underbrace{\left(\frac{\partial u_i}{\partial x_j}+\frac{\partial u_j}{\partial x_i}\right)}_{(\nabla\vec{V}=2\bar{\bar{e}})}-\frac{2}{3\rho}\left(\rho k+\mu_t\frac{\partial u_k}{\partial x_k}\right)\delta_{ij} \quad (7.23)$$

where,

$\mu_t \equiv turbulent\ viscosity$

The second term of the right-hand equation is negligible:

$$\boxed{\Rightarrow -\overline{u'_i u'_j}=2\frac{\mu_t}{\rho}\bar{\bar{e}}} \quad (7.24)$$

where, $\bar{\bar{e}}=\frac{1}{2}\nabla\vec{V}$

The Boussinesq hypothesis is used in several models as: the Spalart-Allmaras model, the $k-\epsilon$ models, and the $k-\omega$ models. The purpose of all these models is to calculate the turbulent viscosity, μ_t. In this thesis is used *standard* $k-\epsilon$ *model* to model the turbulent flow. In this case two additional transport equations (for the turbulence kinetic energy, k, and the turbulence dissipation rate, ϵ) are solved, and μ_t is computed as a function of k and ϵ. The disadvantage of the Boussinesq hypothesis as presented is that it assumes μ_t is an isotropic scalar quantity, which is not strictly true. In many cases, models based on the Boussinesq hypothesis perform very well, and the additional computational expense of other models is not justified.

The standard $k-\epsilon$ model is a semi-empirical model based on model transport equations for the turbulence kinetic energy (k) and its dissipation rate (ϵ). The model transport equation for k is derived from the exact equation, while the model transport equation for ϵ was obtained using physical reasoning and bears little resemblance to its mathematically exact counterpart.

In the derivation of the $k-\epsilon$ model, the assumption is that the flow is fully turbulent, and the effects of molecular viscosity are negligible. The standard $k-\epsilon$ model is therefore valid only for fully turbulent flows.

Transport equations for the standard $k-\epsilon$ model [1]

The turbulence kinetic energy, k, and its rate of dissipation, ϵ , are obtained from the following transport equations:

$$\frac{\partial}{\partial t}(\rho k)+\frac{\partial}{\partial x_i}(\rho k u_i)=\frac{\partial}{\partial x_j}\left[\left(\mu+\frac{\mu_t}{\sigma_k}\right)\frac{\partial k}{\partial x_j}\right]+G_k+G_b-\rho\epsilon-Y_M \qquad (7.25)$$

and,

$$\frac{\partial}{\partial t}(\rho \epsilon)+\frac{\partial}{\partial x_i}(\rho \epsilon u_i)=\frac{\partial}{\partial x_j}\left[\left(\mu+\frac{\mu_t}{\sigma_\epsilon}\right)\frac{\partial \epsilon}{\partial x_j}\right]+C_{1\epsilon}\frac{\epsilon}{k}(G_k+C_{3\epsilon}G_b)-C_{2\epsilon}\rho\frac{\epsilon^2}{k} \qquad (7.26)$$

In these equations, G_k represents the generation of turbulence kinetic energy due to the mean velocity gradients. G_b is the generation of turbulence kinetic energy due to buoyancy. Y_M represents the contribution of the fluctuating dilatation in compressible turbulence to the overall dissipation rate. $C_{1\epsilon}$, $C_{2\epsilon}$, and $C_{3\epsilon}$ are constants. σ_k and σ_ϵ are the turbulent Prandtl numbers for k and ϵ , respectively.

The turbulent (or eddy) viscosity, μ_t , is computed by combining k and ϵ as follows:

$$\mu_t=\rho C_\mu\frac{k^2}{\epsilon} \qquad (7.27)$$

where, C_μ is a constant.

The model constants $C_{1\epsilon}, C_{2\epsilon}, C_\mu, \sigma_k$ and σ_ϵ have the following default values:

$$C_{1\epsilon}=1.44, \qquad C_{2\epsilon}=1.92, \qquad C_\mu=0.09, \qquad \sigma_k=1.0, \qquad \sigma_\epsilon=1.3$$

These default values have been determined from experiments with air and water for fundamental turbulent shear flows including homogeneous shear flows and decaying isotropic grid turbulence. They have been found to work fairly well for a wide range of wall-bounded and free shear flows.

The term G_k, representing the production of turbulence kinetic energy, is defined from the exact equation for the transport of k as:

$$G_k=-\rho\overline{u'_\iota u'_\jmath}\frac{\partial u_j}{\partial x_i} \qquad (7.28)$$

To evaluate G_k in a manner consistent with the Boussinesq hypothesis,

$$G_k=\mu_t S^2 \qquad (7.29)$$

where, S is the modulus of the mean rate-of-strain tensor, defined as:

$$S \equiv \sqrt{2S_{ij}S_{ij}} \tag{7.30}$$

The generation of turbulence due to buoyancy is given by:

$$G_b = \beta g_i \frac{\mu_t}{Pr_t}\frac{\partial T}{\partial x_i} \tag{7.31}$$

where, Pr_t is the turbulent Prandtl number for energy and g_i is the component of the gravitational vector in the ith direction. The default value of Pr_t is 0.85. The coefficient of thermal expansion, β, is defined as:

$$\beta = -\frac{1}{\rho}\left(\frac{\partial \rho}{\partial T}\right)_P \tag{7.32}$$

The degree to which ϵ is affected by the buoyancy is determined by the constant $C_{3\epsilon}$. This constant is calculated according to the following relation:

$$C_{3\epsilon} = tanh\left|\frac{v}{u}\right| \tag{7.33}$$

where, v is the component of the flow velocity parallel to the gravitational vector and u is the component of the flow velocity perpendicular to the gravitational vector. In this way, $C_{3\epsilon}$ will become 1 for buoyant shear layers for which the main flow direction is aligned with the direction of gravity. For buoyant shear layers that are perpendicular to the gravitational vector, $C_{3\epsilon}$ will become zero.

As is assumed incompressible flow, the term that represents the contribution of the fluctuating dilatation in compressible turbulence to the overall dissipation rate (Y_M) can be neglected in the turbulence kinetic energy generation.

Heat transfer in turbulent flow ($k-\epsilon$ Models) [1]

Turbulent heat transport is modelled using the concept of Reynolds' analogy to turbulent momentum transfer. The "modelled" energy equation is thus given by the following:

$$\frac{\partial}{\partial t}(\rho e) + \nabla \cdot \left(\vec{V}\rho e\right) = -\nabla \cdot \vec{q} + \rho \vec{f} \cdot \vec{V} - \nabla \cdot \left(P\vec{V}\right) + \nabla \cdot \left(\bar{\bar{\tau}}_{eff} \cdot \vec{V}\right) \tag{7.34}$$

where, (e) is the total energy per unit mass. The contributions to the specific energy e are the internal energy u, the kinetic energy $V^2/2$, and the potential energy gz.

$$e = u + \frac{1}{2}V^2 + gz \tag{7.35}$$

In this problem, the contribution of the kinetic and potential energy to the specific energy can be neglected assuming that most of the total energy is due to the internal energy ($e \approx u$).

As mentioned above, the conductive term of the energy conservation equation is modelled by *Fourier's law*. Neglecting body forces and assuming steady state:

$$\frac{\partial}{\partial x_i}(v_i \rho u) = \frac{\partial}{\partial x_j}\left(k_{eff}\frac{\partial T}{\partial x_j} + v_i\left(\tau_{ij}\right)_{eff}\right) \tag{7.36}$$

k_{eff} is the effective thermal conductivity, and $\left(\tau_{ij}\right)_{eff}$ is the deviatoric stress tensor, defined as:

$$\left(\tau_{ij}\right)_{eff} = \mu_{eff}\left(\frac{\partial v_j}{\partial x_i} + \frac{\partial v_i}{\partial x_j}\right) \tag{7.37}$$

The term involving $\left(\tau_{ij}\right)_{eff}$ represents the viscous heating. For this turbulent model (standard $k - \epsilon\ model$), the effective thermal conductivity is given by:

$$k_{eff} = k + \frac{c_p \mu_t}{Pr_t} \tag{7.38}$$

where, k, in this case, is the thermal conductivity. The default value of the turbulent Prandtl number is 0.85. $\left(\mu_{eff} = \mu_t\right)$.

Internal energy u is defined as: $u = c_p T$

$$\frac{\partial}{\partial x_i}\left(\rho c_p v_i T\right) = \frac{\partial}{\partial x_j}\left(k_{eff}\frac{\partial T}{\partial x_j} + \mu_{eff} v_i\left(\frac{\partial v_j}{\partial x_i} + \frac{\partial v_i}{\partial x_j}\right)\right) \tag{7.39}$$

Chapter 8

Full simplified mathematical model of the selected heat exchanger

The set of equations presented in the previous chapter describe the model accurately. These equations are solved using "commercial code" (e.g. *FLUENT 6.3*) to determinate the temperature and pressure distribution in the working medium. In this project the solution is determined by solving a simplified mathematical model. This model is described below.

The thermal process in the rock under the ground (without groundwater movement) is governed by heat conduction process. The same process takes place in the pipes and casing walls.

Thermal conduction is governed by *Fourier's law*. For steady state conditions, the Fourier's law can be written as [2] [7] [8]:

$$\boldsymbol{q}'' = -\lambda \nabla T \tag{8.1}$$

Where ∇ is the three-dimensional *del* operator and T is the scalar temperature field. $\boldsymbol{q}''$ (the heat transfer rate per unit area normal to the direction of heat flow) is proportional to the temperature gradient where the proportionality constant λ is a transport property known as the thermal conductivity and is a characteristic of the material. The minus sign is a consequence of the fact that heat is transferred in the direction of decreasing temperature.
We note that q'' is a vector quantity called heat flux vector.

Assuming radial symmetry and neglecting axial conduction, Fourier's law can be expressed in a one-dimensional form (radial dimension):

$$q''_r = -\lambda \frac{\partial T}{\partial r} \qquad ; \qquad q''_r \neq constant \tag{8.2}$$

$$q''_z = -\lambda \frac{\partial T}{\partial z} \cong 0$$

For a cylindrical coordinates, the conductive thermal power per meter borehole $q'_r[W/m]$ is written by multiplying equation (8.2) by de cylinder perimeter as expressed in equation (8.3).

$$q'_r = -2\pi r\lambda \frac{\partial T}{\partial r} \tag{8.3}$$

Integrating in both sides of the equation (8.3):

$$\int_{r_1}^{r_2} q'_r \frac{\partial r}{r} = \int_{T_1}^{T_2} -2\pi\lambda \partial T \quad ; \quad r_2 > r_1 \quad T_1 > T_2 \quad q'_r = constant$$

$$\Longrightarrow q'_r ln\frac{r_2}{r_1} = 2\pi\lambda(T_1 - T_2) \tag{8.4}$$

Hence, the conduction thermal resistance per unit length will be expressed in cylindrical coordinates as the following equation:

$$R'_{th}(conduction) = \frac{(T_1 - T_2)}{q'_r} = \frac{ln\frac{r_2}{r_1}}{2\pi\lambda}\left[\frac{m \cdot K}{W}\right] \tag{8.5}$$

Between internal surfaces pipes and inner flows the thermal process is governed by convection. For the convective heat transfer, the Newton's cooling law can be expressed for internal flow in a DCHE channel as [2] [7] [8]:

$$q''_r = h(T_s - T_m) \tag{8.6}$$

Where:

$q''_r = heat\ transfer\ rate\ per\ unit\ area.$
$h = local\ convection\ heat\ transfer\ coefficient.$
$T_s = internal\ pipe\ surface\ temperature.$
$T_m = mean\ reference\ fluid\ temperature\ at\ a\ given\ cross\ section.$

The convective thermal power per meter borehole $q'_r[W/m]$ is written as:

$$q'_r = 2\pi r h(T_s - T_m) \tag{8.7}$$

Hence, the convection thermal resistance per unit length will be expressed in cylindrical coordinates as the following equation:

$$R'_{th}(convection) = \frac{(T_s - T_m)}{q'_r} = \frac{1}{2\pi r h}\left[\frac{m \cdot K}{W}\right] \tag{8.8}$$

In the simplified model of a closed geothermal well, the casing is closed at the bottom without any perforations. The water flows downward through the annulus between

the coaxial casing and tubing. Since the adjacent rock is warmer than the circulating water, the water temperature increases in the direction of the flow.

An axisymmetric thermal inhomogeneity is developed around the well together with radial heat conduction toward the well. This is the heat supply of the system. The warmed up water flows upward through the tubing while its temperature slightly decreases, depending mainly on the thermal resistance of the tubing. The system is analogous to a countercurrent heat exchanger. The main difference is the increasing adjacent rock temperature distribution with the depth. Thus the familiar methods for design of heat exchangers are not sufficient for this case.

Below is shown the thermal resistances diagram for an elemental length of the tube in the vertical direction (dz):

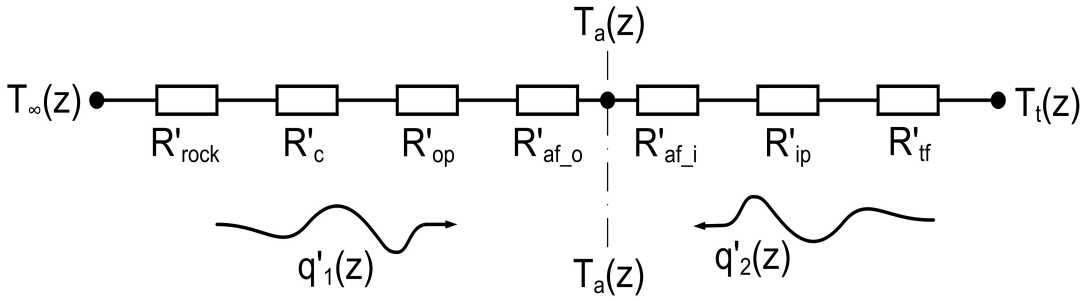

Fig. 8.1: Thermal resistances diagram.

Where,

$R'_{tf} = tubing\ fluid\ thermal\ resistance\ (convection).$
$R'_{ip} = inner\ pipe\ thermal\ resistance\ (conduction).$
$R'_{af_i} = annulus\ fluid\ thermal\ resistance\ inner\ pipe\ side\ (convection).$
$R'_{af_o} = annulus\ fluid\ thermal\ resistance\ outer\ pipe\ side\ (convection).$
$R'_{op} = outer\ pipe\ thermal\ resistance\ (conduction).$
$R'_{c} = casing\ thermal\ resistance\ (conduction).$
$R'_{rock} = rocks\ thermal\ resistance\ (conduction).$

$T_\infty(z) = undisturbed\ natural\ rock\ temperature.$
$T_a(z) = annulus\ temperature.$
$T_t(z) = tubing\ temperature.$

Below are written the thermal resistances expressions that are involved in our heat exchanger:

$$R'_{tf} = \frac{1}{2\pi r_1 h_{tf}} \qquad\qquad R'_{ip} = variable$$

$$R'_{af_i} = \frac{1}{2\pi r_2 h_{af_i}} \qquad R'_{af_o} = \frac{1}{2\pi r_3 h_{af_o}}$$

$$R'_{op} = \frac{ln\,(r_4/r_3)}{2\pi\lambda_{op}} \qquad R'_{c} = \frac{ln\,(r_5/r_4)}{2\pi\lambda_{c}}$$

$$R'_{rock} = \frac{\ln(r_6/r_5)}{2\pi\lambda_{rock}}$$

Where; h_{af_i}, h_{af_o} are the heat transfers coefficients referring to the inner and outer surface of the annulus and h_{tf} is the heat transfer coefficient on the tubing surface.

The downflowing fluid in the annulus of the closed-loop geothermal system is heated from two directions independently: across the tubing (dQ_2) and across the casing (dQ_1) (fig. 8.1). These heat fluxes can be varied independently. It is obvious, that two independent heat transfer coefficients and two different *Nusselt numbers* are obtained on the inner and the outer wall of the annulus.

The main objective in this point of the thesis is find the temperature and pressure distribution in the working medium solving the approximate model. The assumptions that describe the approximate model are summarized below:

Assumptions

- The area around the heat exchanger is divided into six coaxial cylinders.
- There is no groundwater movement in the soil.
- Forced convection in fully developed turbulent pipe flow.
- Smooth tubes.
- Radial symmetry (heat flux is absorbed by the heat exchanger radially).
- Axial heat conduction is negligible.
- Temperatures $T_a(z)$ (annulus) and $T_t(z)$ (tubing) are cross-sectional average values.
- The properties of the annular fluid are evaluated at the average of the annular bulk fluid temperature.
- The properties of the tubing fluid are evaluated at the average of the tubing bulk fluid temperature.
- The thermal conductivity of the pipes, casing and surrounding rocks are constant along the heat exchanger.
- Constant heat transfer coefficients along the heat exchanger (average values).
- No power generated within the heat exchanger.
- The undisturbed natural rock temperature, T_∞ its distribution linear with depth.

$$\boxed{T_\infty(z) = T_s + \gamma \cdot z}$$

where, T_s is the annual mean temperature at the surface and γ is the geothermal gradient.

- Steady-state.
- $h_{af_i} = h_{af_o}$ (is assumed that the convective coefficients are the same in both annular surfaces).

It is convenient to separate the system into two subsystems. One of them is the flowing fluid, in which the convective heat transfer is dominant. The other is the adjacent rock mass around the well, with a radial conductive heat flux. Thus the internal energy balance can be written for the two subsystems in a simplified form.
Cylindrical coordinates are chosen. The radial coordinate *r* is measured from the axis of the coaxial cylinders, while *z* lies along the axis directed downward. The steady, axisymmetric turbulent flow is taken to be uniform at a cross-section, the velocity *v* and temperature *T* are cross-sectional average values. The *t* and *a* indices refer to the tubing and the annulus.

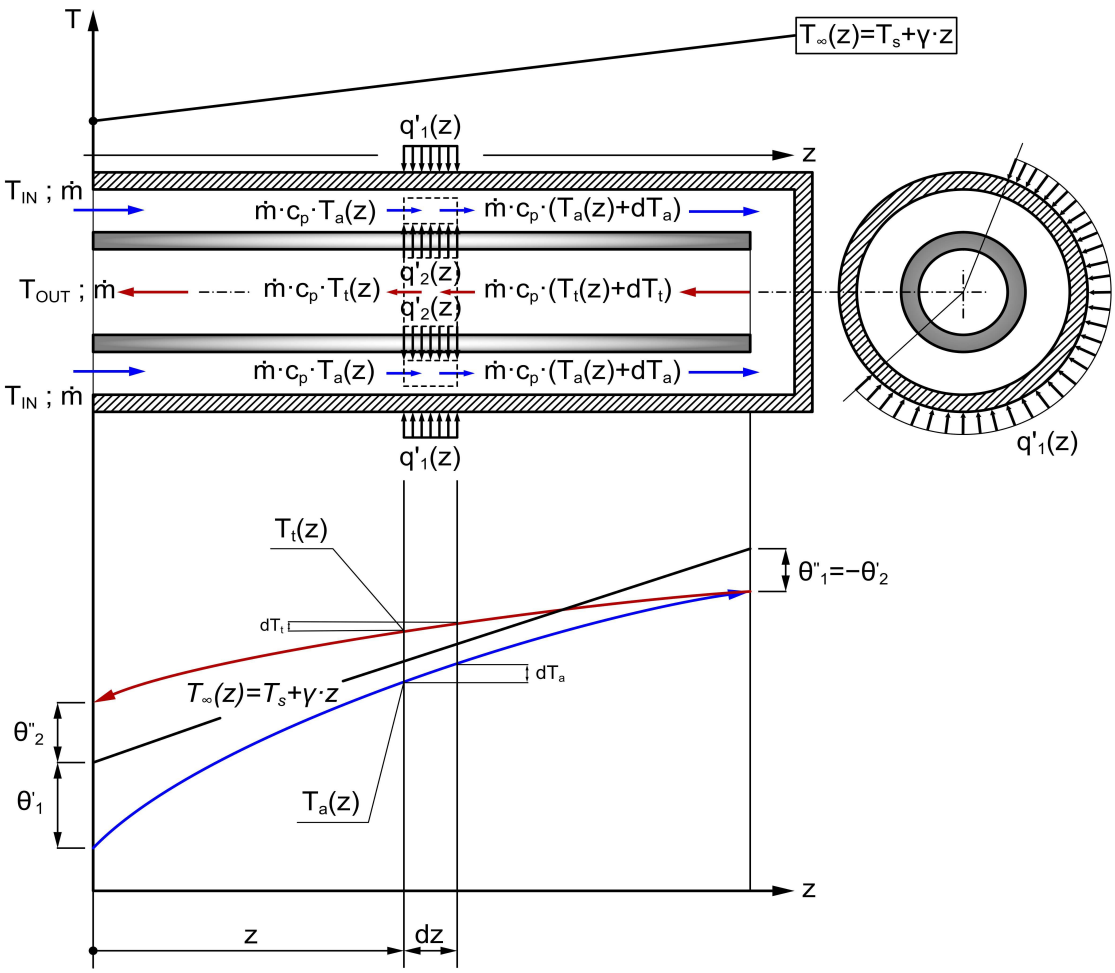

Fig. 8.2: DCHE energy balance description.

Thus the balance equation of the internal energy for the flow across the tubing is (fig. 8.2):

$$\dot{m} \cdot c_p \cdot \frac{dT_t}{dz} = 2 \cdot \pi \cdot r_1 \cdot U_{r_1} \cdot (T_t - T_a) \tag{8.9}$$

In which $\dot{m}$ is the mass flow rate, c_p is the heat capacity of the fluid, U_{r_1} is the overall heat transfer coefficient referring the inner radius of the tubing. For the annular flow we get (fig. 8.2):

$$\dot{m} \cdot c_p \cdot \frac{dT_a}{dz} = 2 \cdot \pi \cdot r_3 \cdot U_{r_3} \cdot (T_\infty - T_a) + 2 \cdot \pi \cdot r_1 \cdot U_{r_1} \cdot (T_t - T_a) \tag{8.10}$$

U_{r_3} is the overall heat transfer coefficient referring the inner radius of the annulus.

Overall heat transfer expressions are written below:

$$U_{r_1} = \frac{1}{A_{r_1} \cdot \sum R_i} = \frac{1}{\frac{r_1}{r_2 \cdot h_{af_i}} + R_{ip} + \frac{1}{h_{tf}}} \left[\frac{W}{m^2 \cdot K}\right]$$

$$U_{r_3} = \frac{1}{A_{r_3} \cdot \sum R_i} = \frac{1}{\frac{r_3 \cdot \ln\left({}^{r_6}/_{r_5}\right)}{\lambda_{rock}} + \frac{r_3 \cdot \ln\left({}^{r_5}/_{r_4}\right)}{\lambda_c} + \frac{r_3 \cdot \ln\left({}^{r_4}/_{r_3}\right)}{\lambda_{op}} + \frac{1}{h_{af_o}}} \left[\frac{W}{m^2 \cdot K}\right]$$

To get the temperatures distributions expressions for the flow across the tubing and annulus along the heat exchanger it is necessary to solve the set of differential equations (equation (8.9) and equation (8.10)). It is solved using the method of d'Alembert [14].

Using the following substitution of variables:

$$\theta_1(z) = T_\infty - T_a \qquad \theta_2(z) = T_t - T_\infty$$

$$a = \frac{2\pi r_1 U_{r_1}}{\dot{m} c_p} \qquad b = \frac{2\pi r_3 U_{r_3}}{\dot{m} c_p}$$

the equation (8.10) becomes:

$$\frac{dT_a}{dz} = a(T_t - T_a) + b(T_\infty - T_a) = a\left[\underbrace{(T_t - T_\infty)}_{\theta_2} + \underbrace{(T_\infty - T_a)}_{\theta_1}\right] + b\,\underbrace{(T_\infty - T_a)}_{\theta_1} \tag{8.11}$$

and equation (8.9) assumes the form:

$$\frac{dT_t}{dz} = a(T_t - T_a) = a\left[\underbrace{(T_t - T_\infty)}_{\theta_2} + \underbrace{(T_\infty - T_a)}_{\theta_1}\right] \tag{8.12}$$

$$\begin{pmatrix} T_a = T_\infty - \theta_1 = T_s + \gamma z - \theta_1 \Longrightarrow \frac{dT_a}{dz} = \gamma - \frac{d\theta_1}{dz} \\ T_t = T_\infty + \theta_2 = T_s + \gamma z + \theta_2 \Longrightarrow \frac{dT_t}{dz} = \gamma + \frac{d\theta_2}{dz} \end{pmatrix}$$

Equations (8.11) and (8.12) can thus be reduced to the following form:

$$\begin{cases} \frac{d\theta_1}{dz} = -(a+b)\theta_1 - a\theta_2 + \gamma & (8.13) \\ \frac{d\theta_2}{dz} = a\theta_1 + a\theta_2 - \gamma & (8.14) \end{cases}$$

Multiplying equations (8.13) and (8.14) by a constant *p* and *q*, respectively, and adding the two equations:

$$\frac{d(p\theta_1)}{dz} + \frac{d(q\theta_2)}{d\theta z} = -p(a+b)\theta_1 - pa\theta_2 + p\gamma + qa\theta_1 + qa\theta_2 - q\gamma \tag{8.15}$$

Applying linearity and factorizing in above equation:

$$\frac{d}{dz}(p\theta_1 + q\theta_2) = (-p(a+b) + qa)\theta_1 + (-p+q)a\theta_2 + (p-q)\gamma \tag{8.16}$$

If the condition is:

$$\frac{-p(a+b) + qa}{p} = \frac{(-p+q)a}{q} = v^2 \tag{8.17}$$

Therefore equation (8.16) can be written as:

$$\frac{d}{dz}(p\theta_1 + q\theta_2) = v^2(p\theta_1 + q\theta_2) + (p-q)\gamma \tag{8.18}$$

A new function is defined as:

$$S_i = p_i\theta_1 + q_i\theta_2 \qquad (i = 1, 2) \tag{8.19}$$

Hence, equation (8.18) becomes a linear equation of the first order:

$$\frac{dS_i}{dz} = v_i^2 S_i + (p_i - q_i)\gamma \qquad (i = 1, 2) \tag{8.20}$$

To solve this differential equation should be solved, at first, the homogeneous linear equation:

$$\frac{dS_i}{dz} = v_i^2 S_i \Longrightarrow \frac{dS_i}{S_i} = v_i^2 dz \Longrightarrow \int \frac{dS_i}{S_i} = \int v_i^2 dz \Longrightarrow ln(S_i) = v_i^2 z + C_i \Longrightarrow exp[ln(S_i)]$$
$$= exp\left[v_i^2 z + C_i\right] \Longrightarrow S_{i_h} = exp\left(v_i^2 z\right) \cdot exp(C_i) \Longrightarrow$$
$$\Longrightarrow S_{i_h} = C_i \cdot exp\left(v_i^2 z\right) \qquad (i = 1, 2)$$

The solution of a no homogeneous differential linear equation has two parts. The homogeneous part and the particular part. Hence:

$$S_i = S_{i_h} + S_{i_p} = C_i \cdot exp\left(v_i^2 z\right) + S_{i_p} \qquad (i = 1, 2) \tag{8.21}$$

where, S_{i_p} is a constant.

Differentiating equation (8.21):

$$\frac{dS_i}{dz} = v_i^2 \cdot C_i \cdot exp\left(v_i^2 z\right)$$

Replacing $\frac{dS_i}{dz}$ and S_i in equation (8.20):

$$v_i^2 \cdot C_i \cdot exp\left(v_i^2 z\right) = v_i^2 \left(C_i \cdot exp\left(v_i^2 z\right) + S_{i_p}\right) + (p_i - q_i)\gamma =$$
$$= v_i^2 \cdot C_i \cdot exp\left(v_i^2 z\right) + v_i^2 \cdot S_{i_p} + (p_i - q_i)\gamma$$
$$\Longrightarrow v_i^2 \cdot S_{i_p} + (p_i - q_i)\gamma = 0 \Longrightarrow S_{i_p} = -\frac{(p_i - q_i)\gamma}{v_i^2}$$

Therefore equation (8.21) is rewritten as:

$$S_i = C_i \cdot exp\left(v_i^2 z\right) - \frac{(p_i - q_i)\gamma}{v_i^2} \qquad (i = 1, 2) \tag{8.22}$$

Equation (8.17) can be written as:

$$\begin{cases} \dfrac{-p_i(a+b) + q_i a}{p_i} = -(a+b) + \dfrac{q_i}{p_i} a = v_i^2 \Longrightarrow \left(\dfrac{q_i}{p_i}\right) = \dfrac{v_i^2 + (a+b)}{a} (i = 1, 2) & (8.23) \\ \dfrac{(-p_i + q_i)a}{q_i} = -\dfrac{p_i}{q_i} a + a = v_i^2 \Longrightarrow \left(\dfrac{p_i}{q_i}\right) = \dfrac{a - v_i^2}{a} \qquad (i = 1, 2) & (8.24) \end{cases}$$

Equating equations (8.23) and (8.24):

$$\frac{v_i^2 + (a+b)}{a} = \frac{a - v_i^2}{a} \Longrightarrow v_i^4 + b v_i^2 - ab = 0 \qquad (i = 1, 2) \tag{8.25}$$

Where, v_i^2 is a root of the algebraic equation (8.25) and has the value:

$$v_i^2 = \frac{-b \pm \sqrt{b^2 + 4ab}}{2} \qquad (i = 1, 2) \tag{8.26}$$

Equating equations (8.19) and (8.22) are obtained the next expressions:

$$p_1\theta_1 + q_1\theta_2 = C_1 \cdot exp(v_1^2 z) - \frac{(p_1 - q_1)\gamma}{v_1^2} \tag{8.27}$$

$$p_2\theta_1 + q_2\theta_2 = C_2 \cdot exp(v_2^2 z) - \frac{(p_2 - q_2)\gamma}{v_2^2} \tag{8.28}$$

From equations (8.27) and (8.28), the use of appropriate transformations and after the introduction of new integration constants C_1^* and C_2^* functions θ_1 and θ_2 take the form:

$$\theta_1 = C_1^* \cdot exp(v_1^2 z) - C_2^* \cdot exp(v_2^2 z) \tag{8.29}$$

$$\theta_2 = C_2^* \left(\frac{p_1}{q_1}\right) \cdot exp(v_2^2 z) - C_1^* \left(\frac{p_2}{q_2}\right) \cdot exp(v_1^2 z) + a\gamma \tag{8.30}$$

The constants of integration (C_1^*, C_2^*) can be determined satisfying the following boundary conditions.

1) $T_a(z = 0) = T_{IN}$, where T_{IN} is the temperature of the cooled injected fluid.

   $\Longrightarrow \theta_1(z = 0) = \theta_1' = (T_\infty - T_{IN})$

2) $T_a(z = L) = T_t(z = L)$, the bottomhole temperatures in the annulus and in the tubing are the same.

   $\Longrightarrow \theta_1(z = L) = -\theta_2(z = L) \Longrightarrow -\theta_2' = \theta_1''$

3) The energy increase of the circulating fluid is equal to the integral of the heat flux across the borehole wall between the bottom and the surface:

$$\dot{m}c_p(T_{OUT} - T_{IN}) = \int_0^L q(z)dz$$

   where, T_{OUT} is the temperature of the outflowing fluid at the wellhead.

The obtained equations from the boundary conditions 1) and 2) are:

1) $C_1^* - C_2^* = \theta_1' \Longrightarrow C_2^* = C_1^* - \theta_1'$ (8.31)

2) $C_1^* \cdot exp(\nu_1^2 L) - C_2^* \cdot exp(\nu_2^2 L) = -C_2^* \left(\frac{p_1}{q_1}\right) \cdot exp(\nu_2^2 L) + C_1^* \left(\frac{p_2}{q_2}\right) \cdot exp(\nu_1^2 L) - a\gamma$ (8.32)

Finally combining equations (8.31) and (8.32) are obtained the constants of integration:

$$C_1^* = \frac{a\gamma - \theta_1' \cdot exp(\nu_2^2 L)\left[\frac{p_1}{q_1} - 1\right]}{exp(\nu_1^2 L)\left[\frac{p_2}{q_2} - 1\right] - exp(\nu_2^2 L)\left[\frac{p_1}{q_1} - 1\right]} \tag{8.33}$$

$$C_2^* = \frac{a\gamma - \theta_1' \cdot exp(\nu_1^2 L)\left[\frac{p_2}{q_2} - 1\right]}{exp(\nu_1^2 L)\left[\frac{p_2}{q_2} - 1\right] - exp(\nu_2^2 L)\left[\frac{p_1}{q_1} - 1\right]} \tag{8.34}$$

The set of equations cited above are used only if the fluid properties are constant. In this project the energy balance is solved considering that the fluid properties are varying with temperature. For this reason is used a numerical solution to determinate the temperature profiles along the heat exchanger. In the next chapter is described this method.

Chapter 9

Determination of temperature and pressure distribution in the working medium

9.1 Temperature distribution along the heat exchanger

At this point is written the algorithm used for find the temperature distribution. This algorithm is solved using *"Mathcad"*. This *software* solve the system of differential equations due to the energy balance in the annular and tubing side by numerical analysis using the *Runge-Kutta* method.

The algorithm consists in a iterative process. At first are assumed the value of the DCHE inlet temperature (T_{IN}), DCHE outlet temperature (T_{OUT}) and the bottomhole temperature (T_L). Then is obtained two differents temperatures distributions, one for the annular region [$T_a(z)$] and the other one for the inner tube region [$T_t(z)$]. Finally are calculated the new value of the assumed variables. In fig. 9.1 is shown the iterative diagram for the temperature distribution calculation.

Below is described in detail the algorithm.

Temperatures assumptions

1) DCHE's inlet temperature assumption(T_{IN}).
2) DCHE's outlet temperature assumption(T_{OUT}).

Calculation of the convective coefficient for the tubing flow

3) Distribution of the properties of the working fluid inside the inner tubing according with the temperature.

$$\begin{cases} \rho(T_t) \\ c_p(T_t) \\ \lambda(T_t) \\ \mu(T_t) \end{cases}$$

4) Geometric characteristics.

$D_{h_t} = "tubing\ hydraulic\ diameter" = 2r_1$
$A_t = "tubing\ cross\ section\ area" = \pi r_1^2$
$G_t = \dfrac{\dot{m}}{A_t}$

5) Determination of the *Reynold's number* distribution.

$$Re_t(T_t) = \frac{G_t \cdot D_{h_t}}{\mu(T_t)}$$

6) Determination of the *Prandtl number* distribution.

$$Pr_t(T_t) = \frac{\mu(T_t) \cdot c_p(T_t)}{\lambda(T_t)}$$

7) Calculation of the friction coefficient distribution.

$$f_t(T_t) = \frac{1}{(1{,}58 ln Re_t(T_t) - 3{,}28)^2}$$

8) Calculation of the heat transfer coefficient distribution.

$$Nu_t(T_t) = \frac{(f_t(T_t)/2)(Re_t(T_t) - 1000)Pr_t(T_t)\left[1 + \left(\frac{D_{h_t}}{L}\right)^{2/3}\right]}{1 + 12{,}7(f_t(T_t)/2)^{1/2}\left(Pr_t^{\frac{2}{3}}(T_t) - 1\right)}$$

9) Calculation of the convective coefficient distribution for the tubing flow.

$$h_t(T_t) = \frac{Nu_t(T_t) \cdot \lambda(T_t)}{D_{h_t}}$$

Calculation of the convective coefficient for the annular flow

10) Distribution of the properties of the working fluid inside the annulus according with the temperature.

$$\begin{cases} \rho(T_a) \\ c_p(T_a) \\ \lambda(T_a) \\ \mu(T_a) \end{cases}$$

11) Geometric characteristics.

$$A_a = "annulus\ cross\ section\ area" = \pi(r_3^2 - r_2^2)$$

$$p_{w_a} = "wetted\ perimeter\ in\ the\ annular\ region" = 2\pi(r_2 + r_3)$$

$$D_{h_a} = "annulus\ hydraulic\ diameter" = \frac{4A_a}{p_{w_a}}$$

$$G_a = \frac{\dot{m}}{A_a}$$

12) Determination of the *Reynold's number* distribution.

$$Re_a(T_a) = \frac{G_a \cdot D_{h_a}}{\mu(T_a)}$$

13) Determination of the *Prandtl number* distribution.

$$Pr_a(T_a) = \frac{\mu(T_a) \cdot c_p(T_a)}{\lambda(T_a)}$$

14) Calculation of the friction coefficient distribution.

$$f_a(T_a) = \frac{1}{(1{,}58 ln Re_a(T_a) - 3{,}28)^2}$$

15) Calculation of the heat transfer coefficient distribution.

$$Nu_a(T_a) = \frac{(f_a(T_a)/2)(Re_a(T_a) - 1000)Pr_a(T_a)\left[1 + \left(\frac{D_{h_a}}{L}\right)^{2/3}\right]}{1 + 12{,}7(f_a(T_a)/2)^{1/2}\left(Pr_a^{\frac{2}{3}}(T_a) - 1\right)}$$

16) Calculation of the convective coefficient distribution for the annular flow.

$$h_{af_i}(T_a) = h_{af_o}(T_a) = \frac{Nu_a(T_a) \cdot \lambda(T_a)}{D_{h_a}}$$

Overall heat transfer coefficients

17) Calculation of the overall heat transfer coefficients distribution (U_{r_1}, U_{r_3}).

$$U_{r_1}(T_t, T_a) = \frac{1}{\frac{r_1}{r_2 \cdot h_{af_i}(T_a)} + R_{ip} + \frac{1}{h_{tf}(T_t)}}$$

$$U_{r_3}(T_a) = \frac{1}{\frac{r_3 \cdot \ln\left({}^{r_6}/_{r_5}\right)}{\lambda_{rock}} + \frac{r_3 \cdot \ln\left({}^{r_5}/_{r_4}\right)}{\lambda_c} + \frac{r_3 \cdot \ln\left({}^{r_4}/_{r_3}\right)}{\lambda_{op}} + \frac{1}{h_{af_o}(T_a)}}$$

Solution of the differential equations system

18) Solution of the differential equations system using the *Runge-Kutta* method.

From the enthalpy balance in the tubing and annulus region we obtain:

$$\begin{cases} \dot{m} \cdot \dfrac{dh_t}{dz} = 2 \cdot \pi \cdot r_1 \cdot U_{r_1}(T_t, T_a) \cdot (T_t - T_a) & (9.1) \\ \dot{m} \cdot \dfrac{dh_a}{dz} = 2 \cdot \pi \cdot r_3 \cdot U_{r_3}(T_a) \cdot (T_\infty - T_a) + 2 \cdot \pi \cdot r_1 \cdot U_{r_1}(T_t, T_a) \cdot (T_t - T_a) & (9.2) \\ T_\infty(z) = T_s + \gamma \cdot z & (9.3) \end{cases}$$

·) Using water as a working fluid:

$$h = h_{ref} + cT + v\left(P - P_{ref}\right) \quad (9.4)$$

$$\frac{dh}{dz} = c\frac{dT}{dz} + v\frac{dP}{dz} \quad ; \quad v = \frac{1}{\rho}$$

The pressure distribution in the tubing looks like (see section 9.2):

$$P_t(z) = \underbrace{P_L}_{cte} - f_t \frac{(L - z)}{D_{h_t}} \frac{\dot{m}^2}{2\rho A_t^2} - \rho g(L - z) \quad ; \quad P_L = P_t(z = L) \quad (9.5)$$

$$\Longrightarrow \frac{dP_t(z)}{dz} = \frac{f_t}{D_{h_t}} \frac{\dot{m}^2}{2\rho A_t^2} + \rho g \quad ; \quad \rho \cong cte = 1000\, {}^{kg}/_{m^3}$$

The pressure distribution in the annulus looks like (see section 9.2):

$$P_a(z) = P_0 - f_a \frac{z}{D_{h_a}} \frac{\dot{m}^2}{2\rho A_a^2} + \rho g z \quad ; \quad P_0 = P_a(z=0) \tag{9.6}$$

$$\Longrightarrow \frac{dP_a(z)}{dz} = -\frac{f_a}{D_{h_a}} \frac{\dot{m}^2}{2\rho A_a^2} + \rho g \quad ; \quad \rho \cong cte = 1000\, {}^{kg}/_{m^3}$$

Therefore, the enthalpy balance in the case of the water takes the following form:

$$\begin{cases} \dfrac{dT_t}{dz} = \dfrac{2\pi r_1 U_{r_1}(T_t, T_a)}{\dot{m}c}(T_t - T_a) - \dfrac{g}{c} - \dfrac{f_t}{D_{h_t}} \dfrac{\dot{m}^2}{2c\rho^2 A_t^2} \\ \dfrac{dT_a}{dz} = \dfrac{2\pi r_3 U_{r_3}(T_a)}{\dot{m}c}(T_\infty - T_a) + \dfrac{2\pi r_1 U_{r_1}(T_t, T_a)}{\dot{m}c}(T_t - T_a) - \dfrac{g}{c} + \dfrac{f_a}{D_{h_a}} \dfrac{\dot{m}^2}{2c\rho^2 A_a^2} \\ T_\infty(z) = T_s + \gamma \cdot z \end{cases}$$

·) Using air as a working fluid:

$$h = h_{ref} + c_p T \tag{9.7}$$

$$\Longrightarrow \frac{dh}{dz} = c_p \frac{dT}{dz}$$

Therefore, the enthalpy balance in the case of the air takes the following form:

$$\begin{cases} \dfrac{dT_t}{dz} = \dfrac{2\pi r_1 U_{r_1}(T_t, T_a)}{\dot{m}c_p(T_t)}(T_t - T_a) \\ \dfrac{dT_a}{dz} = \dfrac{2\pi r_3 U_{r_3}(T_a)}{\dot{m}c_p(T_a)}(T_\infty - T_a) + \dfrac{2\pi r_1 U_{r_1}(T_t, T_a)}{\dot{m}c_p(T_a)}(T_t - T_a) \\ T_\infty(z) = T_s + \gamma \cdot z \end{cases}$$

$$First\ type\ boundary\ conditions = T_{init} = \begin{cases} T_t(z=0) \\ T_a(z=0) \end{cases} = \begin{cases} T_{OUT} \\ T_{IN} \end{cases}$$

Annulus temperature distribution(T_a) and tubing temperature distribution(T_t) are obtained.

Calculation of the new DCHE outlet temperature

19) The DCHE outlet temperature$\left(T_{OUT_{new}}\right)$ is recalculated:

$$T_{OUT_{new}} = T_a(z=L) - (T_t(z=L) - T_{OUT}) = T_{a_L} - \left(T_{t_L} - T_{OUT}\right)$$
$$T_{OUT} = T_t(z=0)$$

This new value will be assigned to the DCHE outlet temperature(T_{OUT}) in the point 2) of the algorithm and the entire model from the point 2) will be recalculated. This process takes place in a iterative way till the variable $T_{OUT_{new}}$ don't change more. Hence:

$$T_{OUT_{new}} \cong T_{OUT}$$

Calculation of the new DCHE inlet temperature

20) The DCHE inlet temperature($T_{IN_{new}}$) is recalculated as explained in section (6.2):

$$T_{IN_{new}} = T_{OUT} - \left(\frac{\dot{Q}_H - \frac{\dot{Q}_H}{COP}}{\dot{m} \cdot c_p(T_{OUT})} \right)$$

This new value will be assigned to the DCHE inlet temperature(T_{IN}) in the point 1) of the algorithm and the entire model from the point 1) will be recalculated. This process takes place in a iterative way till the variable $T_{IN_{new}}$ don't change more. Hence:

$$T_{IN_{new}} \cong T_{IN}$$

Validation of the application range of the Gnielinski equation

Using water as a working fluid *($r_1 = 30\ mm,\ R_{ip} = 0.02\ m^2K/W\ ,\ P_I = 1.038 \cdot 10^5\ Pa$)*:

$$\overline{Re_t} = 1.206 \cdot 10^4 \Longrightarrow 3000 < \overline{Re_t} < 5 \times 10^6$$
$$\overline{Pr_t} = 9.818 \Longrightarrow 0{,}5 < \overline{Pr_t} < 2000$$

$$\overline{Re_a} = 4.006 \cdot 10^3 \Longrightarrow 3000 < \overline{Re_a} < 5 \times 10^6$$
$$\overline{Pr_a} = 10.5 \Longrightarrow 0{,}5 < \overline{Pr_a} < 2000$$

Using air as a working fluid *($r_1 = 25\ mm,\ R_{ip} = 0.03\ m^2K/W\ ,\ P_I = 8.517 \cdot 10^5\ Pa$)*:

$$\overline{Re_t} = 2.868 \cdot 10^6 \Longrightarrow 3000 < \overline{Re_t} < 5 \times 10^6$$
$$\overline{Pr_t} = 0.72 \Longrightarrow 0{,}5 < \overline{Pr_t} < 2000$$

$$\overline{Re_a} = 9.065 \cdot 10^5 \Longrightarrow 3000 < \overline{Re_a} < 5 \times 10^6$$
$$\overline{Pr_a} = 0.72 \Longrightarrow 0{,}5 < \overline{Pr_a} < 2000$$

Where, $\overline{Re}$ and $\overline{Pr}$ are the average of the *Reynolds* and *Prandtl numbers*, respectively.

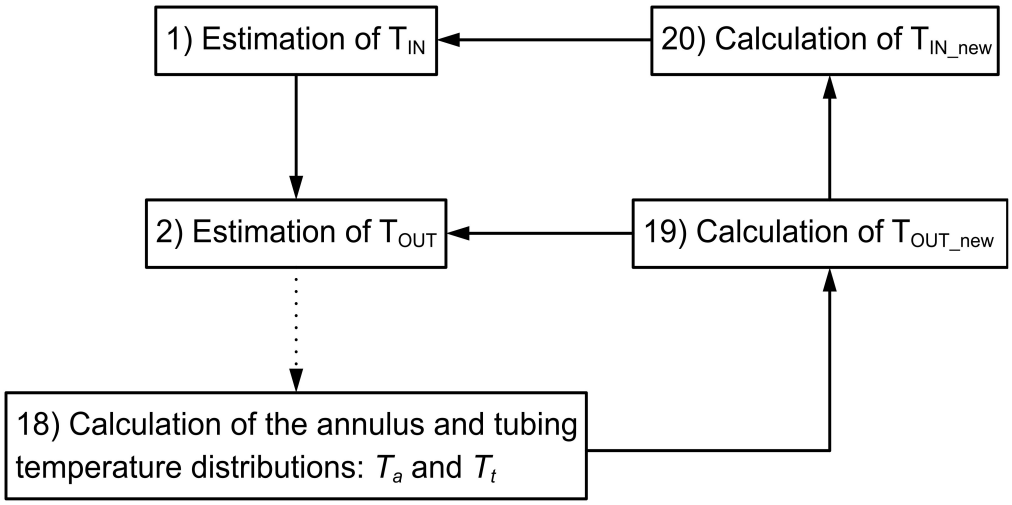

Fig. 9.1: Iterative diagram of the algorithm to calculate the temperatures profiles.

Graphic of the temperature distribution and results

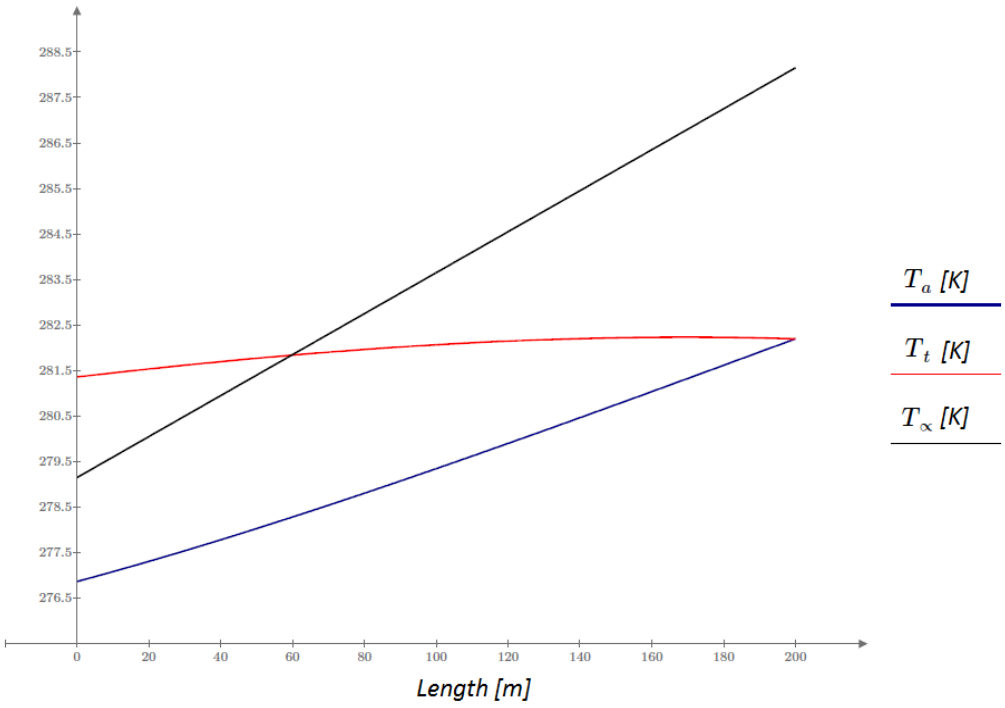

Fig. 9.2: Temperature distribution along the heat exchanger using water as a working fluid. $(r_1 = 30\ mm,\ R_{ip} = 0.02\ m^2K/W\ ,\ P_I = 1.038 \cdot 10^5\ Pa)$

$$T_{IN} = 276.867\ K \quad ; \quad T_{OUT} = 281.359\ K \quad ; \quad T_L = 282.189\ K \quad ; \quad \Delta T = 4.492\ K$$

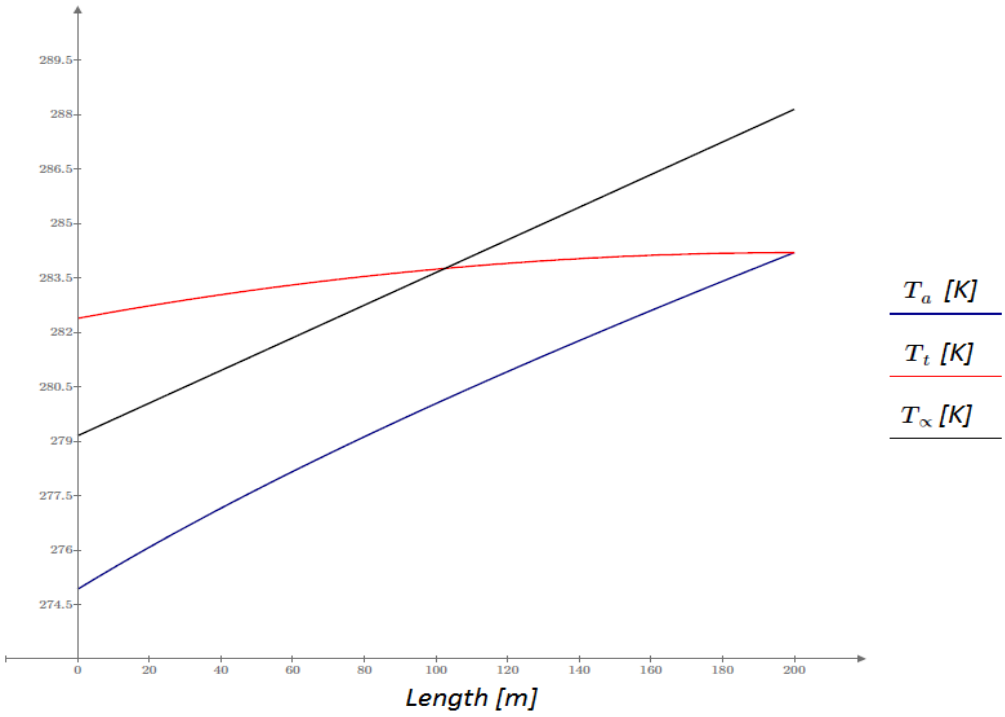

Fig. 9.3: Temperature distribution along the heat exchanger using air as a working fluid. $(r_1 = 25\ mm,\ R_{ip} = 0.03\ m^2K/W\ ,\ P_I = 8.517 \cdot 10^5\ Pa)$

$T_{IN} = 274.918\ K \quad ; \quad T_{OUT} = 282.387\ K \quad ; \quad T_L = 284.201\ K \quad ; \quad \Delta T = 7.469\ K$

9.2 Pressure distribution along the heat exchanger

Pressure drop corresponding to the frictional head loss for a viscous fluid flowing between two points can be calculated as [9]:

$$\Delta P = P_1 - P_2 = f\frac{L}{D_h}\frac{\rho V^2}{2} \tag{9.1}$$

Where:

- ·) f is the friction factor obtained from correlation developed by *Filonenko*.
- ·) L is the length between both points.
- ·) D_h is the hydraulic diameter.
- ·) ρ is the mean density between both points⇒ $\rho = \frac{1}{2}(\rho_1 + \rho_2)$
- ·) V is the mean velocity between both points⇒ $V = \frac{1}{2}(V_1 + V_2)$

Equation (9.1) is known as the *Darcy Formula*. This equation is used in pipe sizing, in a pump selection analysis and other engineering applications. It must be emphasized

that this equation should be used to calculate pressure drop due to flow friction between two points located on a straight piece of pipe.

Equation (9.1) can be rewritten using the next relations:

$$Q_v(= "Volume\ flowrate") = V \cdot A(= Area) \Rightarrow \frac{\dot{m}}{\rho} = V \cdot A \Rightarrow V = \frac{\dot{m}}{\rho \cdot A}$$

Hence, substituting V by $\frac{\dot{m}}{\rho \cdot A}$ in the *Darcy Formula*:

$$\Delta P = P_1 - P_2 = f\frac{L}{D_h} \cdot \frac{\dot{m}^2}{2\rho A^2} = f\frac{L}{D_h} \cdot \frac{G^2}{2\rho} \tag{9.2}$$

Where,

$$G = \frac{\dot{m}}{A}$$

Darcy Formula describes pressure drop in straight pipes due to the viscosity of the fluid and the surface condition of the pipe wall. This is known as *skin friction*. Should also be consider other conditions that result in pressure drop by disturbing the flow such twist, turn, or partial obstruction of the flow. These may result in flow separation and consequently irreversible energy loss to the fluid flow. Similar to the *Darcy* pressure drop, this also results in unrecoverable pressure drop.
Losses due to twist, turn, and flow obstruction are generally due to geometries features such as sudden contractions, enlargements, bends and protuberances.

These kinds of losses are also expressed in terms of specific kinetic energy [9]:

$$\Delta P = K\frac{\rho V^2}{2} = K\frac{\dot{m}^2}{2\rho A^2} \tag{9.3}$$

Where K is referred to as *loss coefficient*.
In the next figure is shown the expressions of loss coefficient associated with sudden change in flow area.

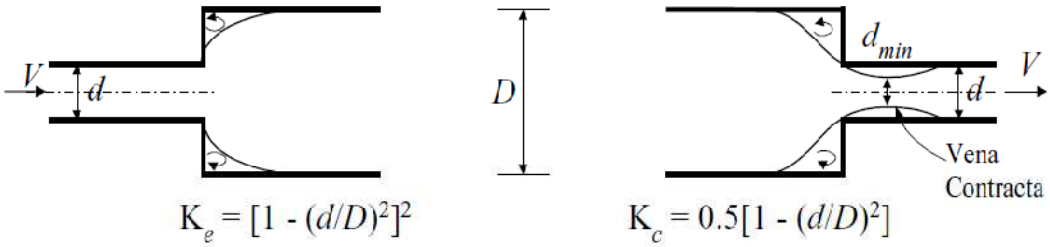

Fig. 9.4: Loss coefficient associated with sudden change in flow area [9].

In this case the loss coefficient for sudden expansion is:

$$K_e = [1 - (d/D)^2]^2 \tag{9.4}$$

And the loss coefficient for sudden contraction is:

$$K_c = 0.5[1 - (d/D)^2] \tag{9.5}$$

For both cases of sudden expansion and contraction, the corresponding head loss is found in terms of the velocity in the smaller pipe.

Below is determined the pressure distribution along the heat exchanger, for this reason must be considered various differential pressure terms a part of the friction pressure drop. These terms are described as follows:

$$\Delta P_{grav} = \rho g \Delta z \tag{9.6}$$

$$\Delta P_{fric} = \left(f\frac{L}{D_h} + \sum K\right)\frac{\dot{m}^2}{2\rho A^2} \tag{9.7}$$

$$\begin{cases} \Delta P_{vel} = \left[\dfrac{1}{A_2^2} - \dfrac{1}{A_1^2}\right]\dfrac{\dot{m}^2}{2\rho} & (9.8) \\ \Delta P_{acc} = \left[\dfrac{1}{\rho_2} - \dfrac{1}{\rho_1}\right]\dfrac{\dot{m}^2}{A^2} & (9.9) \end{cases}$$

The first term is the pressure difference due to gravity (ΔP_{grav}). The second term is the friction pressure drop (ΔP_{fric}) which always impedes the flow. The third and fourth terms are the differential pressure terms due to a change in flow velocity. This is either due to change in the flow area (ΔP_{vel}) or in the fluid density (ΔP_{acc}) (fig. 9.5). If there is a sudden change in flow area, the associated frictional loss is accounted for by (ΔP_{fric}). Hence, (ΔP_{vel}) accounts only for the recoverable pressure difference. The change on the fluid density occurs when the fluid flow is heated up or cooled down. In the case of heat addition $(\rho_2 < \rho_1)$ the flow is accelerated. If the flow is cooled down $(\rho_2 > \rho_1)$ the flow is decelerated.

In the next figure are represented the different cases.

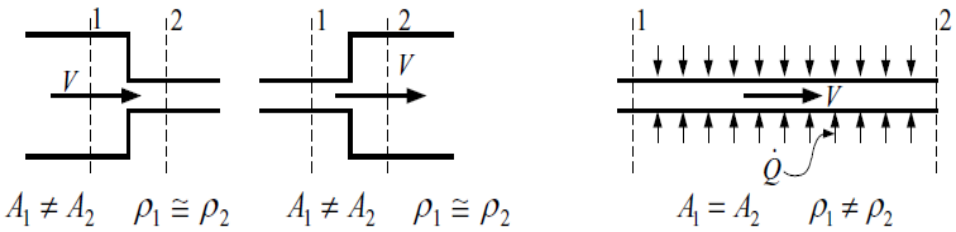

Fig. 9.5: ΔP_{vel} due to sudden area change and ΔP_{acc} due to density change [9].

With respect to the heat exchanger studied in this thesis we can differentiate four different regions for pressure drop: *entrance, exit, change of flow direction and length of the heat exchanger*.
Below is shown a figure with the details of the entrance and exit region.

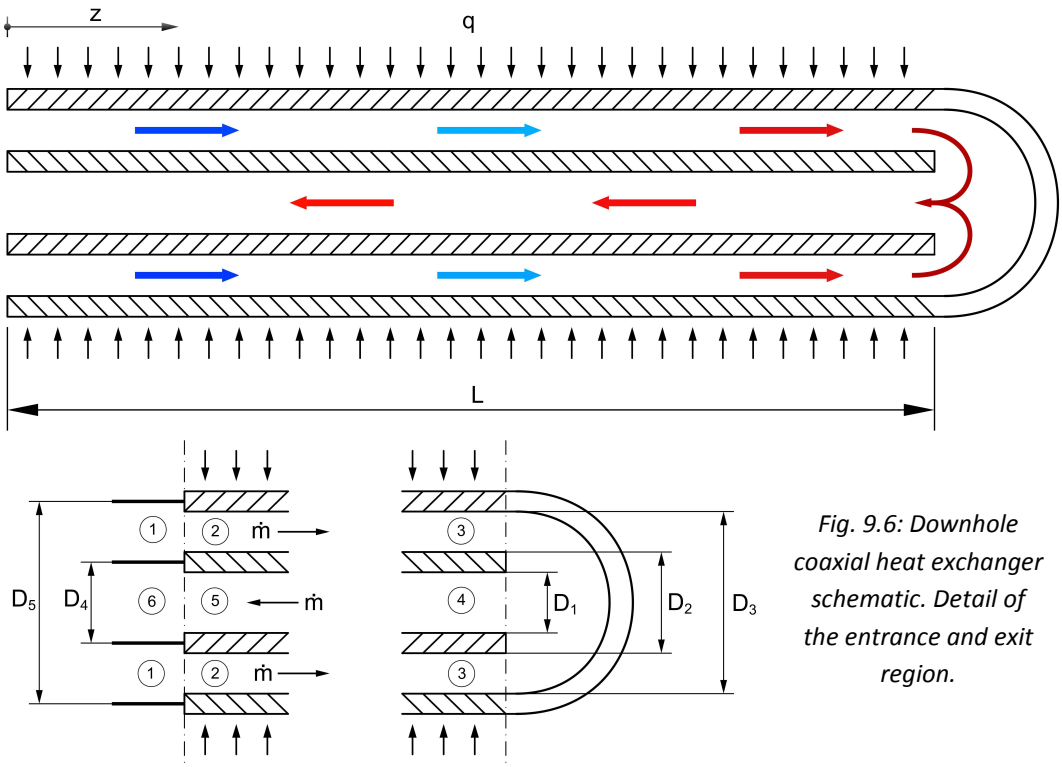

Fig. 9.6: Downhole coaxial heat exchanger schematic. Detail of the entrance and exit region.

The pressure distribution along the heat exchanger will be determinate for two different working fluids; liquid (water) and perfect gas (air).

In the case of the water can be assumed incompressible flow and consequently constant density ($\rho = constant$). Hence:

$$\rho_1 = \rho_2 = \cdots = \rho_6 = \rho \cong 1000\ {}^{kg}/_{m^3}$$

Below are written the equations for the pressure distribution calculation along the heat exchanger for the case of water as working fluid (The expressions numbering refers to fig. 9.6).

$$A_1 = \frac{\pi}{4}\left(D_5^2 - D_4^2\right) \qquad A_2 = A_3 = \frac{\pi}{4}\left(D_3^2 - D_2^2\right) \qquad A_4 = A_5 = \frac{\pi D_1^2}{4} \qquad A_6 = \frac{\pi D_4^2}{4}$$

$$K_c = 0.5\left(1 - \frac{A_2}{A_1}\right) \qquad K_e = \left(1 - \frac{A_5}{A_6}\right)^2$$

$$V_1 = \frac{\dot{m}}{\rho A_1} \qquad V_2 = V_3 = \frac{\dot{m}}{\rho A_2} \qquad V_4 = V_5 = \frac{\dot{m}}{\rho A_4} \qquad V_6 = \frac{\dot{m}}{\rho A_6}$$

$$\Delta P_{12} = P_1 - P_2 = \Delta P_{vel\_12} + \Delta P_{fric\_12} = \frac{\rho(V_2^2 - V_1^2)}{2} + \frac{K_c \cdot \dot{m}^2}{2\rho A_2^2}$$

For ΔP_{23}, $f_{23} = \bar{f}_a \qquad D_{h_2} = D_{h_3} = \frac{4A_2}{p_{w_2}} = (D_3 - D_2)$

$$\Delta P_{23} = P_2 - P_3 = \Delta P_{fric\_23} + \Delta P_{grav\_23} = f_{23}\frac{L}{D_{h_2}}\frac{\dot{m}^2}{2\rho A_2^2} + \rho g(-L - 0)$$

For ΔP_{34}, the pressure drop is due to the change of flow direction. In this case is assumed a *loss coefficient* of ($K_{34} = 1.5$):

$$\Delta P_{34} = P_3 - P_4 = \Delta P_{vel\_34} + \Delta P_{fric\_34} = \frac{\rho(V_4^2 - V_3^2)}{2} + K_{34}\frac{\dot{m}^2}{2\rho A_4^2}$$

For ΔP_{45}, $f_{45} = \bar{f}_t \qquad D_{h_4} = D_{h_5} = D_1$

$$\Delta P_{45} = P_4 - P_5 = \Delta P_{fric\_45} + \Delta P_{grav\_45} = f_{45}\frac{L}{D_1}\frac{\dot{m}^2}{2\rho A_4^2} + \rho g\big(0 - (-L)\big)$$

$$\Delta P_{56} = \Delta P_{vel\_56} + \Delta P_{fric\_56} = \frac{\rho\big(V_6^2 - V_5^2\big)}{2} + \frac{K_e \cdot \dot{m}^2}{2\rho A_5^2}$$

$\Delta P_{Total} = \Delta P_{12} + \Delta P_{23} + \Delta P_{34} + \Delta P_{45} + \Delta P_{56}$

Hence,

$P_1 = P_I = f(r_1) \quad (The\ DCHE's\ inlet\ pressure\ is\ a\ function\ of\ the\ variable\ r_1)$

$P_2 = P_I - \Delta P_{12}$

$$P_{2-3}(z) = P_I - \Delta P_{12} - \Delta P_{23}(z) = P_I - \Delta P_{12} - f_{23}\frac{z}{D_{h_2}}\frac{\dot{m}^2}{2\rho A_2^2} + \rho g z$$

$$P_4 = P_I - \Delta P_{12} - \Delta P_{23}(L) - \Delta P_{34} = P_I - \Delta P_{12} - f_{23}\frac{L}{D_{h_2}}\frac{\dot{m}^2}{2\rho A_2^2} + \rho g L - \Delta P_{34}$$

$$P_{4-5}(z) = P_I - \Delta P_{12} - \Delta P_{23}(L) - \Delta P_{34} - \Delta P_{45}(z) =$$
$$= P_I - \Delta P_{12} - f_{23}\frac{L}{D_{h_2}}\frac{\dot{m}^2}{2\rho A_2^2} + \rho g L - \Delta P_{34} - f_{45}\frac{(L-z)}{D_1}\frac{\dot{m}^2}{2\rho A_4^2}$$
$$- \rho g(L - z)$$

$$P_6 = P_I - \Delta P_{12} - \Delta P_{23}(L) - \Delta P_{34} - \Delta P_{45}(0) - \Delta P_{56} =$$
$$= P_I - \Delta P_{12} - f_{23}\frac{L}{D_{h_2}}\frac{\dot{m}^2}{2\rho A_2^2} + \rho g L - \Delta P_{34} - f_{45}\frac{L}{D_1}\frac{\dot{m}^2}{2\rho A_4^2} - \rho g L$$
$$- \Delta P_{56}$$

Fig. 9.7 shows a graph with the pressure distribution. The horizontal axis represents the length along the working fluid $[l]$. The range between $0 - 200\ m$ corresponds to the annular region while the range between $200 - 400\ m$ corresponds to the inner pipe. The vertical axis represents the pressure $[P(l)]$ along the heat exchanger.

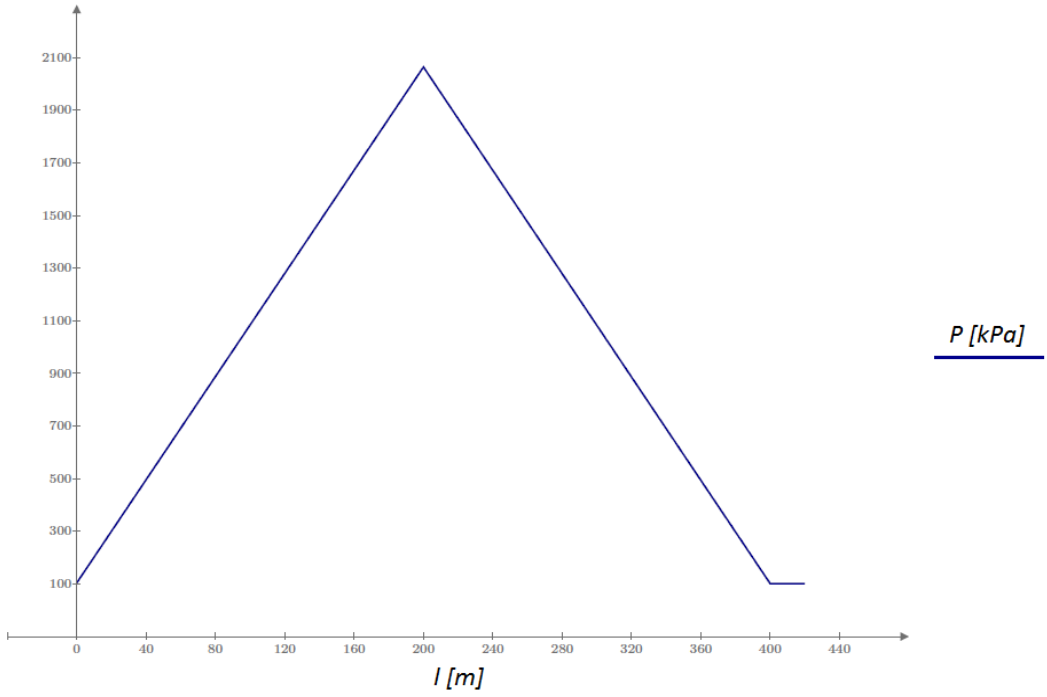

Fig. 9.7: Pressure distribution along the heat exchanger using water as a working fluid. $(r_1 = 30\ mm,\ R_{ip} = 0.02\ m^2K/W\ ,\ P_I = 1.038 \cdot 10^5\ Pa)$

From the fig. 9.7 is noting that the local pressure along the heat exchanger depends, basically, to the gravity term. This is because of the high density of the water.

In the next table are summarized the value of the different terms of the pressure drop along the heat exchanger using water as a working fluid for this particular configuration: $r_1 = 30\ mm,\ R_{ip} = 0.02\ m^2K/W\ ,\ P_I = 1.038 \cdot 10^5\ Pa$.

Cross Section Areas					
A₁	***A₂***	***A₃***	***A₄***	***A₅***	***A₆***
0.0053 m^2	0.004 m^2	0.004 m^2	0.0028 m^2	0.0028 m^2	0.0033 m^2
Velocities					

V_1	V_2	V_3	V_4	V_5	V_6
0.150 m/s	0.200 m/s	0.200 m/s	0.283 m/s	0.283 m/s	0.241 m/s
Loss coefficients					
K_c		K_e		K_{34}	
0.125		0.022		1.5	
Friction coefficients and hydraulic diameters					
f_{23}	D_{h_23}		f_{45}	D_{h_45}	
0.01035	0.03 m		0.00747	0.06 m	
ΔP_{12} (pressure drop 1-2)					
ΔP_{vel_12}	ΔP_{fric_12}		ΔP_{Total_12}		
8.726 Pa	2.493 Pa		11.219 Pa		
ΔP_{23} (pressure drop 2-3)					
ΔP_{fric_23}	ΔP_{grav_23}		ΔP_{Total_23}		
$1.377 \cdot 10^3$ Pa	$-1.962 \cdot 10^6$ Pa		$-1.961 \cdot 10^6$ Pa		
ΔP_{34} (pressure drop 3-4)					
ΔP_{vel_34}	ΔP_{fric_34}		ΔP_{Total_34}		
20.083 Pa	60.042 Pa		80.125 Pa		
ΔP_{45} (pressure drop 4-5)					
ΔP_{fric_45}	ΔP_{grav_45}		ΔP_{Total_45}		
996.918 Pa	$1.962 \cdot 10^6$ Pa		$1.963 \cdot 10^6$ Pa		
ΔP_{56} (pressure drop 5-6)					
ΔP_{vel_56}	ΔP_{fric_56}		ΔP_{Total_56}		
-10.967	0.876		-10.091 Pa		
$\Delta P_{Total} = \Delta P_{12} + \Delta P_{23} + \Delta P_{34} + \Delta P_{45} + \Delta P_{56} = 2.455 \cdot 10^3$ Pa					

Table 9.1: Pressure drop values along the heat exchanger using water as a working fluid ($r_1 = 30\ mm,\ R_{ip} = 0.02\ m^2K/W\ ,\ P_I = 1.038 \cdot 10^5\ Pa$).

In the case of air, incompressible flow cannot be assumed and consequently density fluid change along the heat exchanger due to a heat flux ($\rho \not\approx constant$).

$$\rho_1 \cong \rho_2 \qquad \rho_3 \neq \rho_2 \qquad \rho_4 \cong \rho_3 \qquad \rho_5 \neq \rho_4 \qquad \rho_6 \cong \rho_5$$

$$\rho[kg/m^3] = \frac{3.484 \cdot P_I[kPa]}{T[K]} \tag{9.10}$$

Below are written the equations for the pressure distribution calculation along the heat exchanger for the case of air as working fluid (The expressions numbering refers to fig. 9.6).

$$V_1 = \frac{\dot{m}}{\rho_1 A_1} \qquad V_2 = \frac{\dot{m}}{\rho_1 A_2} \qquad V_3 = \frac{\dot{m}}{\rho_3 A_3} \qquad V_4 = \frac{\dot{m}}{\rho_3 A_4} \qquad V_5 = \frac{\dot{m}}{\rho_5 A_5} \qquad V_6 = \frac{\dot{m}}{\rho_5 A_6}$$

$$\Delta P_{12} = \Delta P_{vel\_12} + \Delta P_{fric\_12} = \frac{\rho_1 (V_2^2 - V_1^2)}{2} + \frac{K_c \cdot \dot{m}^2}{2\rho_1 A_2^2}$$

For $\Delta P_{23},\ f_{23} = \bar{f_a} \qquad D_{h_2} = D_{h_3} = \frac{4A_2}{p_{w_2}} = (D_3 - D_2)$

$$\overline{T}_{23} = \overline{T}_a = \frac{(T_3 + T_2)}{2} \qquad \overline{\rho}_{23} = \overline{\rho}_a[kg/m^3] = \frac{3.484 \cdot P_I[kPa]}{\overline{T}_{23}[K]}$$

$$\Delta P_{23} = \Delta P_{fric\_23} + \Delta P_{acc\_23} + \Delta P_{grav\_23} =$$
$$= f_{23}\frac{L}{D_{h_2}}\frac{\dot{m}^2}{2\overline{\rho}_{23}A_2^2} + \left(\frac{1}{\rho_3} - \frac{1}{\rho_2}\right)\frac{\dot{m}^2}{A_2^2} + \bar{\rho}_{23}g(-L - 0)$$

For ΔP_{34}, the pressure drop is due to the change of flow direction. In this case is assumed a *loss coefficient* of ($K_{34} = 1.5$):

$$\Delta P_{34} = \Delta P_{vel\_34} + \Delta P_{fric\_34} = \frac{\rho_4(V_4^2 - V_3^2)}{2} + K_{34}\frac{\dot{m}^2}{2\rho_4 A_4^2}$$

For ΔP_{45}, $f_{45} = \bar{f}_t \qquad D_{h_4} = D_{h_5} = D_1$

$$\overline{T}_{45} = \overline{T}_t = \frac{(T_5 + T_4)}{2} \qquad \overline{\rho}_{45} = \overline{\rho}_t[kg/m^3] = \frac{3.484 \cdot P_I[kPa]}{\overline{T}_{45}[K]}$$

$$\Delta P_{45} = \Delta P_{fric\_45} + \Delta P_{acc\_45} + \Delta P_{grav\_45} =$$
$$= f_{45}\frac{L}{D_1}\frac{\dot{m}^2}{2\overline{\rho}_{45}A_4^2} + \left(\frac{1}{\rho_5} - \frac{1}{\rho_4}\right)\frac{\dot{m}^2}{A_4^2} + \rho g\big(0 - (-L)\big)$$

$$\Delta P_{56} = \Delta P_{vel\_56} + \Delta P_{fric\_56} = \frac{\rho_5\big(V_6^2 - V_5^2\big)}{2} + \frac{K_e \cdot \dot{m}^2}{2\rho_5 A_5^2}$$

$\Delta P_{Total} = \Delta P_{12} + \Delta P_{23} + \Delta P_{34} + \Delta P_{45} + \Delta P_{56}$

Hence,

$P_1 = P_I = f(r_1) \quad (The\ DCHE's\ inlet\ pressure\ is\ a\ function\ of\ the\ variable\ r_1)$

$P_2 = P_I - \Delta P_{12}$

$$P_{2-3}(z) = P_I - \Delta P_{12} - \Delta P_{23}(z) =$$
$$= P_I - \Delta P_{12}$$
$$- \left(f_{23}\frac{z}{D_{h_2}}\frac{\dot{m}^2}{2\overline{\rho}_{a_{(2-z)}}A_2^2} + \left(\frac{1}{\rho_{a_{(z)}}} - \frac{1}{\rho_2}\right)\frac{\dot{m}^2}{A_2^2} - \overline{\rho}_{a_{(2-z)}}gz\right)$$

$$P_4 = P_I - \Delta P_{12} - \Delta P_{23}(L) - \Delta P_{34} =$$
$$= P_I - \Delta P_{12}$$
$$- \left(f_{23}\frac{L}{D_{h_2}}\frac{\dot{m}^2}{2\overline{\rho}_{a_{(2-L)}}A_2^2} + \left(\frac{1}{\rho_{a_{(L)}}} - \frac{1}{\rho_2}\right)\frac{\dot{m}^2}{A_2^2} - \overline{\rho}_{a_{(2-L)}}gL\right) - \Delta P_{34}$$

$$P_{4-5}(z) = P_I - \Delta P_{12} - \Delta P_{23}(L) - \Delta P_{34} - \Delta P_{45}(z) =$$
$$= P_I - \Delta P_{12}$$
$$- \left(f_{23} \frac{L}{D_{h_2}} \frac{\dot{m}^2}{2\overline{\rho}_{a_{(2-L)}} A_2^2} + \left(\frac{1}{\rho_{a_{(L)}}} - \frac{1}{\rho_2} \right) \frac{\dot{m}^2}{A_2^2} - \overline{\rho}_{a_{(2-L)}} gL \right) - \Delta P_{34}$$
$$- \left(f_{45} \frac{(L-z)}{D_1} \frac{\dot{m}^2}{2\overline{\rho}_{t_{(4-z)}} A_4^2} + \left(\frac{1}{\rho_{t_{(z)}}} - \frac{1}{\rho_4} \right) \frac{\dot{m}^2}{A_4^2} + \overline{\rho}_{t_{(4-z)}} g(L-z) \right)$$

$$P_6 = P_I - \Delta P_{12} - \Delta P_{23}(L) - \Delta P_{34} - \Delta P_{45}(0) - \Delta P_{56} =$$
$$= P_I - \Delta P_{12}$$
$$- \left(f_{23} \frac{L}{D_{h_2}} \frac{\dot{m}^2}{2\overline{\rho}_{a_{(2-L)}} A_2^2} + \left(\frac{1}{\rho_{a_{(L)}}} - \frac{1}{\rho_2} \right) \frac{\dot{m}^2}{A_2^2} - \overline{\rho}_{a_{(2-L)}} gL \right) - \Delta P_{34}$$
$$- \left(f_{45} \frac{L}{D_1} \frac{\dot{m}^2}{2\overline{\rho}_{t_{(4-0)}} A_4^2} + \left(\frac{1}{\rho_{t_{(0)}}} - \frac{1}{\rho_4} \right) \frac{\dot{m}^2}{A_4^2} + \overline{\rho}_{t_{(4-z)}} gL \right) - \Delta P_{56}$$

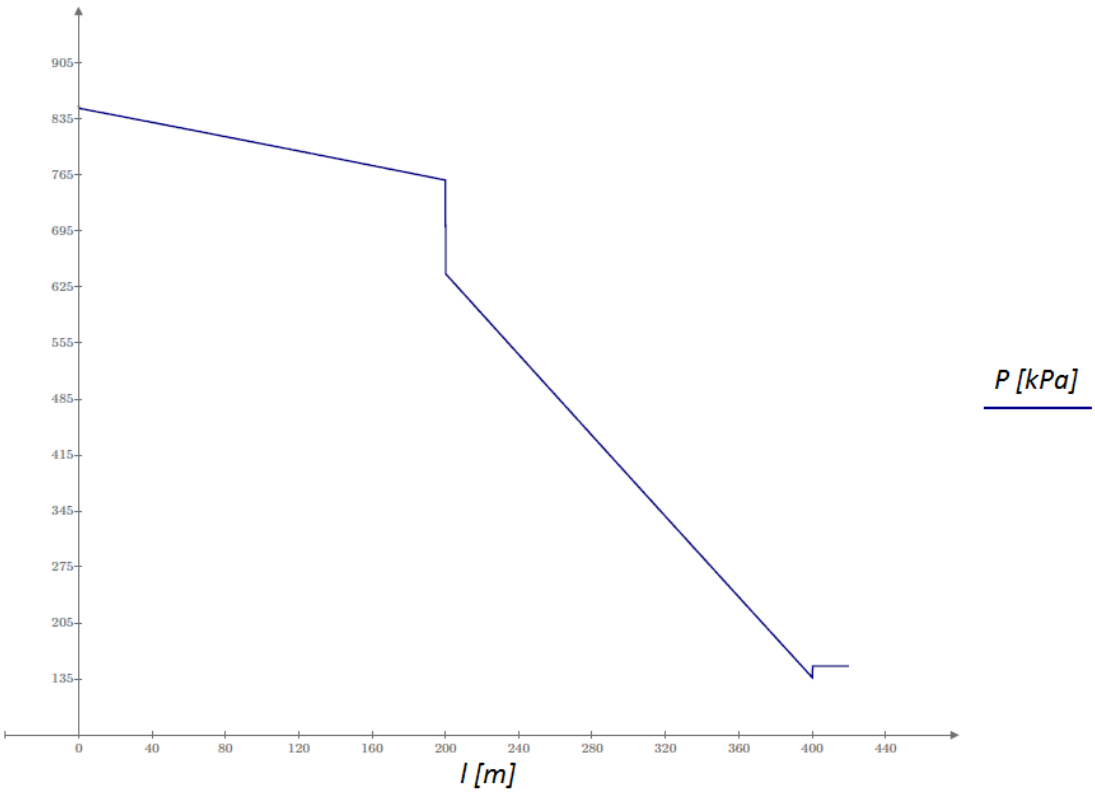

Fig. 9.8: Pressure distribution along the heat exchanger using air as a working fluid.
($r_1 = 25\ mm,\ R_{ip} = 0.03\ m^2K/W\ ,\ P_I = 8.517 \cdot 10^5\ Pa$)

Unlike the pressure profile obtained using water as working fluid, for the air, there is not too much pressure drop due to the gravity. In this case the most of the pressure drop is due to the friction of the fluid flow with the pipe's walls (compare fig. 9.7 and fig. 9.8). In the calculation of the total pressure drop along the heat exchanger the gravity term no affects to the result. This is because the total balance of gravity

pressure drop accounting to the annulus and tubing is zero. In the next table are summarized the value of the different terms of pressure drop for the particular case simulated in fig. 9.8.

Areas					
A_1	A_2	A_3	A_4	A_5	A_6
0.0063 m^2	0.005 m^2	0.005 m^2	0.002 m^2	0.002 m^2	0.0024 m^2
Velocities					
V_1	V_2	V_3	V_4	V_5	V_6
29.491 m/s	36.864 m/s	38.108 m/s	97.557 m/s	96.935 m/s	80.111 m/s
Loss coefficients					
K_c		K_e		K_{34}	
0.1		0.03		1.5	
Friction coefficients, hydraulic diameters and average densities					
f_{23}	D_{h_23}	$\bar{\rho}_a$	f_{45}	D_{h_45}	$\bar{\rho}_t$
0.00296	0.04 m	10.614 kg/m^3	0.00245	0.05 m	10.474 kg/m^3
ΔP_{12} (pressure drop 1-2)					
ΔP_{vel_12}		ΔP_{fric_12}		ΔP_{Total_12}	
$2.64 \cdot 10^3$ Pa		733.378 Pa		$3.374 \cdot 10^3$ Pa	
ΔP_{23} (pressure drop 2-3)					
ΔP_{fric_23}		ΔP_{acc_23}	ΔP_{grav_23}	ΔP_{Total_23}	
$1.102 \cdot 10^5$ Pa		495.272 Pa	$-2.083 \cdot 10^4$ Pa	$8.989 \cdot 10^4$ Pa	
ΔP_{34} (pressure drop 3-4)					
ΔP_{vel_34}		ΔP_{fric_34}		ΔP_{Total_34}	
$4.21 \cdot 10^4$ Pa		$7.453 \cdot 10^4$ Pa		$1.166 \cdot 10^5$ Pa	
ΔP_{45} (pressure drop 4-5)					
ΔP_{fric_45}		ΔP_{acc_45}	ΔP_{grav_45}	ΔP_{Total_45}	
$4.849 \cdot 10^5$ Pa		-633.997 Pa	$2.055 \cdot 10^4$ Pa	$5.048 \cdot 10^5$ Pa	
ΔP_{56} (pressure drop 5-6)					
ΔP_{vel_56}		ΔP_{fric_56}		ΔP_{Total_56}	
$-1.565 \cdot 10^4$ Pa		$1.487 \cdot 10^3$ Pa		$-1.416 \cdot 10^4$ Pa	
$\Delta P_{Total} = \Delta P_{12} + \Delta P_{23} + \Delta P_{34} + \Delta P_{45} + \Delta P_{56} = 7.005 \cdot 10^5$ Pa					

Table 9.2: Pressure drop values along the heat exchanger using air as a working fluid ($r_1 = 25\ mm,\ R_{ip} = 0.03\ m^2K/W\ ,\ P_I = 8.517 \cdot 10^5\ Pa$).

In the next section will be analyzed the pressure distribution along the heat exchanger for different values of the inner's pipe diameter.

DCHE's inlet pressure distribution and analysis of the pressure distribution along the heat exchanger

As is mentioned in section 6.4, the DCHE's inlet pressure depends on the value of the inner radius of the inner pipe (r_1). The DCHE's inlet pressure is calculated using an iterative process. The DCHE's outlet pressure is fixed and calculating the total of the pressure drop along the heat exchanger is determined the inlet pressure. In the case of water the outlet pressure (P_{OUT}) is assumed to be *1 atm* and for the air *1.5 atm*. In fig. 9.9 and fig. 9.10 are shown the results.

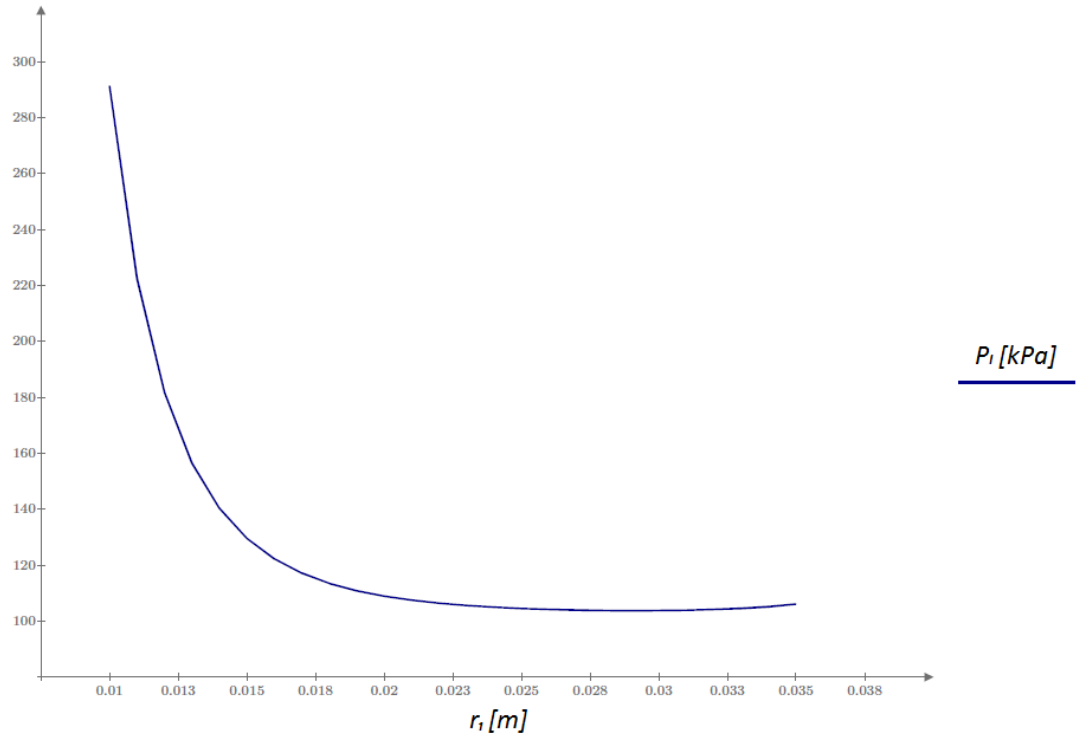

Fig. 9.9: DCHE's inlet pressure distribution according with the value of the inner radius of the inner pipe (r_1) using water as a working fluid.

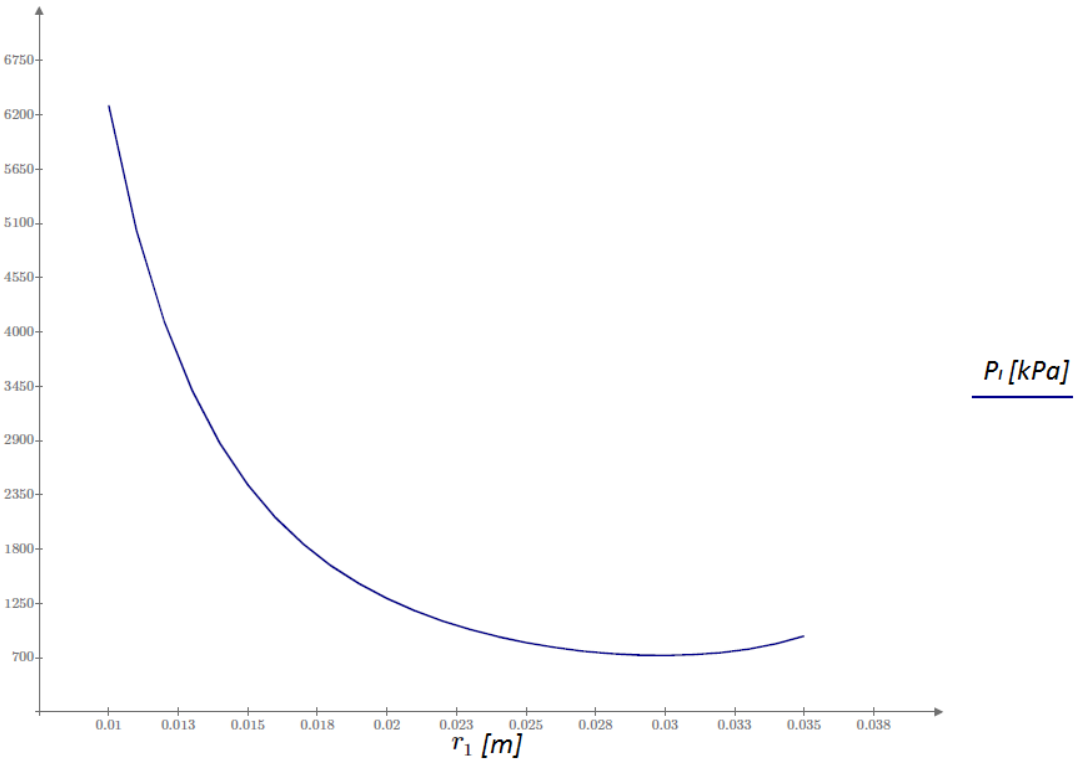

Fig. 9.10: DCHE's inlet pressure distribution according with the value of the inner radius of the inner pipe (r_1) using air as a working fluid.

Comparing the two previous graphs is concluded that the inlet pressure in the case of the air is higher than in the case of the water. Therefore the total of the pressure drop is higher for the air than using water as a working fluid. The reason is that the density of the air is about one thousand times lower than the density of the water and consequently the friction effects are much significant.

Below is analyzed the pressure distribution along the heat exchanger using air as a working fluid for different configurations according with the variable (r_1).

The pressure drop in the annulus of the downhole, coaxial heat exchanger is expressed as:

$$\Delta P_a = \Delta P_{a_{fric}} + \Delta P_{a_{\Delta\rho}} + \Delta P_{a_{grav}} = \bar{f}_a \frac{L}{D_{h_a}} \frac{\dot{m}^2}{2\bar{\rho}_a {A_a}^2} + \left(\frac{1}{\rho_{a_L}} - \frac{1}{\rho_{a_0}}\right)\frac{\dot{m}^2}{{A_a}^2} + \bar{\rho}_a g(0 - L)$$

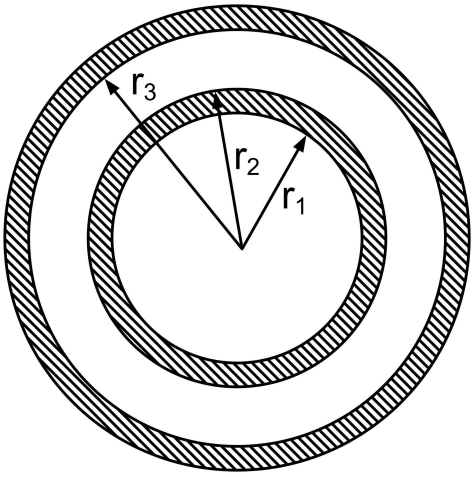

Fig. 9.11: DCHE radius description.

$$D_{h_a} = 2 \cdot (r_3 - r_2)$$

$$\bar{\rho}_a = \frac{3.484 \cdot P_I[kPa]}{\bar{T}_a}$$

$$A_a = \pi(r_3^2 - r_2^2)$$

$$\rho_{a_L} = \frac{3.484 \cdot P_I[kPa]}{T_{a_L}}$$

$$\rho_{a_0} = \frac{3.484 \cdot P_I[kPa]}{T_{a_0}}$$

Where, P_I is the DCHE's inlet pressure.

The pressure drop in the tubing is expressed as:

$$\Delta P_t = \Delta P_{t_{fric}} + \Delta P_{t_{\Delta\rho}} + \Delta P_{t_{grav}} = \bar{f}_t \frac{L}{D_{h_t}} \frac{\dot{m}^2}{2\bar{\rho}_t {A_t}^2} + \left(\frac{1}{\rho_{t_0}} - \frac{1}{\rho_{t_L}}\right)\frac{\dot{m}^2}{{A_t}^2} + \bar{\rho}_t g(L - 0)$$

Where,

$$D_{h_t} = 2r_1$$

$$\bar{\rho}_t = \frac{3.484 \cdot P_I[kPa]}{\bar{T}_t}$$

$$A_t = \pi r_1^2$$

$$\rho_{t_0} = \frac{3.484 \cdot P_I[kPa]}{T_{t_0}}$$

$$\rho_{t_L} = \frac{3.484 \cdot P_I[kPa]}{T_{t_L}}$$

If we compare the pressure drop due to the friction with the walls in the annulus region and in the tubing region we obtain the next relation:

$$\frac{\Delta P_{t_{fric}}}{\Delta P_{a_{fric}}} = \frac{\bar{f}_t \frac{L}{D_{h_t}} \frac{\dot{m}^2}{2\bar{\rho}_t {A_t}^2}}{\bar{f}_a \frac{L}{D_{h_a}} \frac{\dot{m}^2}{2\bar{\rho}_a {A_a}^2}} = \frac{\bar{f}_t \cdot L \cdot \dot{m}^2 \cdot D_{h_a} \cdot 2 \cdot \bar{\rho}_a \cdot {A_a}^2}{\bar{f}_a \cdot L \cdot \dot{m}^2 \cdot D_{h_t} \cdot 2 \cdot \bar{\rho}_t \cdot {A_t}^2}$$

$(\bar{f}_t \cong \bar{f}_a \quad ; \quad \bar{\rho}_t \cong \bar{\rho}_a)$

$$\Rightarrow \frac{\Delta P_{t_{fric}}}{\Delta P_{a_{fric}}} \cong \frac{D_{h_a} \cdot A_a^2}{D_{h_t} \cdot A_t^2} = \frac{(r_3 - r_2)^3 \cdot (r_3 + r_2)^2}{r_1^5} = \underbrace{\text{"}\phi\text{"}}_{\substack{defi \\ nition}}$$

· $r_1 = 0.010\, m;\ r_2 = 0.015\, m;\ r_3 = 0.05\, m\ (P_I = 6.298 \cdot 10^6\ Pa)$

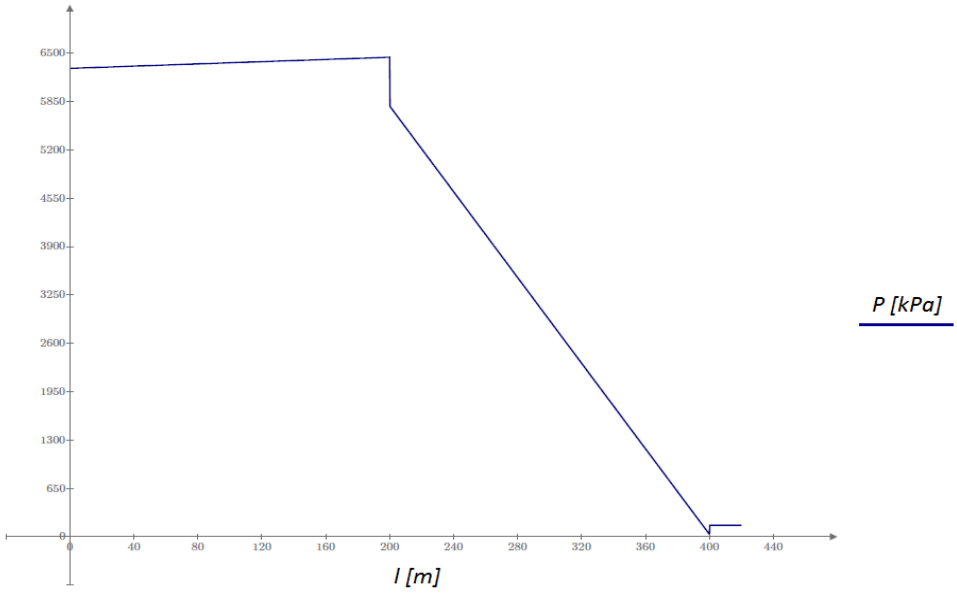

Fig. 9.12: Pressure distribution along the heat exchanger using air as a working fluid.
($r_1 = 10\, mm,\ R_{ip} = 0.03\ m^2K/W\ ,\ P_I = 6.298 \cdot 10^6\ Pa$)

In fig. 9.12 can be observed the great different between the pressure drop in the annulus and the pressure drop in the tubing. The reason is the smallest cross section area of the inner tube. Even, in the annulus, the pressure is increasing. This is because

the pressure gain due to the gravity is higher than the pressure drop due to the friction. Below are quantified the obtained results. Note the high value of the term ϕ for this particular configuration and the relation of this term with the next ratio: $\frac{\Delta P_{t_{fric}}}{\Delta P_{a_{fric}}}$

$\Delta P_{a_{fric}} = 4.094 \cdot 10^3\ Pa$
$\Delta P_{a_{\Delta\rho}} = 29.382\ Pa$
$\Delta P_{a_{grav}} = -1.539 \cdot 10^5\ Pa$
$\Delta P_a = -1.5 \cdot 10^5\ Pa\ (increasing)$

$\bar{f}_a = 0.002871\ ;\ \bar{f}_t = 0.002143 \Longrightarrow \bar{f}_a \cong \bar{f}_t$

$\bar{\rho}_a = 78.447\ kg/m^3\ ;\ \bar{\rho}_t = 77.413 \Longrightarrow \bar{\rho}_a \cong \bar{\rho}_t$

$D_{h_a} = 0.07\ m\ ;\ D_{h_t} = 0.02\ m$

$A_a = 0.007147\ m^2\ ;\ A_t = 0.000314\ m^2$

$\Delta P_{t_{fric}} = 5.609 \cdot 10^6\ Pa$
$\Delta P_{t_{\Delta\rho}} = -1.409 \cdot 10^3\ Pa$
$\Delta P_{t_{grav}} = 1.519 \cdot 10^5\ Pa$
$\Delta P_t = 5.76 \cdot 10^6\ Pa\ (decreasing)$

$$\frac{\Delta P_{t_{fric}}}{\Delta P_{a_{fric}}} = \underline{1375} \quad ; \quad \phi = \frac{D_{h_a} \cdot A_a^2}{D_{h_t} \cdot A_t^2} = \underline{1811}$$

- $\underline{r_1 = 0.025\ m;\ r_2 = 0.030\ m;\ r_3 = 0.05\ m\ (P_I = 8.517 \cdot 10^5\ Pa)}$

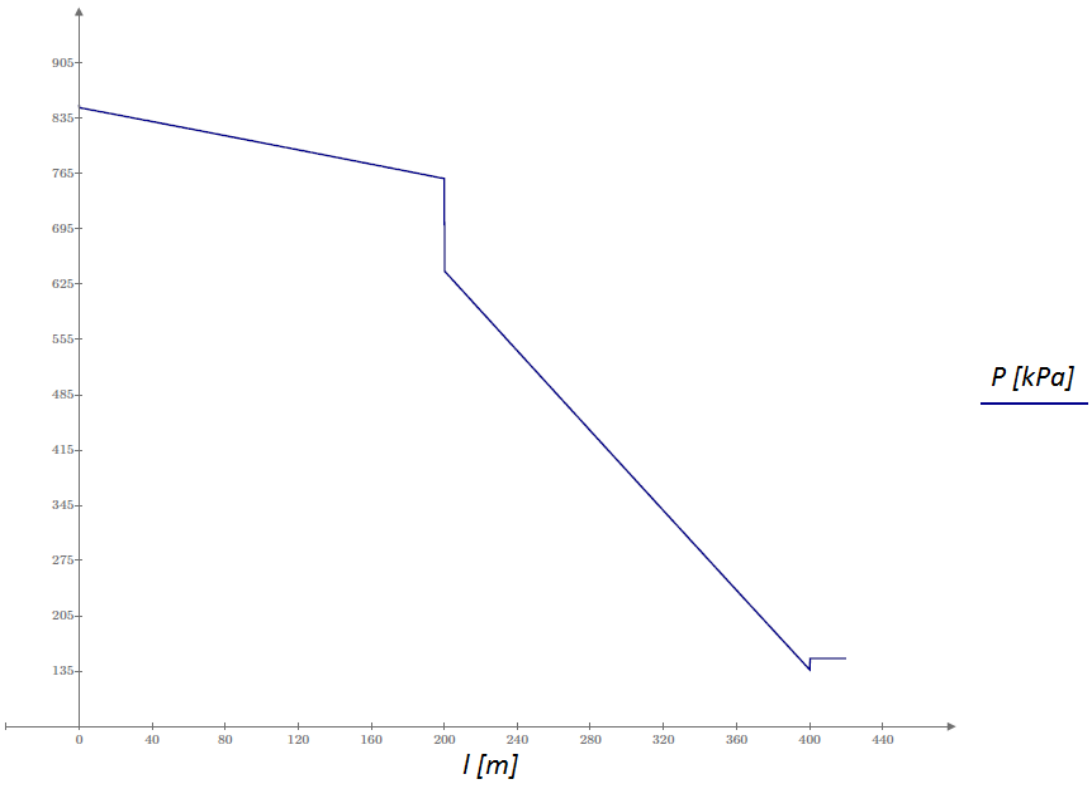

Fig. 9.13: Pressure distribution along the heat exchanger using air as a working fluid.
($r_1 = 25\ mm,\ R_{ip} = 0.03\ m^2K/W\ ,\ P_I = 8.517 \cdot 10^5\ Pa$)

Although the pressure drop in the tubing is higher than in the annulus (fig. 9.13) the difference is not as significant as in the previous case (compare fig. 9.12 and fig. 9.13). The reason lies in the increase of the cross sectional area of the inner pipe. Note, in the below results, that the relation ϕ decreased in comparison with the previous case.

$\Delta P_{a_{fric}} = 1.102 \cdot 10^5\ Pa$
$\Delta P_{a_{\Delta\rho}} = 495.272\ Pa$
$\Delta P_{a_{grav}} = -2.083 \cdot 10^4\ Pa$
$\Delta P_a = 8.989 \cdot 10^4\ Pa\ (decreasing)$

$\bar{f}_a = 0.002956\ ;\ \bar{f}_t = 0.002448 \Longrightarrow \bar{f}_a \cong \bar{f}_t$

$\bar{\rho}_a = 10.614\ kg/m^3\ ;\ \bar{\rho}_t = 10.474 \Longrightarrow \bar{\rho}_a \cong \bar{\rho}_t$

$D_{h_a} = 0.04\ m\ ;\ D_{h_t} = 0.05\ m$

$A_a = 0.005027\ m^2\ ;\ A_t = 0.001963\ m^2$

$\Delta P_{t_{fric}} = 4.849 \cdot 10^5\ Pa$
$\Delta P_{t_{\Delta\rho}} = -633.997\ Pa$
$\Delta P_{t_{grav}} = 2.055 \cdot 10^4\ Pa$
$\Delta P_t = 5.048 \cdot 10^5\ Pa\ (decreasing)$

$$\frac{\Delta P_{t_{fric}}}{\Delta P_{a_{fric}}} = \underline{5.616} \quad ; \quad \phi = \frac{D_{h_a} \cdot A_a^2}{D_{h_t} \cdot A_t^2} = \underline{4.399}$$

- $\underline{r_1 = 0.030\ m;\ r_2 = 0.035\ m;\ r_3 = 0.05\ m\ (P_I = 7.223 \cdot 10^5\ Pa)}$

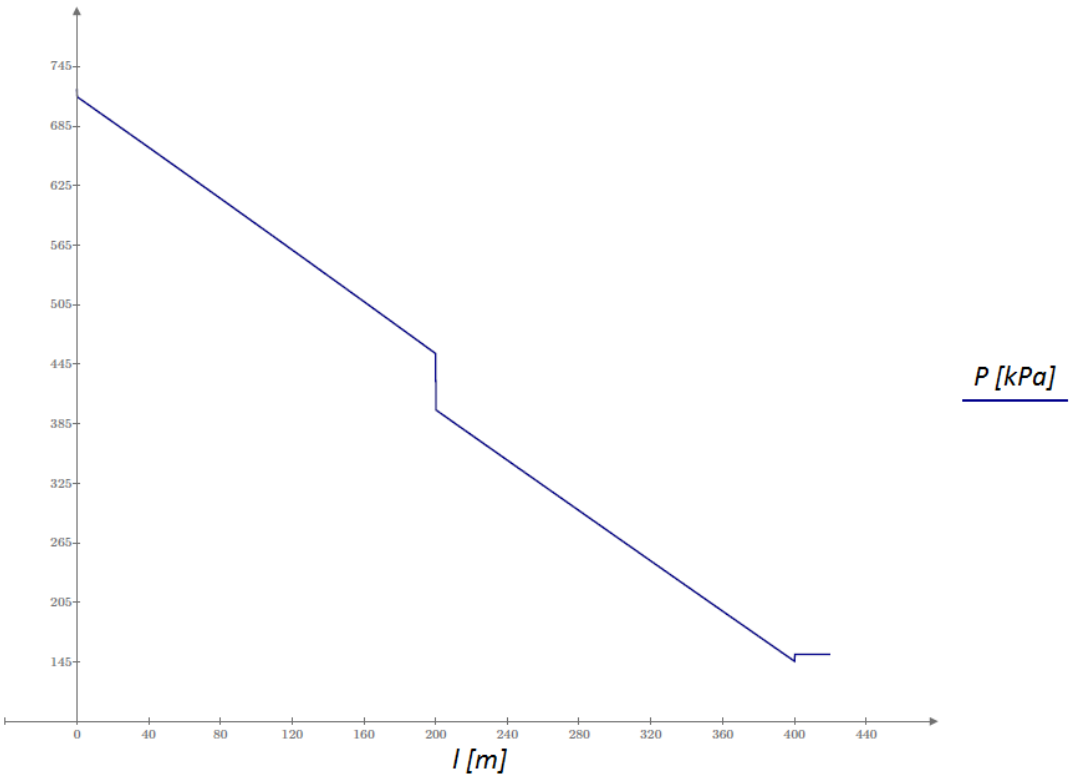

Fig. 9.14: Pressure distribution along the heat exchanger using air as a working fluid.
($r_1 = 30\ mm,\ R_{ip} = 0.03\ m^2K/W\ ,\ P_I = 7.223 \cdot 10^5\ Pa$)

In this case the pressure drop along the annulus is almost the same than in the tubing (fig. 9.14). This appreciation can be also observed through the analysis of the relation ϕ, noting that the calculation of this term is a perfect way to know how to vary the pressure drop along the inner tube in comparison with the annulus. This particular configuration corresponds with the minimal pressure drop case.

$\Delta P_{a_{fric}} = 2.757 \cdot 10^5\ Pa$
$\Delta P_{a_{\Delta\rho}} = 952.415\ Pa$
$\Delta P_{a_{grav}} = -1.766 \cdot 10^4\ Pa$
$\Delta P_a = 2.59 \cdot 10^5\ Pa\ (decreasing)$

$\bar{f}_a = 0.002986\ ;\ \bar{f}_t = 0.002518 \Longrightarrow \bar{f}_a \cong \bar{f}_t$

$\bar{\rho}_a = 9.003\ kg/m^3\ ;\ \bar{\rho}_t = 8.884 \Longrightarrow \bar{\rho}_a \cong \bar{\rho}_t$

$D_{h_a} = 0.03\ m\ ;\ D_{h_t} = 0.06\ m$

$A_a = 0.004006\ m^2\ ;\ A_t = 0.002827\ m^2$

$\Delta P_{t_{fric}} = 2.364 \cdot 10^5\ Pa$
$\Delta P_{t_{\Delta\rho}} = -426.454\ Pa$
$\Delta P_{t_{grav}} = 1.743 \cdot 10^4\ Pa$
$\Delta P_t = 2.534 \cdot 10^5\ Pa\ (decreasing)$

$$\frac{\Delta P_{t_{fric}}}{\Delta P_{a_{fric}}} = \underline{0.858} \quad ; \quad \phi = \frac{D_{h_a} \cdot A_a^2}{D_{h_t} \cdot A_t^2} = \underline{1.003}$$

- $\underline{r_1 = 0.035\ m;\ r_2 = 0.040\ m;\ r_3 = 0.05\ m\ (P_I = 9.198 \cdot 10^5\ Pa)}$

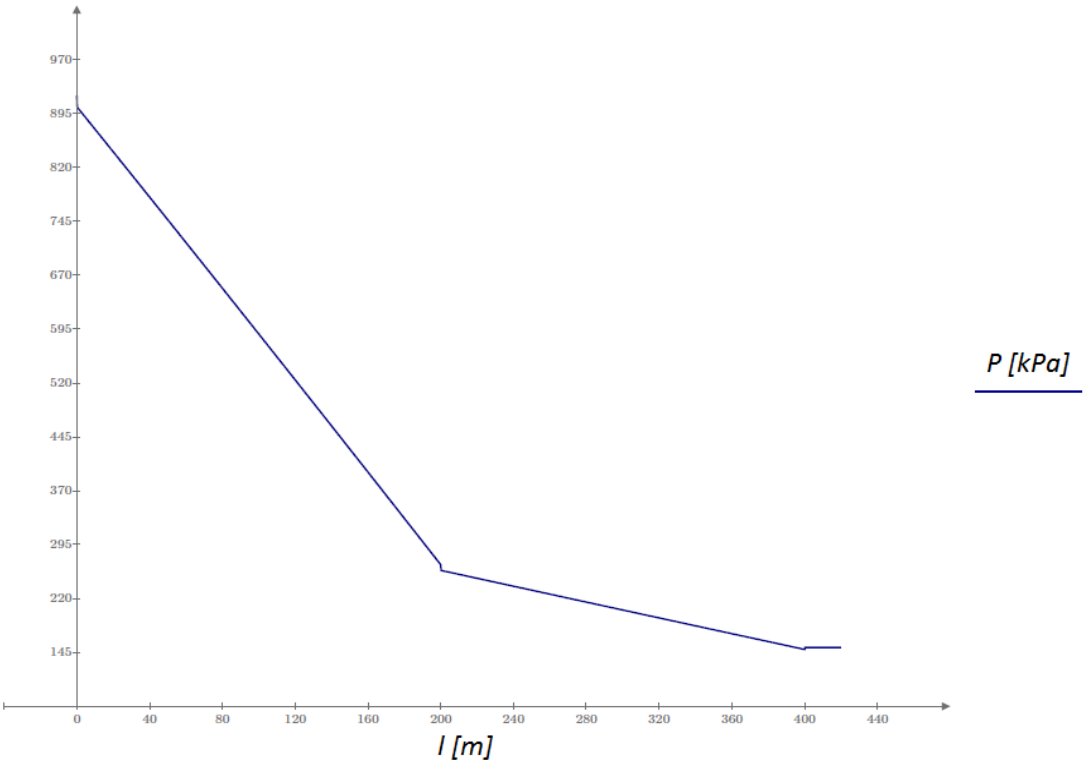

Fig. 9.15: Pressure distribution along the heat exchanger using air as a working fluid.
($r_1 = 35\ mm,\ R_{ip} = 0.03\ m^2K/W\ ,\ P_I = 9.198 \cdot 10^5\ Pa$)

Now, for this particular configuration the pressure drop in the annulus is higher than in the tubing (fig. 9.15). Increasing the diameter of the inner pipe, the annular cross sectional area is decreasing and consequently the friction effects and the pressure drop in the annulus are increasing. Note that now the value of the term ϕ is less than 1.

$\Delta P_{a_{fric}} = 6.583 \cdot 10^5\ Pa$
$\Delta P_{a_{\Delta\rho}} = 1.551 \cdot 10^3\ Pa$
$\Delta P_{a_{grav}} = -2.249 \cdot 10^4\ Pa$
$\Delta P_a = 6.373 \cdot 10^5\ Pa\ (decreasing)$

$\bar{f}_a = 0.003017\ ;\ \bar{f}_t = 0.002582 \Longrightarrow \bar{f}_a \cong \bar{f}_t$

$\bar{\rho}_a = 11.465\ kg/m^3\ ;\ \bar{\rho}_t = 11.314 \Longrightarrow \bar{\rho}_a \cong \bar{\rho}_t$

$D_{h_a} = 0.02\ m\ ;\ D_{h_t} = 0.07\ m$

$A_a = 0.002827\ m^2\ ;\ A_t = 0.003848\ m^2$

$\Delta P_{t_{fric}} = 8.804 \cdot 10^4\ Pa$
$\Delta P_{t_{\Delta\rho}} = -207.882\ Pa$
$\Delta P_{t_{grav}} = 2.22 \cdot 10^4\ Pa$
$\Delta P_t = 1.1 \cdot 10^5\ Pa\ (decreasing)$

$$\frac{\Delta P_{t_{fric}}}{\Delta P_{a_{fric}}} = \underline{0.134} \quad ; \quad \phi = \frac{D_{h_a} \cdot A_a^2}{D_{h_t} \cdot A_t^2} = \underline{0.154}$$

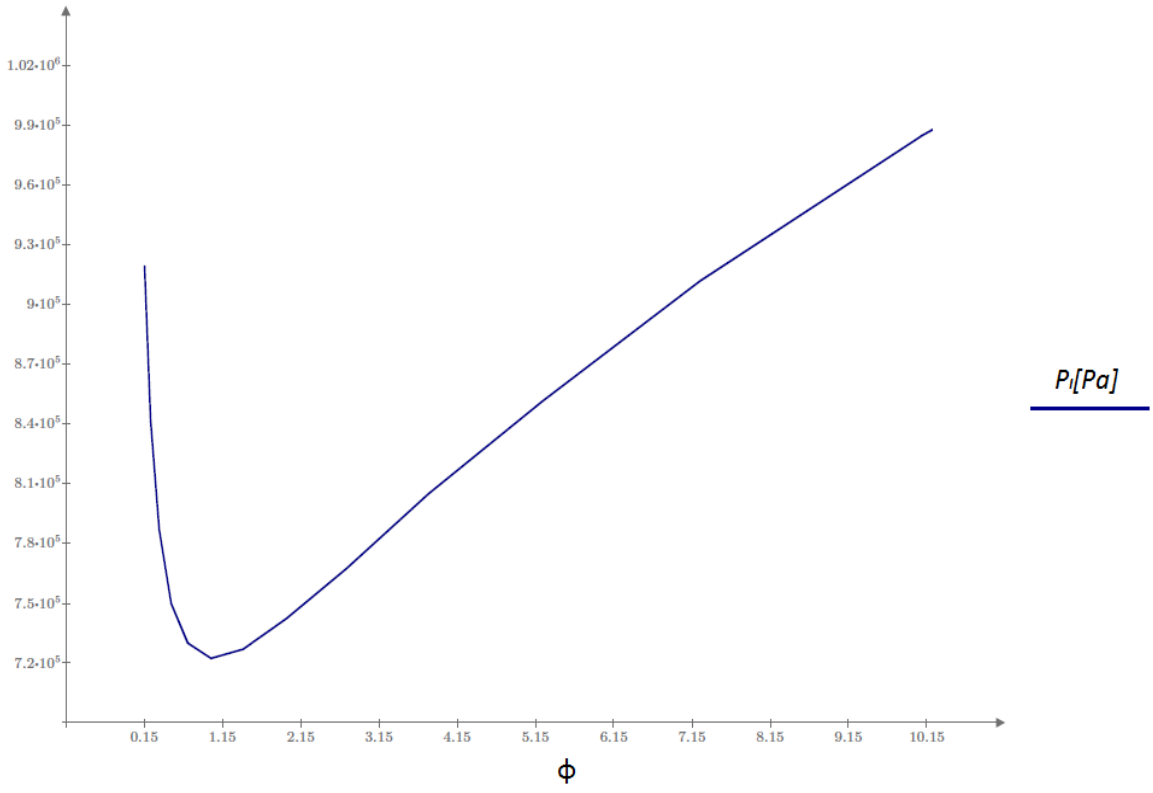

Fig. 9.16: Detail of the DCHE's inlet pressure distribution using air as a working fluid according with the relation ϕ.

In fig. 9.16 is shown how vary the DCHE's inlet pressure according with the relation ϕ. From this figure is again concluded that the minimum of the DCHE's inlet pressure required (minimum pressure drop) corresponds for the configuration that is done the next relation:

$$\phi = \frac{D_{h_a} \cdot A_a^2}{D_{h_t} \cdot A_t^2} = 1$$

This configuration corresponds to the inner radius equal to:

$$r_1 = 30\ mm = 0.03\ m$$

Chapter 10

Determination of the local and total rate of entropy generation in the considered heat exchanger

The entropy balance for any control volume between two states is written as:

$$\frac{dS}{dt} + \sum_{out} \dot{m}_{out} \cdot s_{out} - \sum_{in} \dot{m}_{in} \cdot s_{in} = \int_{A_s} \frac{\dot{Q} dA}{T_s} + \dot{S}_{gen} \quad \left[\frac{W}{K}\right] \qquad (10.1)$$

Where, out refers to the output stream in the control of volume and in refers to the input stream in the control of volume.
$\dot{Q}$ is the heat rate transferred to the stream, T_s is the surface temperature of the control of volume and $\dot{S}_{gen}$ is the rate of entropy generation.

For steady-state $\left(\frac{dS}{dt} = 0\right)$ equation (10.1) becomes:

$$\sum_{out} \dot{m}_{out} \cdot s_{out} - \sum_{in} \dot{m}_{in} \cdot s_{in} = \int_{A_s} \frac{\dot{Q} dA}{T_s} + \dot{S}_{gen} \quad \left[\frac{W}{K}\right] \qquad (10.2)$$

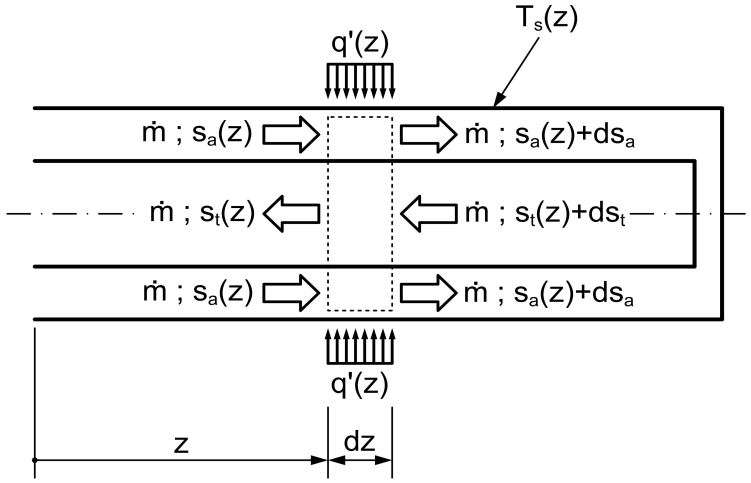

Fig. 10.1: Schematic of the entropy balance for the element length of the DCHE.

For the element length of the downhole, coaxial heat exchanger the entropy balance is expressed in equation (10.3) (fig. 10.1). Axial heat conduction is not considered in the whole of the volume of control.

$$\dot{m}(s_a(z)+ds_a)+\dot{m}s_t(z)-\dot{m}s_a(z)-\dot{m}(s_t(z)+ds_t)=\frac{q'(z)}{T_s(z)}dz+\dot{S}'_{gen}(z)dz \Longrightarrow$$

$$\Longrightarrow \dot{m}ds_a-\dot{m}ds_t=\frac{q'(z)}{T_s(z)}dz+\dot{S}'_{gen}(z)dz$$

$$\Longrightarrow \boxed{\dot{S}'_{gen}(z)=\dot{m}\frac{ds_a}{dz}-\dot{m}\frac{ds_t}{dz}-\frac{q'(z)}{T_s(z)}} \tag{10.3}$$

In this case the heat transfer rate per unit length (q') and the surface temperature (T_s) are not constant along the heat exchanger. Hence must be calculated the heat transfer rate (fig. 10.3 and fig. 10.6) and surface temperature distribution (fig. 10.4 and fig. 10.7) along the external heat exchanger's pipe. The heat transfer rate per unit length is calculated as:

$$q'(z)=2\pi r_3 U_{r3}[T_\infty(z)-T_a(z)] \tag{10.4}$$

The surface temperature distribution is calculated as:

$$T_s(z)=T_\infty(z)-\frac{q'(z)}{2\pi r_3 U_{r3'}} \tag{10.5}$$

Where,

$$U_{r3'}=\frac{1}{\frac{r_3 ln(r_6/r_5)}{\lambda_{rock}}+\frac{r_3 ln(r_5/r_4)}{\lambda_c}+\frac{r_3 ln(r_4/r_3)}{\lambda_{op}}}$$

The DCHE structure can be approximate in a simplified finite element model. Taking 801 nodes and 800 elements the schematic of the model for the DCHE external pipe is shown in figure 10.2.

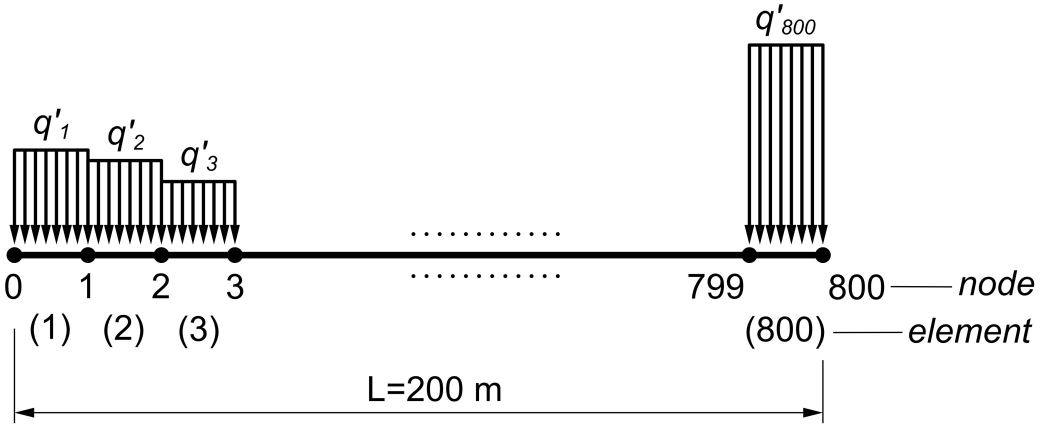

Fig. 10.2: Simplified finite element model for the DCHE external pipe.

Now equation (10.3) can be expressed as:

$$\dot{S}'_{gen}(z) = \dot{m}\Delta s'_a(z) - \dot{m}\Delta s'_t(z) - \frac{q'(z)}{T_s(z)} \quad \left[\frac{W}{m \cdot K}\right] \tag{10.6}$$

Multiplying equation (10.6) by Δz:

$$\dot{S}_{gen}(z) = \dot{m}\Delta s_a(z) - \dot{m}\Delta s_t(z) - \frac{q'(z)}{T_s(z)}\Delta z \quad \left[\frac{W}{K}\right] \tag{10.7}$$

$$\begin{cases} \dot{S}_{gen_1} = \dot{m}\Delta s_{a_1} - \dot{m}\Delta s_{t_1} - \dfrac{q'_1}{T_{s_1}}\Delta z = \dot{m}\left(s_{a_1} - s_{a_0}\right) - \dot{m}\left(s_{t_1} - s_{t_0}\right) - \dfrac{q'_1}{T_{s_1}}\Delta z \\ \dot{S}_{gen_2} = \dot{m}\Delta s_{a_2} - \dot{m}\Delta s_{t_2} - \dfrac{q'_2}{T_{s_2}}\Delta z = \dot{m}\left(s_{a_2} - s_{a_1}\right) - \dot{m}\left(s_{t_2} - s_{t_1}\right) - \dfrac{q'_2}{T_{s_2}}\Delta z \\ \vdots \\ \dot{S}_{gen_i} = \dot{m}\Delta s_{a_i} - \dot{m}\Delta s_{t_i} - \dfrac{q'_i}{T_{s_i}}\Delta z = \dot{m}\left(s_{a_i} - s_{a_{(i-1)}}\right) - \dot{m}\left(s_{t_i} - s_{t_{(i-1)}}\right) - \dfrac{q'_i}{T_{s_i}}\Delta z \\ \vdots \\ \dot{S}_{gen_{800}} = \dot{m}\Delta s_{a_{800}} - \dot{m}\Delta s_{t_{800}} - \dfrac{q'_{800}}{T_{s_{800}}}\Delta z = \dot{m}\left(s_{a_{800}} - s_{a_{799}}\right) - \dot{m}\left(s_{t_{800}} - s_{t_{799}}\right) - \dfrac{q'_{800}}{T_{s_{800}}}\Delta z \end{cases}$$

Where,

$$\Delta z = \frac{200\ m}{800\ elements} = 0.25\ {}^{m}/_{element}$$

In the case of water (incompressible) as a working fluid the entropy of a state is calculated as:

$$s = c_p ln\frac{T[K]}{T_{ref}[K]} \quad \left[\frac{J}{kg \cdot K}\right] \tag{10.8}$$

Where,

$$T_{ref} = T_{\substack{triple \\ point}} = 273.16\ K$$

In the case of air as a working fluid and assuming perfect gas the entropy of a state is calculated as:

$$s = \int_{T_{ref}[K]}^{T[K]} \frac{c_p(T)}{T}dT - R\int_{P_{ref}}^{P} \frac{dP}{P} = \int_{T_{ref}[K]}^{T[K]} \frac{c_p(T)}{T}dT - Rln\left(\frac{P}{P_{ref}}\right)\left[\frac{J}{kg \cdot K}\right] \tag{10.9}$$

Where,

$$\begin{cases} T_{ref} = 298.15\ K \\ P_{ref} = 0.1\ MPa \\ R_{air} = 286.9\ J/kg \cdot K \end{cases}$$

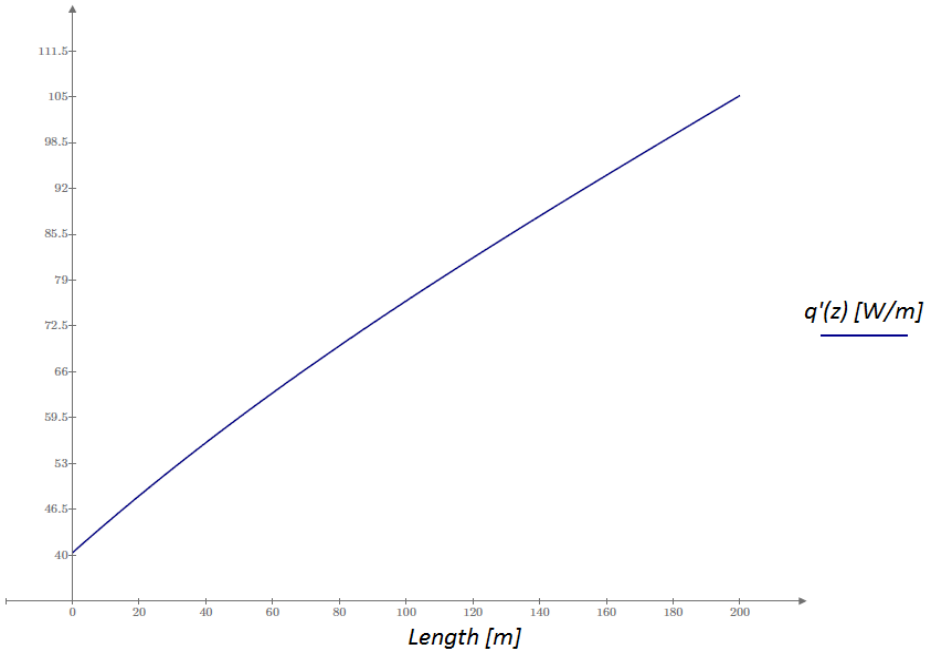

Fig. 10.3: Distribution of the heat transfer rate per unit length along the external DCHE pipe using water as working fluid ($r_1 = 30\ mm,\ R_{ip} = 0.02\ m^2K/W\ ,\ P_I = 1.038 \cdot 10^5\ Pa$).

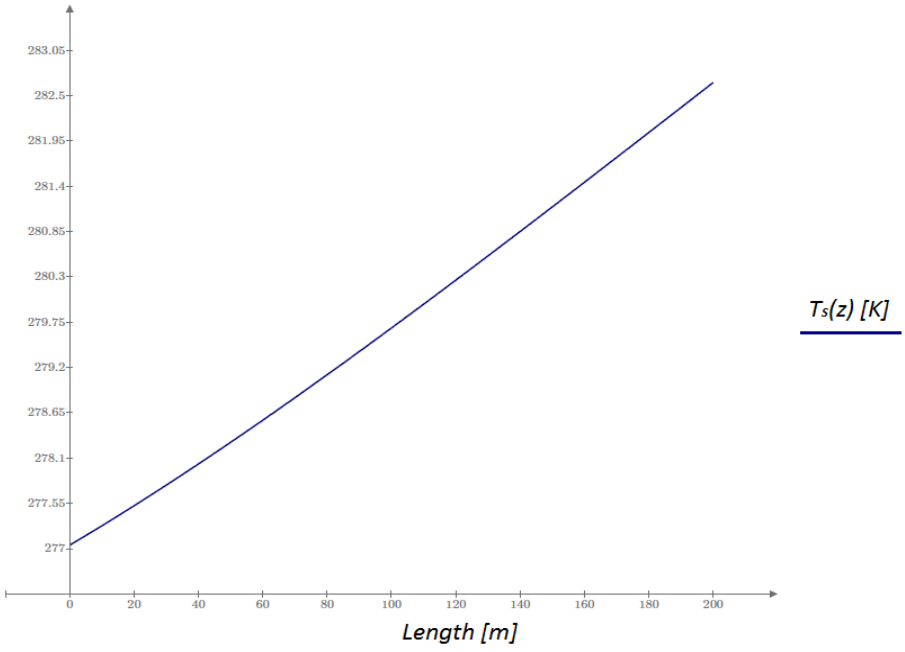

Fig. 10.4: Surface temperature distribution along the external DCHE pipe using water as working fluid ($r_1 = 30\ mm,\ R_{ip} = 0.02\ m^2K/W\ ,\ P_I = 1.038 \cdot 10^5\ Pa$).

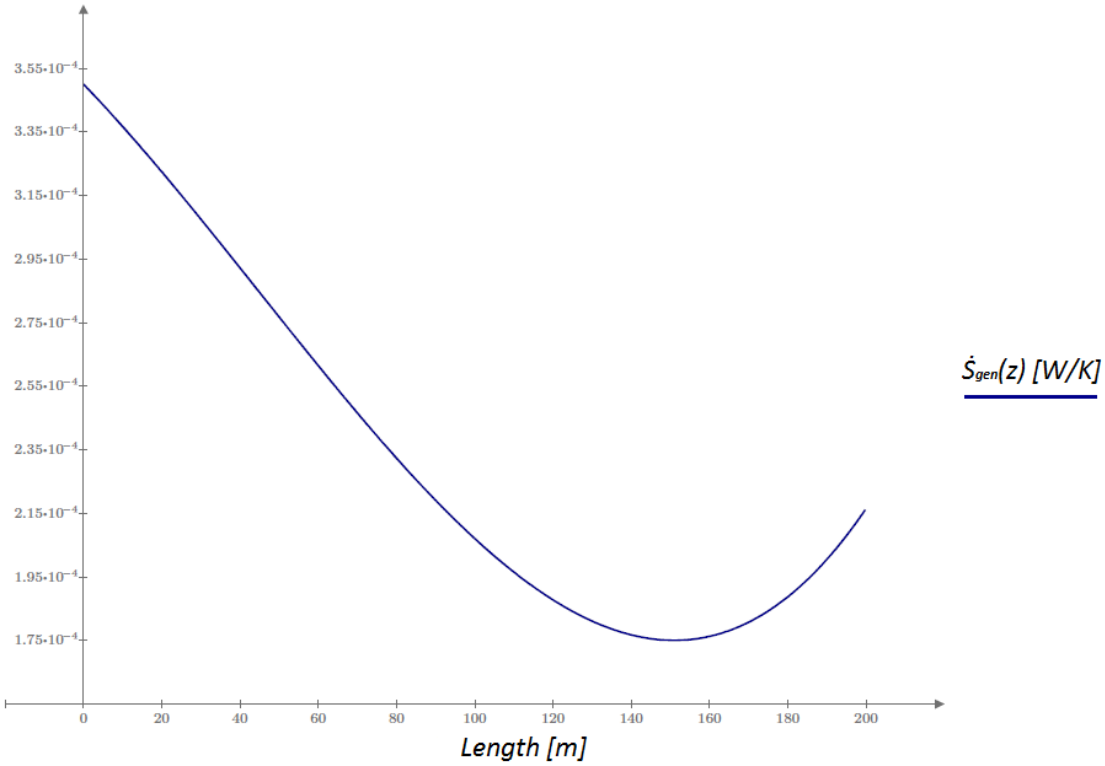

Fig. 10.5: Local rate of entropy generation distribution along the heat exchanger using water as working fluid ($r_1 = 30\ mm,\ R_{ip} = 0.02\ m^2K/W\ ,\ P_l = 1.038 \cdot 10^5\ Pa$).

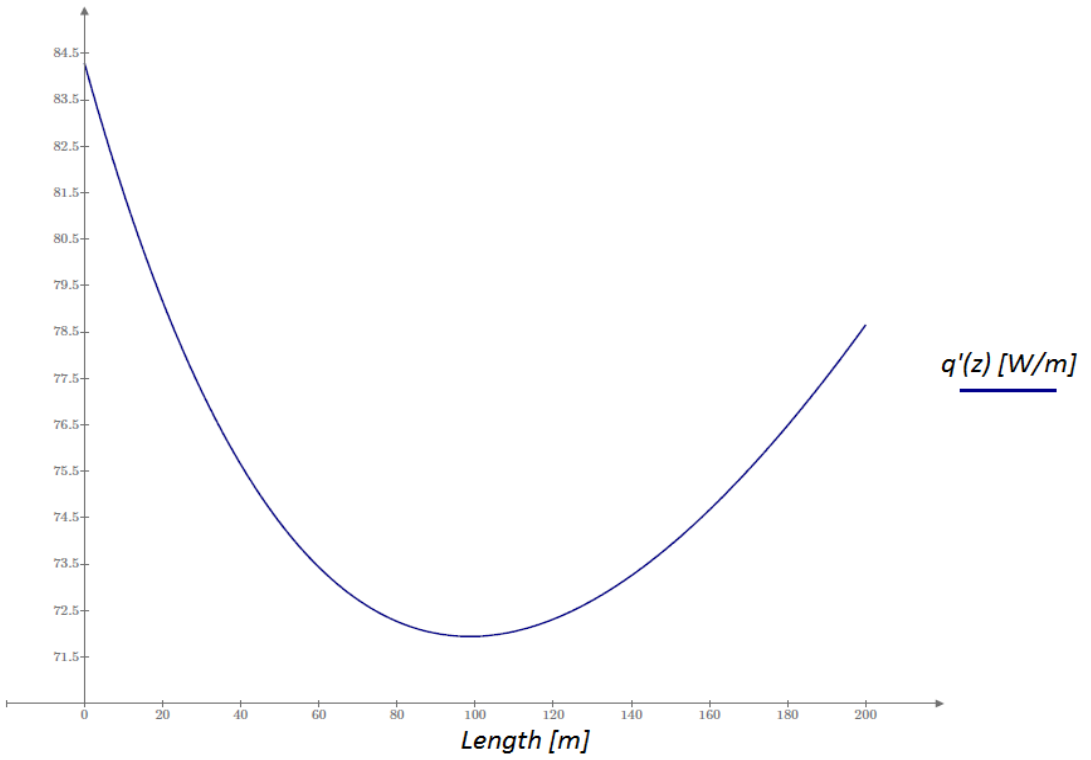

Fig. 10.6: Distribution of the heat transfer rate per unit length along the external DCHE pipe using air as working fluid ($r_1 = 25\ mm,\ R_{ip} = 0.03\ m^2K/W\ ,\ P_l = 8.517 \cdot 10^5\ Pa$).

Figure 10.5 shows the local rate of entropy generation distribution using water as working fluid. Integrating along the whole of the heat exchanger the total rate of entropy generation is obtained.
For, $\left(r_1 = 25\ mm,\ R_{ip} = 0.03\ m^2K/W\,,\ P_I = 8.517 \cdot 10^5\ Pa\right)$:

$$\dot{S}_{gen_{0-L}} = \int_0^L \dot{S}'_{gen}(z)dz \cong \sum_{i=1}^{800} \dot{S}'_{gen} \cdot \Delta z = \boxed{0.6124\ \frac{W}{K}}$$

This case has been chosen just to illustrate the order of magnitude of the entropy generated along the heat exchanger using water as working medium.

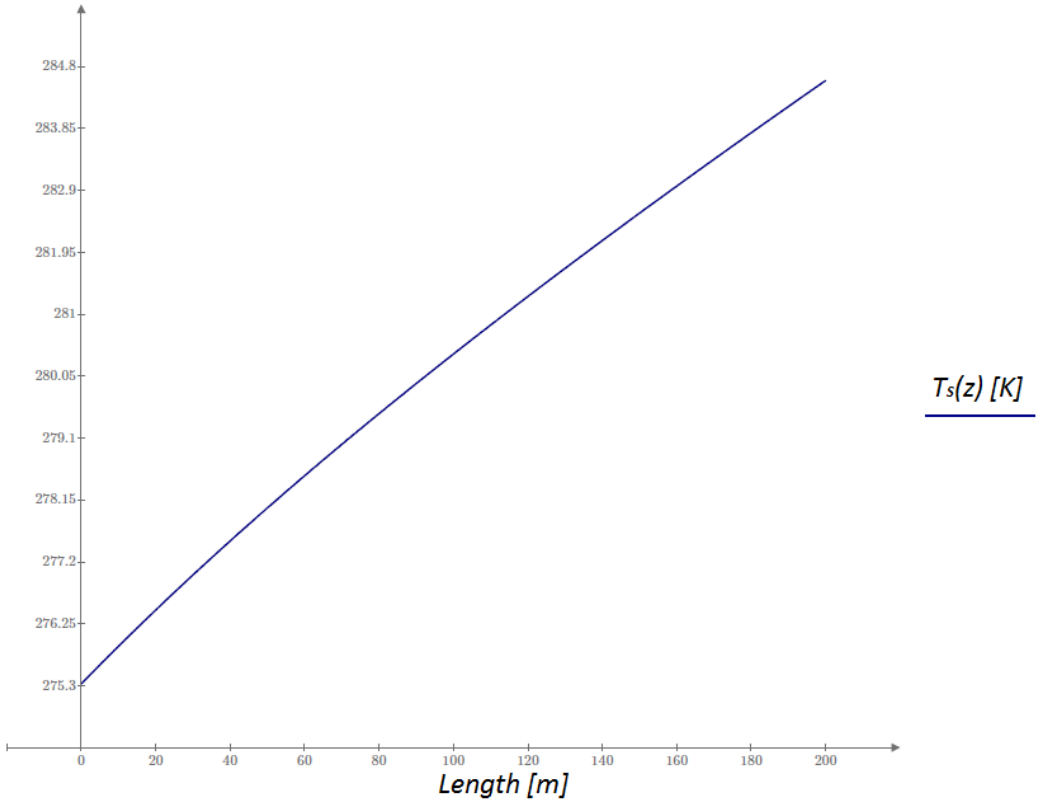

Fig. 10.7: Surface temperature distribution along the external DCHE pipe using air as working fluid $(r_1 = 25\ mm,\ R_{ip} = 0.03\ m^2K/W\,,\ P_I = 8.517 \cdot 10^5\ Pa)$.

Figure 10.8 shows the local rate of entropy generation distribution using air as working fluid. Integrating along the whole of the heat exchanger the total rate of entropy generation is obtained for this particular case represented in figure. 10.8. Hence:

$$\dot{S}_{gen_{0-L}} = \int_0^L \dot{S}'_{gen}(z)dz \cong \sum_{i=1}^{800} \dot{S}'_{gen} \cdot \Delta z = \boxed{951.44\ \frac{W}{K}}$$

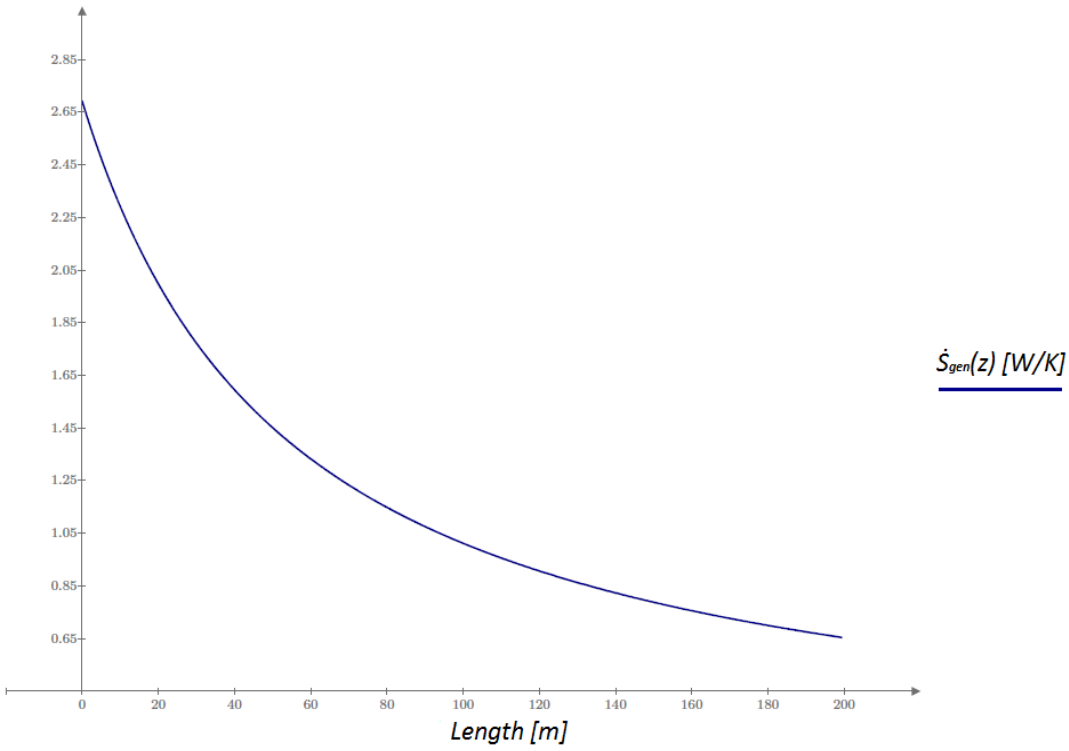

Fig. 10.8: Local rate of entropy generation distribution along the heat exchanger using air as working fluid ($r_1 = 25\ mm,\ R_{ip} = 0.03\ m^2K/W\ ,\ P_I = 8.517 \cdot 10^5\ Pa$).

Chapter 11

Determination of optimal of the diameter and thermal resistance of the inner pipe by minimization of the total entropy generation in the heat exchanger

To determinate the optimal of the inner diameter and thermal resistance of the inner pipe, the total of the entropy generated is calculated for all the configurations (r_1, R_{ip}).

Following are written the numerical value range of the variables, this is due to a physical limits for r_1 and R_{ip}, respectively.

$$10\ mm, 11\ mm, \dots, r_1, \dots, 34\ mm, 35\ mm$$
$$0.008\ \frac{m^2 \cdot K}{W}, 0.009\ \frac{m^2 \cdot K}{W}, \dots, R_{ip}, \dots, 0.099\ \frac{m^2 \cdot K}{W}, 0.1\ \frac{m^2 \cdot K}{W}$$

The objective is to find out the configuration which the total of the entropy generated is minimized.

Working medium: Water

The total of entropy generated distribution in function on the inner radius of the inner pipe (r_1) for different values of the inner pipe's thermal resistance $\left(R_{ip}\right)$ using water as a working fluid is shown in the figures from 11.1 to 11.4.

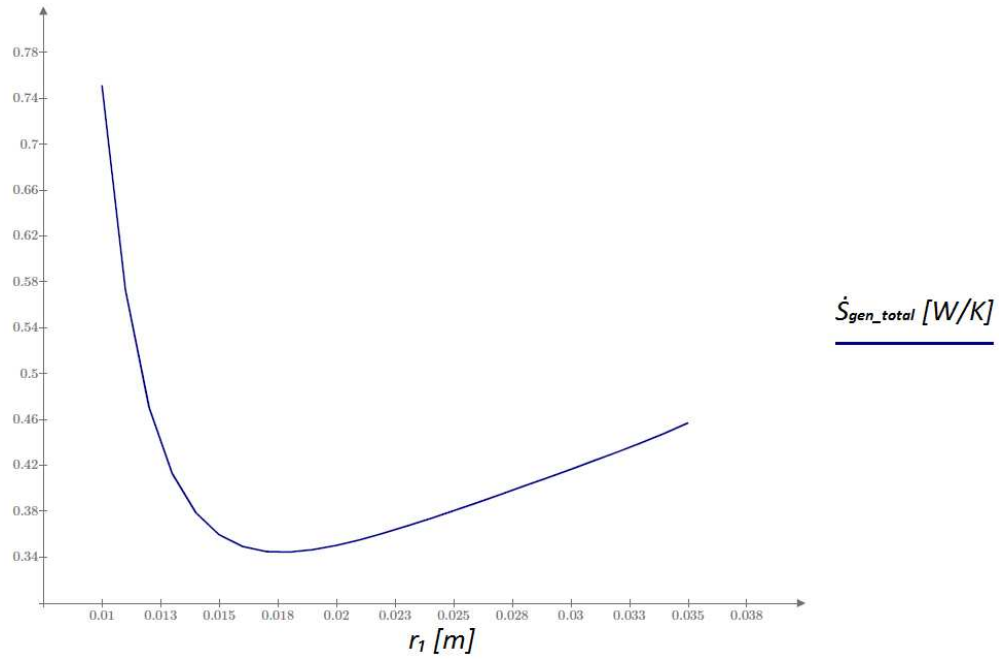

Fig. 11.1: Total of the entropy generated distribution using water $\left(R_{ip} = 0.008\ m^2 \cdot K/W\right)$.

The minimal value of entropy generation corresponds with the following configuration:

$$r_1(optimal) = 0.018\,m \quad ; \quad \dot{S}_{gen_{total}} = 0.3445\ \frac{W}{K}$$

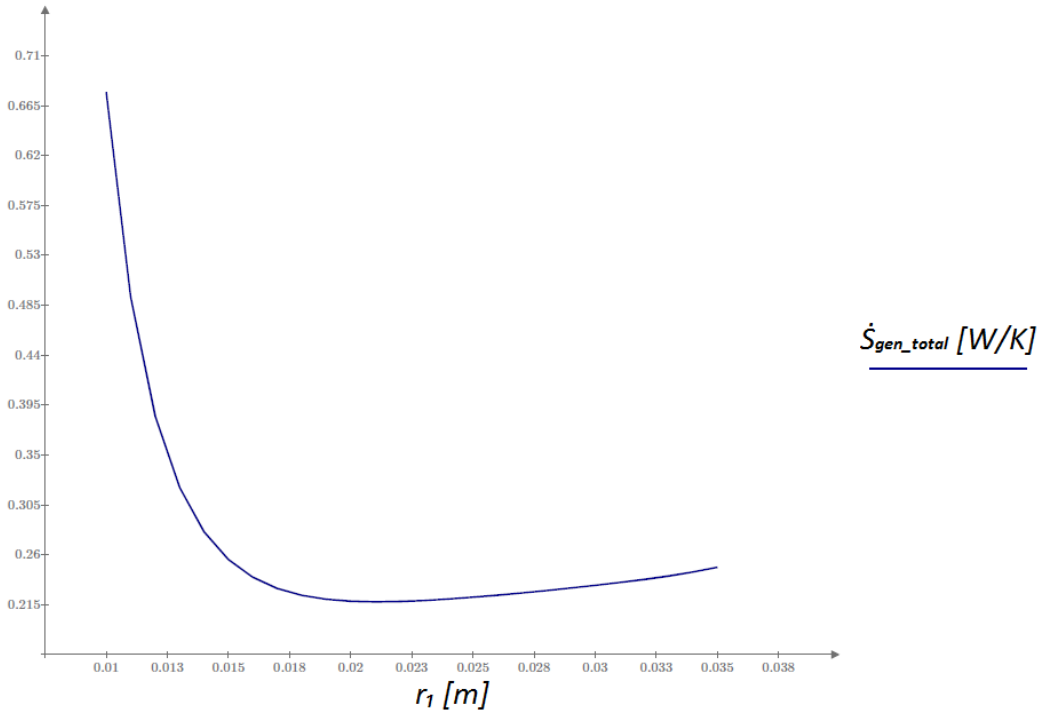

Fig. 11.2: Total of the entropy generated distribution using water $\left(R_{ip} = 0.02\ m^2 \cdot K/W\right)$.

The minimal value of entropy generation corresponds with the following configuration:

$$r_1(optimal) = 0.021\,m \quad ; \quad \dot{S}_{gen_{total}} = 0.2176\,\frac{W}{K}$$

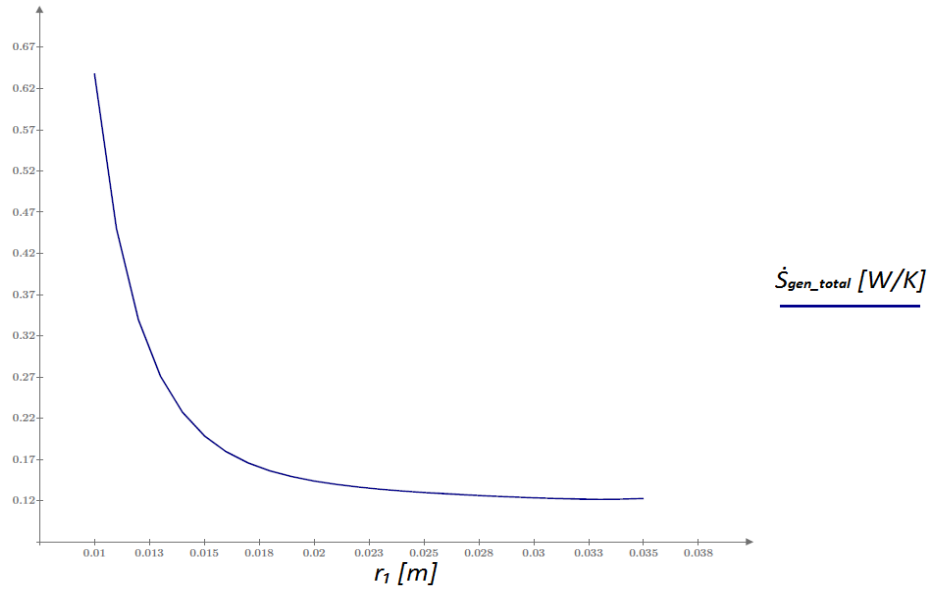

Fig. 11.3: Total of the entropy generated distribution using water $\left(R_{ip} = 0.056\ m^2 \cdot K/W\right)$.

The minimal value of entropy generation corresponds with the following configuration:

$$r_1(optimal) = 0.033\,m \quad ; \quad \dot{S}_{gen_{total}} = 0.1217\,\frac{W}{K}$$

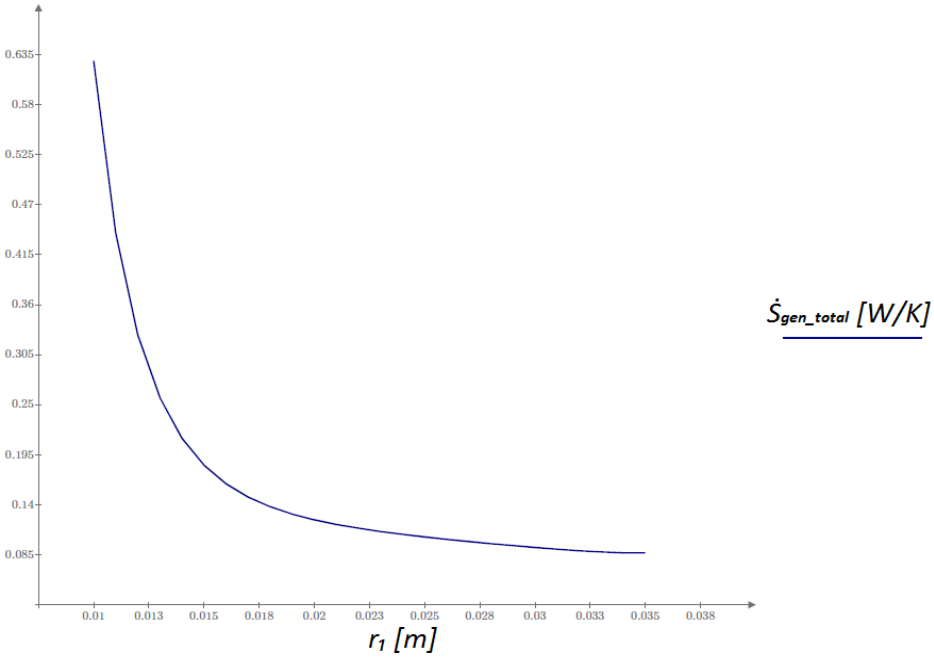

Fig. 11.4: Total of the entropy generated distribution using water $\left(R_{ip} = 0.1\ m^2 \cdot K/W\right)$.

The minimal value of entropy generation corresponds with the following configuration:

$$r_1(optimal) = 0.035\ m \quad ; \quad \dot{S}_{gen_{total}} = 0.0871\ \frac{W}{K}$$

From above graphs is concluded that the minimum of the total of the entropy generated corresponds to the maximum of the thermal resistance and inner radius of the inner pipe. This is corroborated in fig. 11.5, where is observed that the minimal of entropy generation corresponds to the maximal value of the inner's pipe thermal resistance for the optimal radius of the inner pipe ($r_1 = 0.035\ m$).

Hence, the optimal configuration using water as working fluid is:

$$\boxed{\begin{array}{c} r_1(optimal) = 35\ mm \\ R_{ip}(optimal) = 0.1\ \frac{m^2 \cdot K}{W} \end{array}}$$

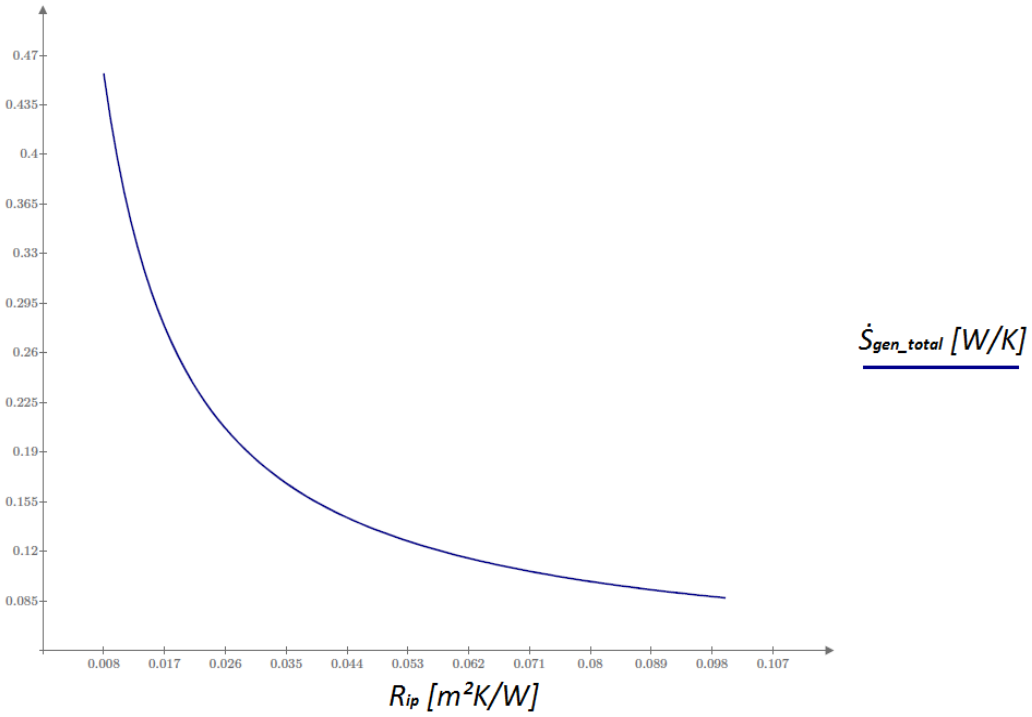

Fig. 11.5: Total of the entropy generated distribution using water ($r_1 = 35\ mm$).

Working medium: Air

The total of entropy generated distribution in function on the inner radius of the inner pipe (r_1) for different values of the inner's pipe thermal resistance (R_{ip}) using air as a working fluid is shown in figures from 11.6 to 11.8.

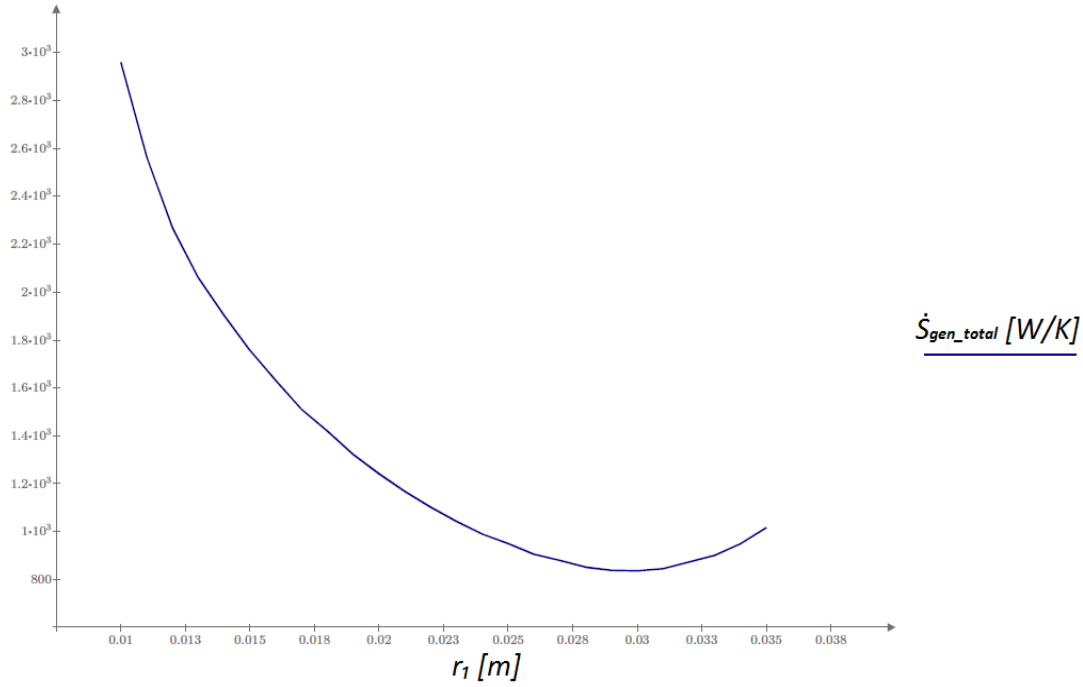

Fig. 11.6: Total of the entropy generated distribution using air $\left(R_{ip} = 0.03\ m^2 \cdot K/W\right)$.

In this case, the function represented in figure 11.6 has a radius which corresponds with the minimum of the entropy generated and is given by the value:

$$r_1(optimal) = 30\ mm \quad ; \quad \dot{S}_{gen_{total}} = 835.77\ \frac{W}{K}$$

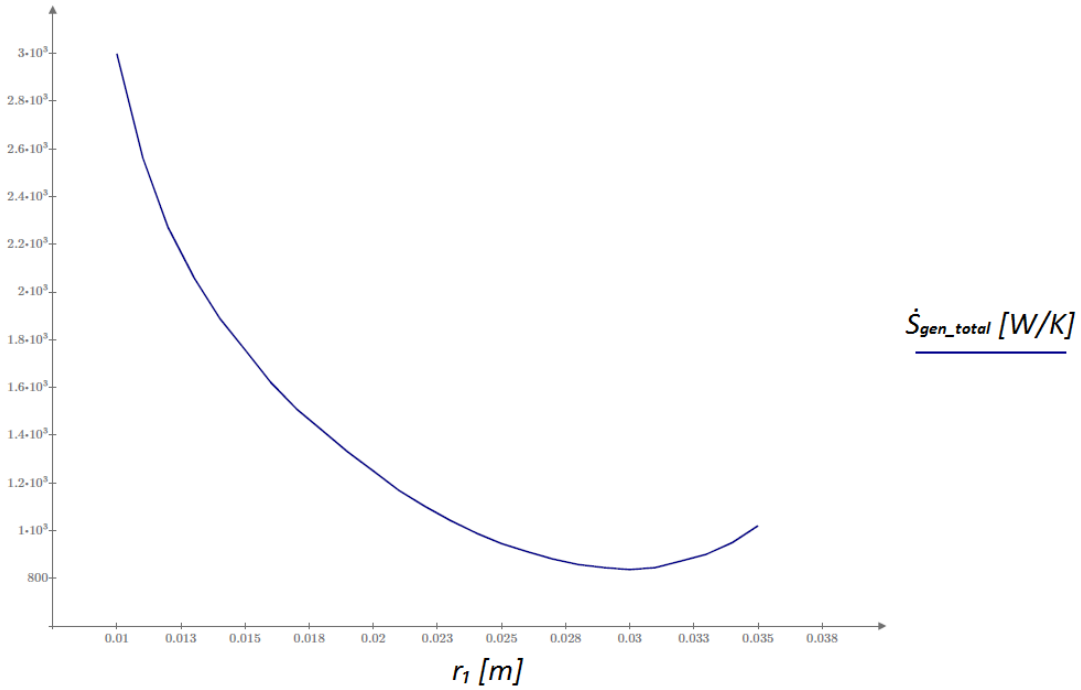

Fig. 11.7: Total of the entropy generated distribution using air $\left(R_{ip} = 0.07\ m^2 \cdot K/W\right)$.

The minimal value of entropy generation for the distribution presented in fig. 11.7 corresponds with the following configuration:

$$r_1(optimal) = 0.030\ m \quad ; \quad \dot{S}_{gen_{total}} = 836.20\ \frac{W}{K}$$

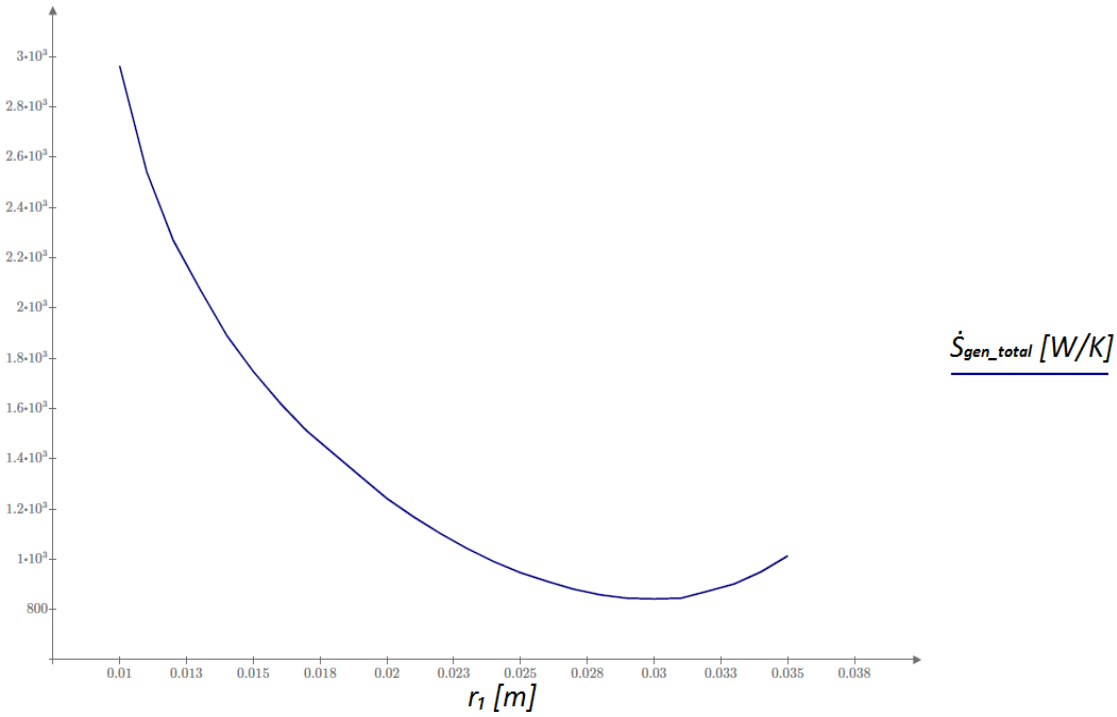

Fig. 11.8: Total of the entropy generated distribution using air $\left(R_{ip} = 0.1\ m^2 \cdot K/W\right)$.

The minimal value of entropy generation for the distribution presented in fig. 11.8 corresponds with the following configuration:

$$r_1(optimal) = 0.030\ m \quad ; \quad \dot{S}_{gen_{total}} = 842.29\ \frac{W}{K}$$

Moreover, for all values of thermal resistance of the inner pipe the minimum of entropy generated corresponds to the same radius of the inner pipe equal to 30 mm.

The optimal thermal resistance $\left(R_{ip}\right)$ is calculated for the optimal radius of the inner pipe. Fig. 11.9 shows the total of the entropy generated distribution according with the thermal resistance for this particular case.

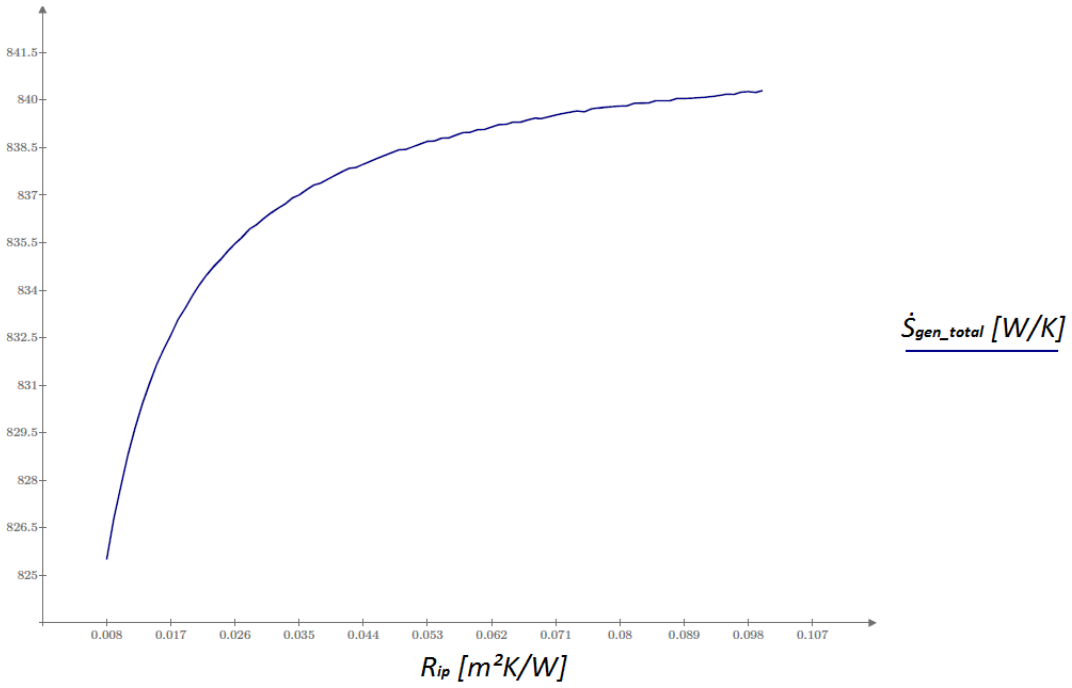

Fig. 11.9: Total of the entropy generated distribution using air ($r_1 = 30\ mm$).

As is observed in fig. 11.9, for the minimum thermal resistance the entropy generated is minimized. But in the other hand the DCHE's outlet temperature is also minimized (see fig. 11.10). So we must find a balance between the entropy generated and the DCHE's outlet temperature to find the optimal thermal resistance.

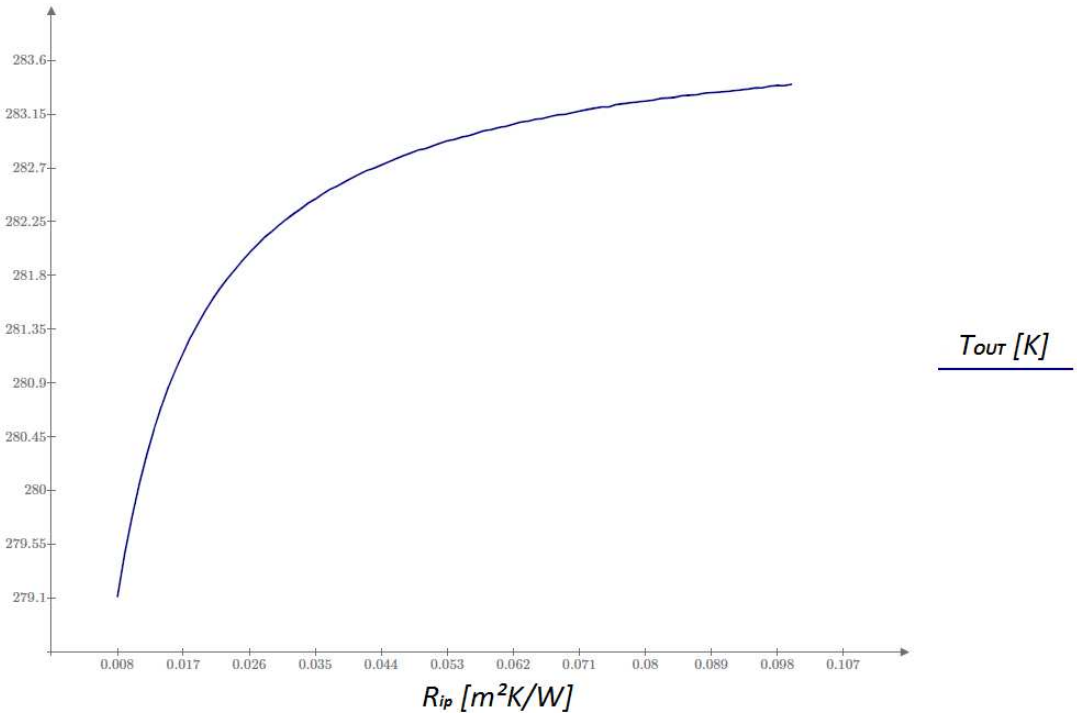

Fig. 11.10: DCHE's outlet temperature distribution using air ($r_1 = 30\ mm$).

In order to determine the optimal configuration, the percentage that increases the total of entropy generated and the DCHE's outlet temperature is calculated for every value of the thermal resistance. The respective expressions to calculate the percentages are written below:

$$\%\, S_{gen_{total}}(R_{ip}) = \left(\frac{S_{gen_{total}}\left(R_{ip} = 0.1\ \frac{m^2K}{W}\right) - S_{gen_{total}}(R_{ip})}{S_{gen_{total}}(R_{ip})} \right) \cdot 100$$

$$\%\, T_{OUT}(R_{ip}) = \left(\frac{T_{OUT}\left(R_{ip} = 0.1\ \frac{m^2K}{W}\right) - T_{OUT}(R_{ip})}{T_{OUT}(R_{ip})} \right) \cdot 100$$

Finally is decided that a 0.3% between the outlet temperature and the maximum outlet temperature is so small that it can be used to select the optimal point (fig. 11.11). This margin of error corresponds to the following thermal resistance:

$$R_{ip}(optimal) = 0.038\ \frac{m^2 \cdot K}{W}$$

$$\Longrightarrow 0.3\% = \left(\frac{T_{OUT}\left(R_{ip} = 0.1\ \frac{m^2K}{W}\right) - T_{OUT}\left(R_{ip} = 0.038\ \frac{m^2K}{W}\right)}{T_{OUT}\left(R_{ip} = 0.038\ \frac{m^2K}{W}\right)} \right) \cdot 100$$

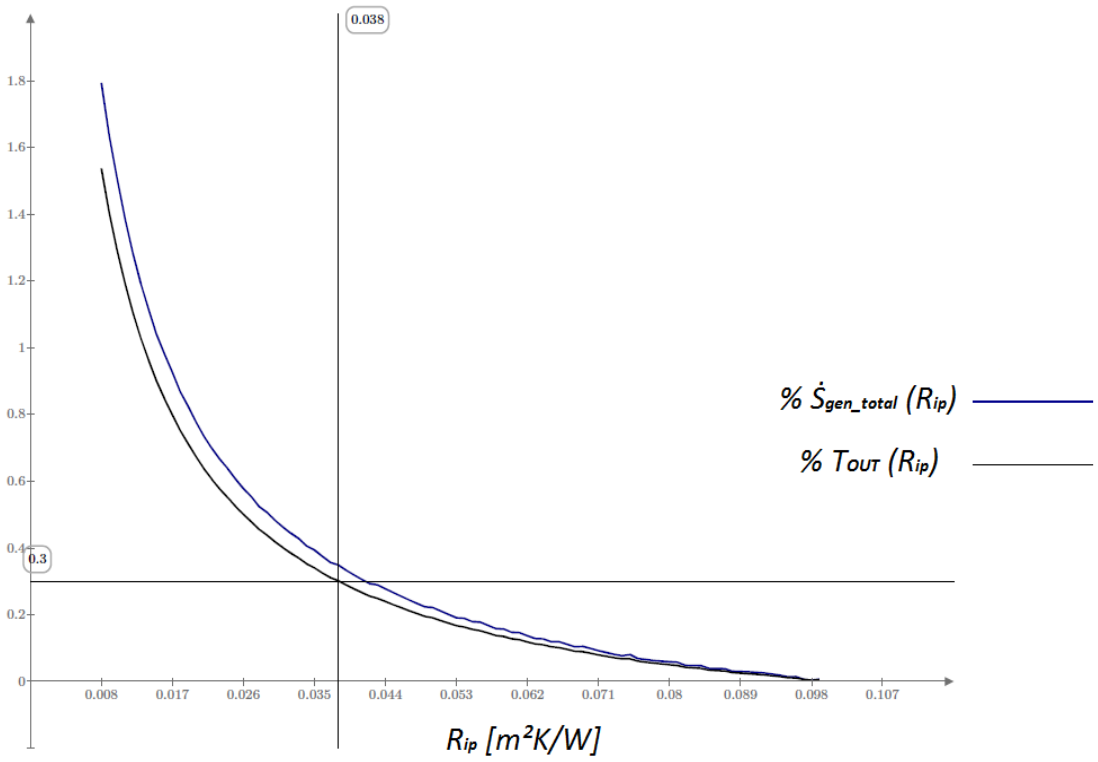

Fig. 11.11: Increasing percentage of the total of entropy generated and DCHE's outlet temperature respect to the maximum value using air $(r_1 = 30\ mm)$.

Hence, the optimal inner radius and thermal resistance of the inner pipe using air as a working fluid are:

$$\boxed{\begin{array}{c} r_1(optimal) = 30\ mm \\ R_{ip}(optimal) = 0.038\ \dfrac{m^2 \cdot K}{W} \end{array}}$$

SUMMARY

The results of the simulation to find the optimal downhole coaxial heat exchanger for both cases according to the working medium studied in this text are summarized in the table 11.1 given below. Corresponding distributions of water temperature, pressure and entropy generation rate are presented in figures from 11.2 to 11.14.

Parameter	Value	Parameter	Value
r_1	35 mm	T_L	282.048 K
R_{ip}	0.1 m^2·K/W	ΔT	4.491 K
P_I	1.061·10^5 Pa	$\overline{Re_a}$	3.819·10^3
D_{h_a}	0.02 m	$\overline{Re_t}$	1.043·10^4
D_{h_t}	0.07 m	$\overline{Pr_a}$	10.394
A_a	0.0028 m^2	$\overline{Pr_t}$	9.722
A_t	0.0038 m^2	ΔP	4.728·10^3 Pa
T_I	277.684 K	$\dot{S}_{gen_{total}}$	0.0871 W/K
T_F	282.175 K		

Table 11.1: Results of the simulation of the optimal DCHE using water as working fluid.

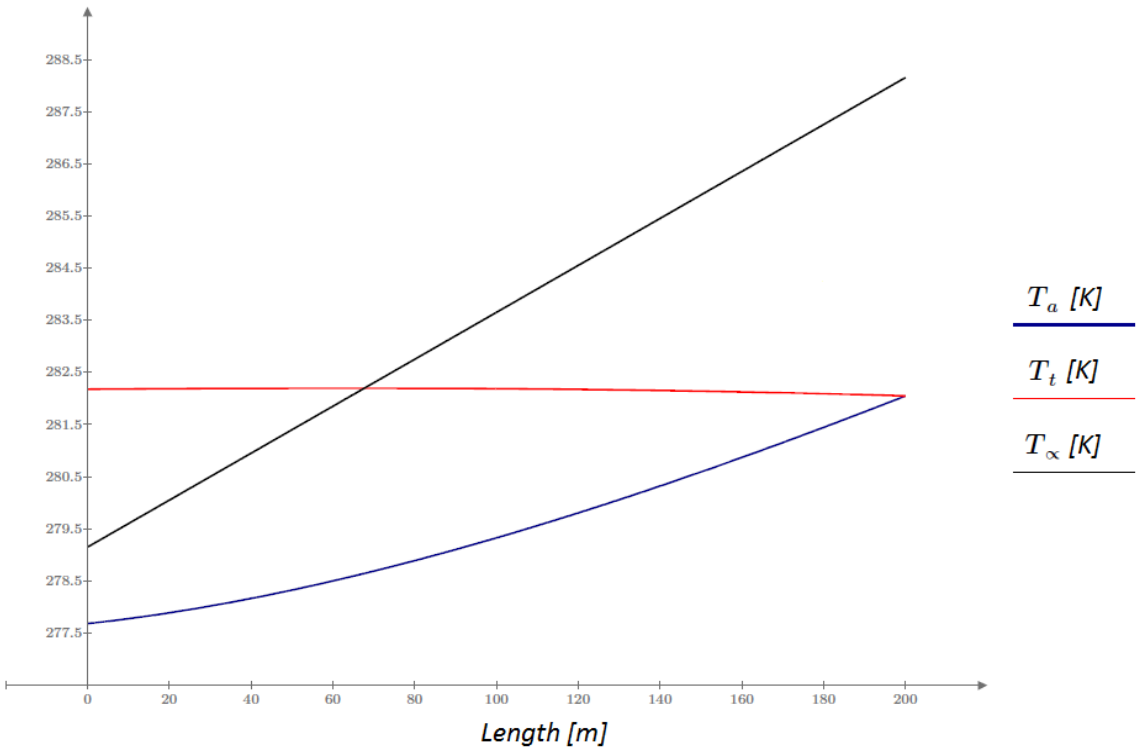

Fig. 11.12: Temperature distribution along the heat exchanger using water as a working fluid. $(r_1 = 35\ mm,\ R_{ip} = 0.1\ m^2K/W,\ P_I = 1.061 \cdot 10^5\ Pa)$

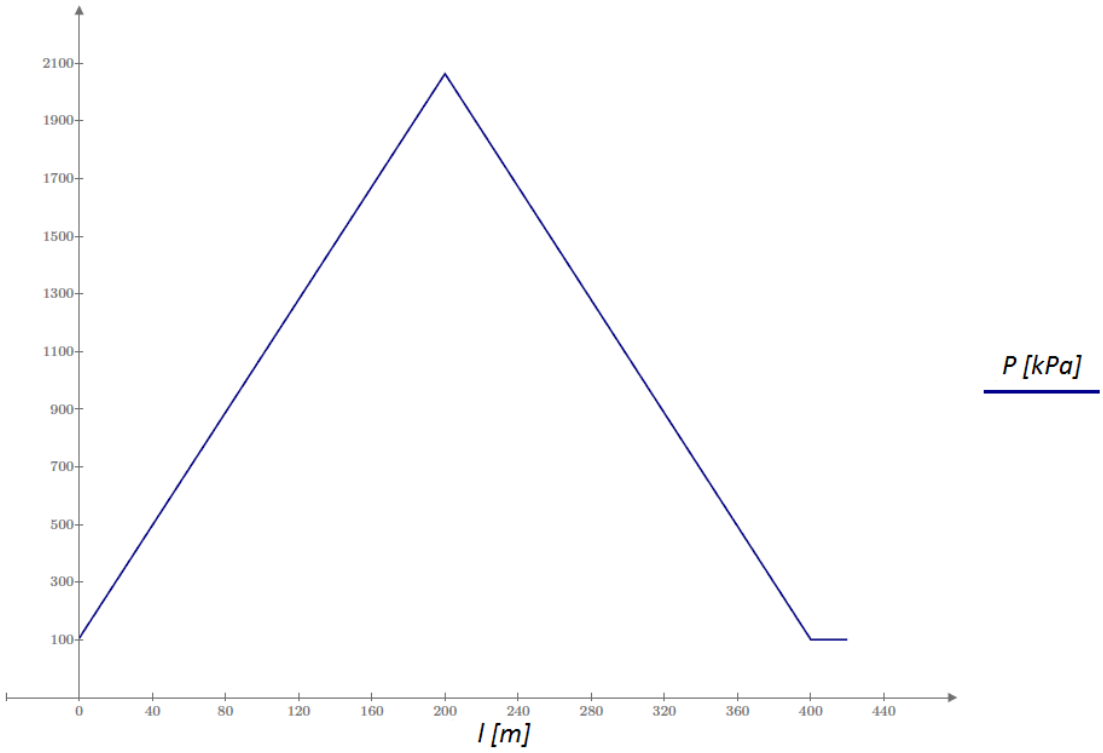

Fig. 11.13: Pressure distribution along the heat exchanger using water as a working fluid. $(r_1 = 35\ mm,\ R_{ip} = 0.1\ m^2K/W\ ,\ P_l = 1.061 \cdot 10^5\ Pa)$

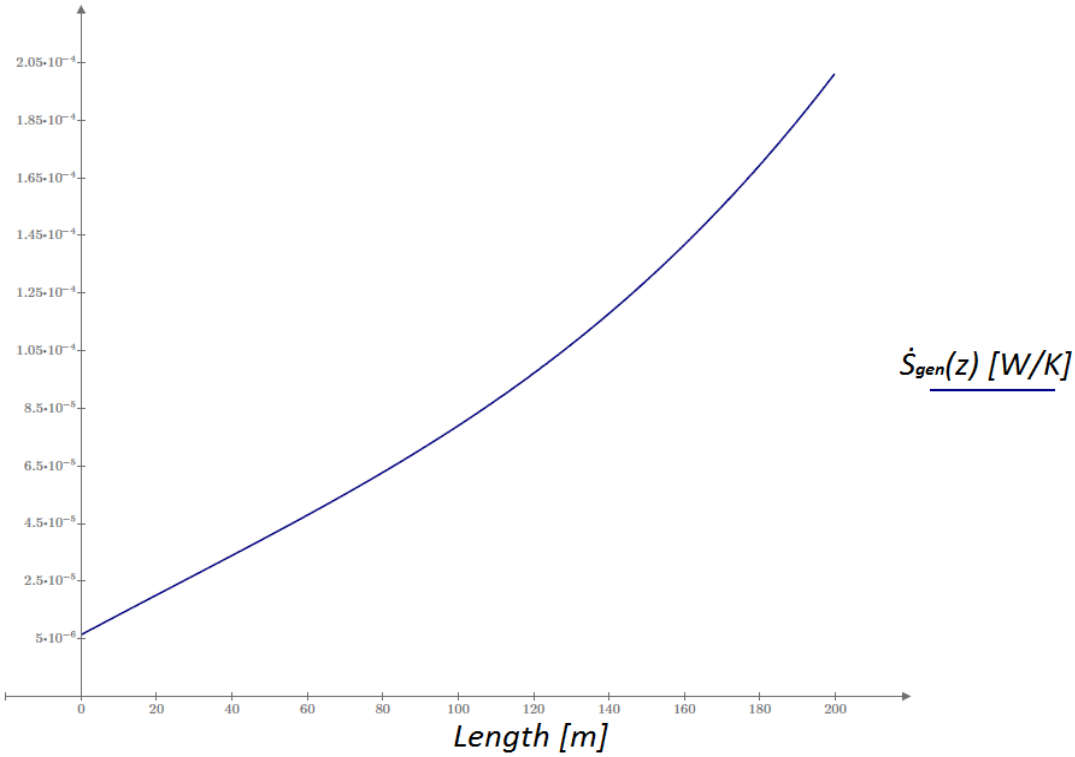

Fig. 11.14: Local rate of entropy generation distribution along the heat exchanger using water as working fluid $(r_1 = 35\ mm,\ R_{ip} = 0.1\ m^2K/W\ ,\ P_l = 1.061 \cdot 10^5\ Pa)$.

Distributions of air temperature, pressure and entropy generation rate corresponding to the optimal values of the inner pipe radius and thermal resistance are given in table 11.2 and presented in figures from 11.15 to 11.17.

Parameter	Value	Parameter	Value
r_1	30 mm	T_L	284.265 K
R_{ip}	0.038 m^2·K/W	ΔT	7.471 K
P_I	7.223·10^5 Pa	$\overline{Re_a}$	8.537·10^5
D_{h_a}	0.03 m	$\overline{Re_t}$	2.392·10^6
D_{h_t}	0.06 m	$\overline{Pr_a}$	0.719
A_a	0.0040 m^2	$\overline{Pr_t}$	0.719
A_t	0.0028 m^2	ΔP	5.698·10^5 Pa
T_I	275.05 K	$\dot{S}_{gen_{total}}$	837.13 W/K
T_F	282.521 K		

Table 11.2: Results of the simulation of the optimal DCHE using air as working fluid.

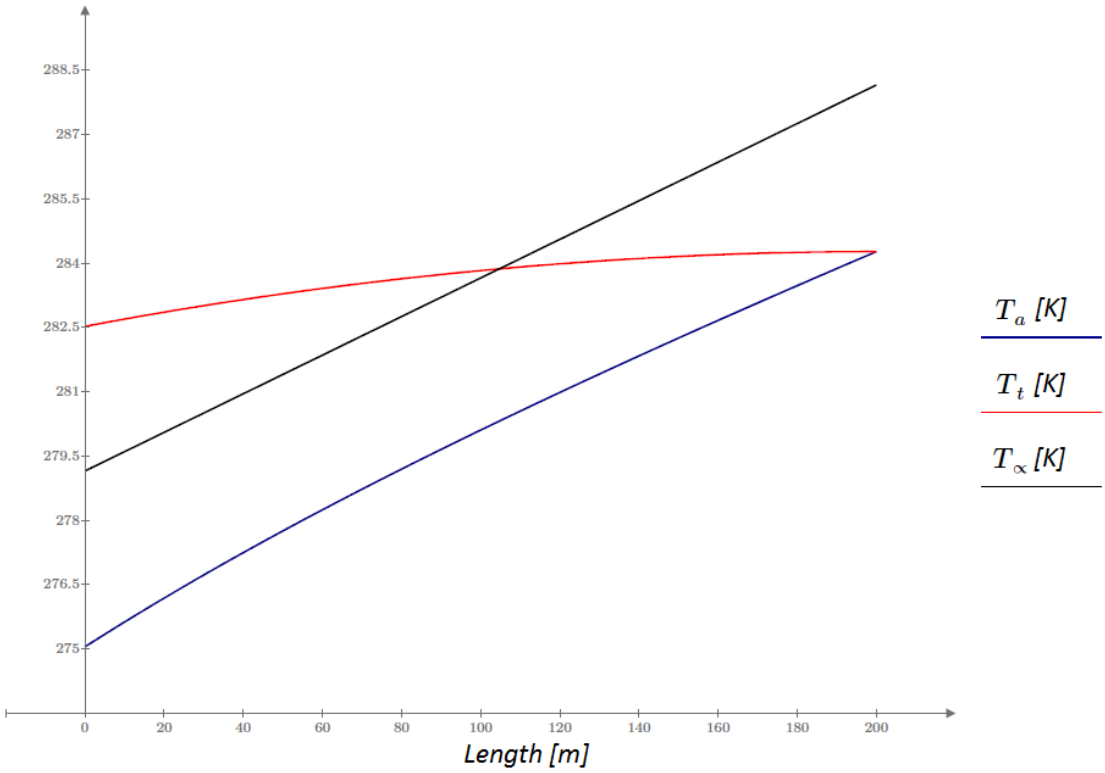

Fig. 11.15: Temperature distribution along the heat exchanger using air as a working fluid. $(r_1 = 30\ mm,\ R_{ip} = 0.038\ m^2K/W,\ P_I = 7.223 \cdot 10^5\ Pa)$

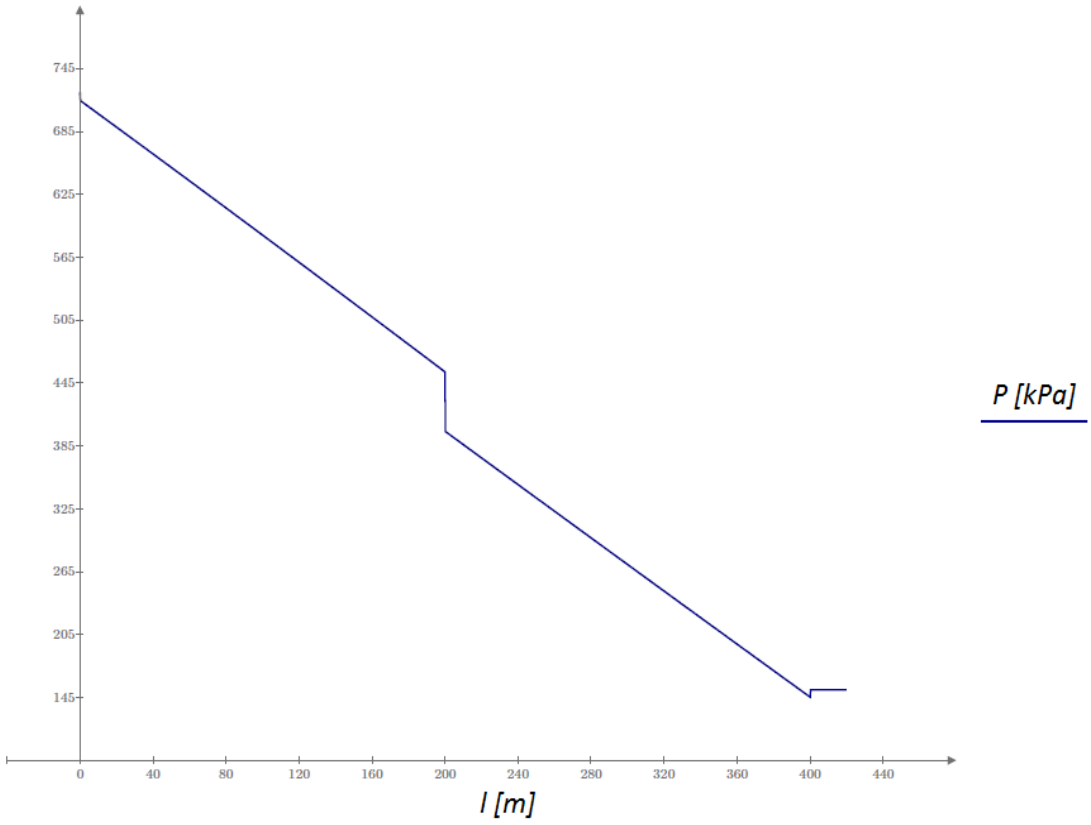

Fig. 11.16: Pressure distribution along the heat exchanger using air as a working fluid. ($r_1 = 30\ mm$, $R_{ip} = 0.038\ m^2K/W$, $P_l = 7.223 \cdot 10^5\ Pa$)

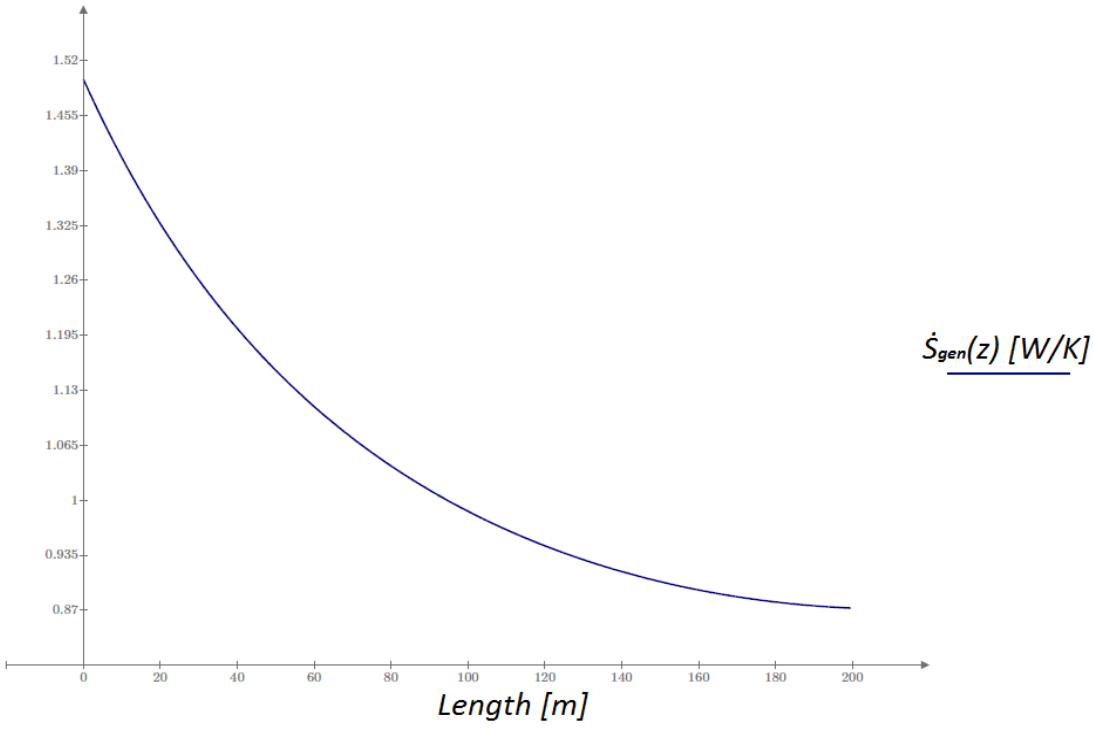

Fig. 11.17: Local rate of entropy generation distribution along the heat exchanger using air as working fluid ($r_1 = 30\ mm$, $R_{ip} = 0.038\ m^2K/W$, $P_l = 7.223 \cdot 10^5\ Pa$).

Chapter 12

Conclusions

The results of DCHE show that the temperature rise along the heat exchanger using air as working fluid is higher than using water. This is because the heat capacity of the air is much smaller and it causes this effect. In the other hand, the air as a working medium has a significant deficiency. It leads to the high pressure drop along the heat exchanger due to the friction of the air with the pipe's walls.

In the case of water, the pressure drop along the heat exchanger does not play a significant role for the heat exchanger design. For the water the effect of the fluid friction with the pipe's wall is not so high. As I mentioned above this is because the relative high density of the water and gravitational effects.

As regards to the entropy generation, this is much higher for the air than for the water. The entropy is generated within the system by action of irreversibilities. The entropy generation is due to two mechanisms: the heat transfer across a finite temperature difference and the flow with friction through ducts. We have to considerer their simultaneous effect on entropy generation, heat transfer and fluid friction irreversibilities tend *to compete* with one another. Adjusting the diameter and thermal resistance of the inner pipe the total rate of entropy generation is minimized. The diameter of the inner pipe is the variable mainly related with the entropy generation due to the flow with friction while the thermal resistance of the inner pipe is the variable mainly related with the entropy generation due to the heat transfer.

In the case of water the entropy generation is basically due to the heat transfer while for the air the entropy generation is basically due to the frictional pressure drop. Take note that, for the water, the entropy generation depends of both variables (r_1, R_{ip}). In the case of the air the entropy generation depends more in the inner radius of the inner pipe - variable strongly related with the frictional pressure drop - than in the thermal resistance of the inner pipe.

Hence, for the air, the optimal configuration from the point of view of the entropy generation is one that minimizes the frictional pressure drop. This is corroborated comparing fig. 9.10 with fig. 11.6, 11.7 and 11.8.

For the water, the optimal configuration is one that maximizes the outlet temperature of the downhole coaxial heat exchanger. Then the heat exchanger irreversibilities are minimized and the heat transfer occurs optimally. Increasing the thermal resistance and the diameter of the inner pipe is the way to reach this goal.

References

[1] Ansys, FLUENT: "FLUENT 6.3 Documentation". http://my.fit.edu/itresources/manuals/fluent6.3/help/index.htm. 20-09-2006.

[2] Bejan, A. and Kraus, A.D.: "Heat transfer Handbook". John Wiley & Sons, INC, USA, 2003.

[3] Bejan, A., Tsatsaronis, G. and Moran, M.: "Thermal design & optimization". John Wiley & Sons, Inc, USA, 1996. p.273-332.

[4] Blomberg, T. and Claesson, J.: "Earth Energy Designer Manual". http://www.buildingphysics.com/index.htm. 17-11-2008.

[5] Bonals, L.A.: "Transferència de calor". Publicacions d'Abast S.L.L. Escola Tècnica Superior d'Enginyeria Industrial de Barcelona-Universitat Politècnica de Catalunya, Barcelona, 2007.

[6] CADDET Centre for Renewable Energy ETSU: "Geothermal and solar heat used to melt snow on roads, *Technical Brochure No.76*". http://www.caddet-re.org/assets/no76.pdf

[7] Incropera, F. P. and DeWitt, D. P.: "Fundamentals of Heat and Mass Transfer". John Wiley, USA, 2007.

[8] Kreith, F.: "The CRC Handbook of thermal engineering". Editor-in-chief Kreith, F. Co-published by CRC press Springer, USA, 2000.

[9] Massoud, M.: "Engineering Thermofluids". Springer, Germany, 2005. p.295-320.

[10] Morita, K.: "One possible way to utilize abandoned deep wells-The application of the DCHE" in: *Geothermal Energy in Underground Mines*. Proceedings of International Scientific Conference "Geothermal Energy in Underground Mines" November 21-23, 2001, Ustroń, Poland. University of Silesia, Faculty of Earth Sciences, Department of Fundamental Geology, 2001. *art.17.*

[11] Morita, K. and Tago, M.: "Operational characteristics of the Gaia snow-melting system in Ninohe, Iwate, Japan". *GEO-HEAT CENTER*, **21**, (4), December 2000. p.5-11. http://geoheat.oit.edu/

[12] Naderer, P., Fruehling, P. and Dinstl, O.: "Transforming liquidated hydrocarbonwells to geothermal deep borehole heat exchangers" *Geothermal Energy Utilization Conference*, 3-4th November 2009, Dallas, USA. http://smu.edu/geothermal/oil&gas/2009/Presentations/Abstracts/Naderer_Abstract_09.pdf

[13] National Chung Hsing University, Department of Mechanical Engineering, *Professor Jung-Yang San*: "Governing equations for turbulent flow". http://wwwme.nchu.edu.tw/Enter/html/lab/lab516/Convective%20Heat%20Transfer(6707)-Pdf/2.2.pdf

[14] Nowak, W., Sobański, R., Kabat, M. and Kujawa, T.: "Systemy pozyskiwania I wykorzystania energii geotermicznej". Politechnika Szczecińska, Katedra Techniki Cieplnej, Szczecin (Poland), 2000. p.54-73.

[15] Sanner, B.: "Shallow geothermal energy". *GEO-HEAT CENTER*, **22**, (2), June 2001. p.19-25. http://geoheat.oit.edu/

[16] Signorelli, S.: "Geoscientific investigations for the use of shallow Low-Enthalpy systems". Zurich, Swiss Federal Institute of Technology Zurich, 2004.

[17] Sobański, R., Kabat, M. and Nowak, W.: "Jak pozyskac ciepło z ziemi". Centralny ósrodek informacji budownictwa, Warsaw (Poland), 2000.

[18] Stanford University, School of Earth Sciences, Department of Energy Resources Engineering: "Design and performance of borehole heat exchanger/Heat pump systems". http://pangea.stanford.edu/ERE/pdf/IGAstandard/ISS/2001Romania/rybach.pdf. 2001

[19] Tóth, A. and Bobok, E.: "Sustainability of a geothermal doublet" in: *1st Knowbridge Conference on Renewables*. Proceedings of the conference held at the University of Miskolc Institute of Environmental Management, Miskolc, Hungary September 27-28, 2010. University of Miskolc, Institute of Environmental Management, 2010. p.90-100. http://www.knowbridge.eu/

[20] Wang, Z.: "Modeling study of a single-well enhanced geothermal system (EGS)". Palo Alto (California), Stanford University 2009. p.28-34.

[21] Wiśniewski, S. and Wiśniwski, T. S.: "Wymiana Ciepła". Wydawnictwa Naukowo-Techniczne, Poland, 1997. p.393-421.